2006

The dissolution and swelling of bituminous coal in N-methyl-pyrrolidone

Joseph M. Stoffa
West Virginia University

The Dissolution and Swelling of Bituminous Coal in N-Methyl-Pyrrolidone

Joseph M. Stoffa

Thesis Submitted to the College of Engineering and Mineral Resources at West Virginia University in partial fulfillment of the requirements for the degree of

Master of Science in Chemical Engineering

Dr. Alfred H. Stiller, Chair
Dr. Peter G. Stansberry
Dr. Richard Turton

Department of Chemical Engineering

West Virginia University

Morgantown, West Virginia

2006

Keywords: Coal dissolution, coal extraction, coal swell, n-methyl-pyrrolidone, solvent extraction, correlation, porosity

Abstract

The Dissolution and Swelling of Bituminous Coal in N-Methyl-Pyrrolidone

Joseph M. Stoffa

Research detailed herein examined the extraction and swelling of a bituminous coal in the super solvent n-methyl-pyrrolidone. Correlations were developed to describe the extraction and swelling observed in the coal-solvent system. These correlations describe swelling and extraction based on experimental parameters such as extraction time and extraction temperature. The research concluded that swelling and extraction may be related processes. The most significant result of the research was a proposed relationship between the rapidness of coal swell and the coal's solubility in the solvent. The research served as support for coal structure models and solvent extraction mechanisms published in peer reviewed literature.

Acknowledgements

I thank Alfred Stiller, his guiding influence enabled me to grow as a professional and as an individual. I thank Peter Stansberry, his unparalleled knowledge of coal solvent systems was a great asset during research. I thank Richard Turton, whose style improved the quality of my research. I thank Elliot Kennel – he helped me improve my (somewhat still) awkward writing style. I thank Jennie Wheeler, who tirelessly performed several hundred coal-solvent extractions, and then analyzed the several hundred resultant solutions. I also thank the DOE for funding the work – nothing would have been accomplished if the DOE lacked the foresight to invest in coal research.

Contents

List of Figures

List of Tables

List of Equations

Chapter 1 – Introduction

Discussion of US energy independence has revitalized interest in coal utilization. Coal is underutilized as a feedstock for liquid fuels and as a base for value added products. This research concerned coal's use as a base for value added products. Specifically, the work focused on the solvent extraction of bituminous coal using the super solvent n-methyl-pyrrolidone. Solvent extraction separates the desirable carbonaceous portion of coal from the undesirable inorganic portion of coal. Solvent extraction removes virtually all inorganic matter from coal, including sulfur in the form of pyrite. Because many undesirable elements, such as arsenic and mercury, are substitutions in the pyrite matrix, solvent extraction will also remove some heavy metals present in coal[1]. The product of solvent extraction, coal extract, is a solid carbonaceous material having almost zero ash. Coal extract have been used as a feedstock for carbon fibers, carbon foams, carbon fuel cell fuel, fuel additives, nuclear grade graphite, pitch additives, and more.

Solvent extraction may also participate in the future of energy production in the United States. New clean coal power plants designed under DOE programs such as Vision 21 and Future Gen will require a purer feed coal to reduce pollution. If progress can be made in lowering the costs of solvent extraction, solvent extraction could compete will less effective conventional coal cleaning methods such as dense medium separation and froth flotation. If solvent extraction is unable to compete economically with conventional coal cleaning technology, it may still play a role in power production. New clean coal power facilities will

be more costly than current power plants. The higher costs of these facilities could be offset by producing a value added feedstock in addition to producing power.

The research detailed herein recorded the swell and extraction of a bituminous coal in the super solvent n-methyl-pyrrolidone. The swell and extraction was described as a function of process parameters, the extraction temperature and extraction time. The relationship between swell and extraction was examined. The porosity of the bituminous coal used in the research was examined using mercury porisimetry. The porosity of the bituminous coal and its relationship to solvent extraction and solvent swelling of coal was examined. To summarize, the research discussed herein accomplished the following.

1) Collected data on the solvent swelling of bituminous coal
2) Collected data on the solvent extraction of bituminous coal
3) Examined the porosity of bituminous coal via mercury porisimetry
4) Correlated the extent of coal swelling to processing parameters
5) Correlate the extent of solvent extraction to processing parameters
6) Determined the relationship between swelling and extraction

Chapter 2 – Background

Section 2.1 – What is Coal

"G.L. Jansen, a geologist and coal petrographer, referred to coal simply as an 'organic sediment'.[2]" Merriam-Webster defines coal as "a black or brownish black solid combustible substance formed by the partial decomposition of vegetable matter without free access of air and under the influence of moisture and often increased pressure and temperature that is widely used as a natural fuel.[3]" "More specifically, it can be said that coal is a combustible solid, usually stratified, which originated from the accumulation, burial, and compaction of partially decomposed vegetation in previous geologic ages.[2]" Coal primarily contains carbon, hydrogen, oxygen, sulfur, and lesser amounts of up to 60 other elements[4]. Coal contains these elements because they were present in the parent material, were incorporated with the coal during coalification, or were mixed with the coal during mining[4].

The coalification process spans millions of years, and there are many levels of coalification. Coalification is a function of how long the parent organic material is buried, and the temperature and pressure to which the parent organic material is exposed. Coal is classified according to rank, a measure of the degree of coalification. The coal ranks, in order of increasing coalification, are lignite, sub-bituminous, bituminous, and anthracite. The coalification cycle is presented graphically in Figure 2-1[5].

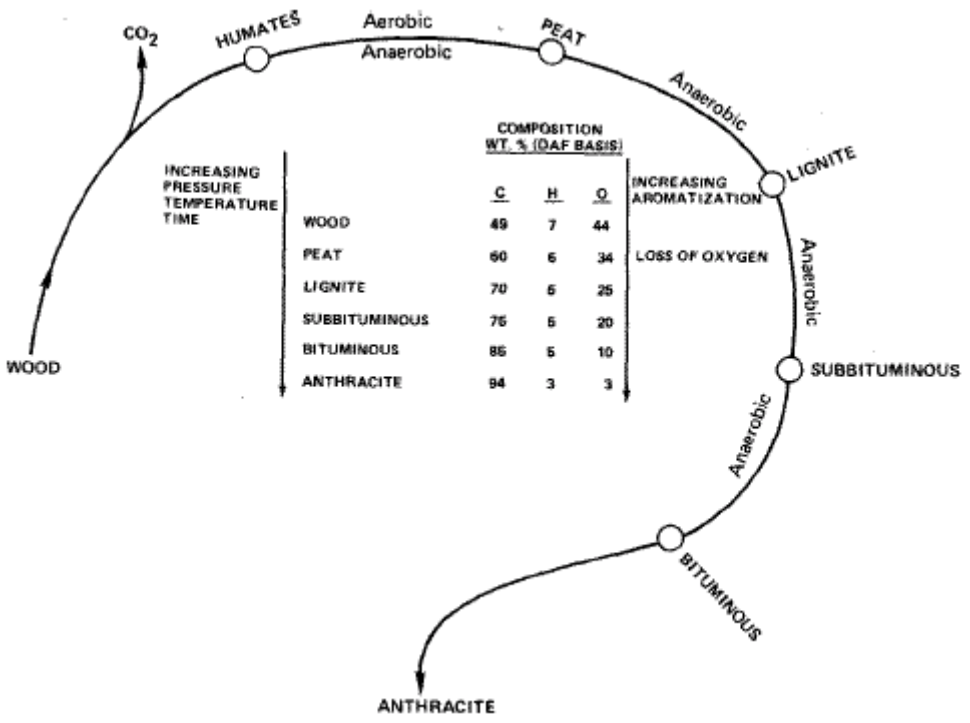

Figure 2-1 – The coalification cycle[5]

Some coal properties are correlated with coalification. As coalification increases, the aromaticity of the coal structure increases. Accompanying this increase in aromaticity is a decrease in hydrogen and oxygen content. When anthracite undergoes further coalification, it is no longer classified as coal, it is classified as graphite. Pure graphite is the most aromatic form of carbon, and contains no hydrogen. Other carbonaceous materials may contain the same constituents as coal, but are not defined as coal because they have a proportionally large amount of inorganic matter, or because they have not undergone a metamorphic change. For example, oil shale and peat are elementally similar to coal, but are not considered coals. The American Standards Testing Methods (ASTM) has definitions of various coal ranks, and these definitions are presented as Table 2-1[6].

Table 2-1 – ASTM classification of various coal ranks[6]

Class		Group	Fixed Carbon Limits (%) (dry mineral-matter -free basis) ≥	<	Volatile Matter Limits (%) (dry mineral-matter (dry ma basis) >	≤	Caloric Value Limits (Btu/lb)[b] (moist[c], mineral-matter -free basis) ≥	<	Agglomerating Characteristics
I. Anthracite	1	Meta-anthracite	98	-	-	2	-	-	Nonagglomerating
	2	Anthracite	92	98	2	8	-	-	
	3	Semianthracite[d]	86	92	8	14	-	-	
II. Bituminous	1	Low volatile bituminous coal	78	86	14	22	-	-	Commonly
	2	Medium-volatile bituminous coal	69	78	22	31	-	-	Agglomerating[f]
	3	High-volatile A bituminous coal	-	69	31	-	14000[e]	-	
	4	High-volatile B bituminous coal	-	-	-	-	13000	14000	
	5	High-volatile C bituminous coal[g]	-	-	-	-	11500	13000	
			-	-	-	-	10500	11500	Agglomerating
III. Subbituminous	1	Subbituminous A coal[g]	-	-	-	-	10500	11500	Nonagglomerating
	2	Subbituminous C coal	-	-	-	-	9500	10500	
	3	Subbituminous B coal	-	-	-	-	8300	9500	
IV. Lignite	1	Lignite A	-	-	-	-	6300	8300	Nonagglomerating
	2	Lignite B	-	-	-	-	-	6300	

While these ranks are useful, they do not describe the non-carbonaceous constituents of coal or the structure of coal. Even though two coals may be of the same rank, High-volatile A bituminous coal for example, they may have varying constituents and structure. Understanding coal requires knowledge of the constituents of coal, how these components are connected, and what chemistry is applicable to coal. For these reasons, the following sections examine the constituents of coal, the structure of coal, and the functional groups of coal.

Section 2.1.1 – Constituents of Coal

Some have described coal as "a very complex heterogenous mixture of organic compounds and minerals, analogous to a fruit cake.[2]" Continuing the analogy, it would be helpful to summarize the ingredients of the fruit cake that is coal. It would be accurate to say that both fruit cake and coal are composed mainly of the elements carbon, oxygen, and hydrogen. With respect to fruit cakes, it would be more specific to say they contain sugar, water, and fruits. With respect to coals, it would be more specific to say they contain various organic groupings. These organic groupings are analyzed and defined by petrographers. Petrography is based on the microscopic examination of materials, and is defined as "the description and systematic classification of rocks[3]." Although coal does not meet all definitions of a rock, petrography is a useful tool for describing and classifying coal.

When coal is examined under magnification, it appears as a collection of smaller organic groups, known as macerals. Macerals in coal are analgous to minerals in rocks, but macerals, unlike minerals, have no fixed chemical composition or definite crystal structure. Macerals are characterized according to their source material, morphology, nature of formation, similarity in chemical composition, internal structure, level of reflectivity or color, and degree of coalification[7].

Coal contains three major maceral groups; Vitrinite, Liptinite (also called Exinite), and Inertinite. Vitrinite macerals are the result of coalified woody tissues. These coalified woody tissues are derived from the stems, roots, and vascular tissue of parent leaf material[7]. The next

most common maceral group is Liptinite, also known as Exinite. "The macerals of the Liptinite maceral group are derived from the resinous and waxy materials of plants, including resins, cuticles, spore and pollen exines, and algal remains that constitute resinite, cutinite, sporonite, and alginate, respectively[7]." Another common maceral group is Inertinite. It is presumed that Inertinite results from the charring of plant tissue. "Inertinite derives its name from the fact that it is inert or semi-inert during normal carbonization processes in a retort.[4]"

The major maceral groups, particular maceral names, origins, and important maceral properties are presented as

Table 2-2[8]. Pictures of Vitrinite (Vitrinite maceral group), Alginite (Liptinite maceral group), and Fusinite (Inertinite maceral groups) are presented below as Figure 2-2[9].

Table 2-2 – Origin and importance of macerals and maceral groups8

Maceral Group	Maceral	Origin	Group Properties
Vitrinite	Collinite telinite	Wood or bark	Principal constituent of coal, readily hydrogenated, oxidized easily, relatively oxygen rich
Liptinite (exinite)	Resinite Cutinite	Plant Resins Needles and leaf cuticles	Yields greatest quantity of by-products when carbonized
	Sporinite Alginite	Spores Algae	Readily hydrogenated in coals with more than 25% volatile
Inertinite	Sclerotinite	Fungal Remains	
	Micrinite macrinite	Granular matter from protoplasm	Relatively inert, not easily hydrogenated or oxidized
	Semifusinite	Wood or bark severely oxidized before burial	An important additive in coke

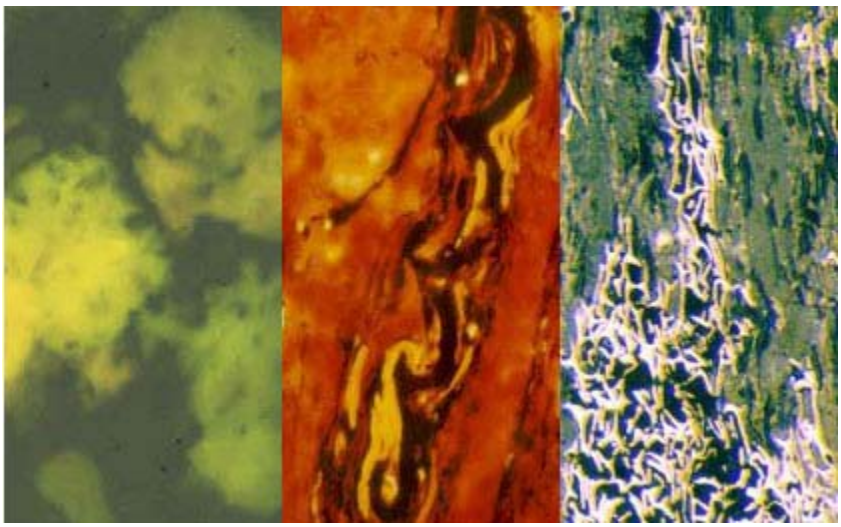

Figure 2-2 – From left to right, Alginite, Vitrinite, and Fusinite[9]

In addition to maceral groups, coal contains inorganic constituents. These inorganics are often incorrectly referred to as ash. Ash is the post-combustion form of inorganic material, but prior to combustion it is proper to refer to these constituent more generally as inorganics. Some examples of inorganic constituents include clay minerals, carbonates, sulfides, oxides, quartz, phosphates, heavy minerals, and accessory minerals[10]. A listing and description of these inorganic compounds is presented below as Table 2-3[10].

Table 2-3 – Summary of the minerals in coal[10]

	First Stage of Coalification: Synergistic Formation, Synsedimentary, Early Diagenetic (intimately intergrown)		Second Stage of Coalification: Epigenetic Formation	
Mineral Group	Transported by Water or Wind	Newly Formed	Deposited in Fissures, Cleats, and Cavities (coarsely intergrown)	Transformation of Synergistic Minerals (intimately intergrown)
Clay Minerals	Kaolinite, illite, sericite, clay minerals with mixed-layer structure, montmorillonite, tonstein			Illite, chlorite
Carbonates		Siderite-ankerite concretions, dolomite, calcite, ankerite, siderite, calcite	Ankerite, calcite, dolomite, ankerite in fusite	
Sulphides		Pyrite concretions, melnikovite-pyrite, coarse pyrite (marcasite), concretion of FeS_2-$CuFeS_2$-ZnS	Pyrite, marcasite, zinc sulphide (sphalerite), lead sulphide (galena), copper sulphide (chalcopyrite, pyrite in fusite	Pyrite from the transformation of syngernetic concretions of $FeCO_3$
Oxides		Hematite	Geothite, lepidocrocite ("needle iron ore")	
Quartz	Quartz Grains	Chalcedony and quartz from the weathering of feldspar and mica	Quartz	
Phosphates	Apatite	Phosphorite, apatite		
Heavy Minerals and accessory minerals	Zircon, rutile, tourmaline, orthoclase, biotite		Chlorides, sulfates, and nitrates	

Section 2.1.2 – Structure of Coal

The focus of research was bituminous coal, so it was important to understand bituminous coal structure. The structure of bituminous coal is not as straightforward as diamond or graphite. Coal is a collection of many different molecular units, coal has no definite structure or exact composition. There is near universal agreement that coal can be modeled as a large three-dimensional crosslinked macromolecular network of polynuclear aromatic clusters connected by relatively strong bonds[11,12]. This description of coal is graphically represented in the Wiser Model of bituminous coal, and has gained wide acceptance[13]. Figure 2-3 is an example of a large polymer-like carbonaceous molecule that exists in coal according to the Wiser Model[13].

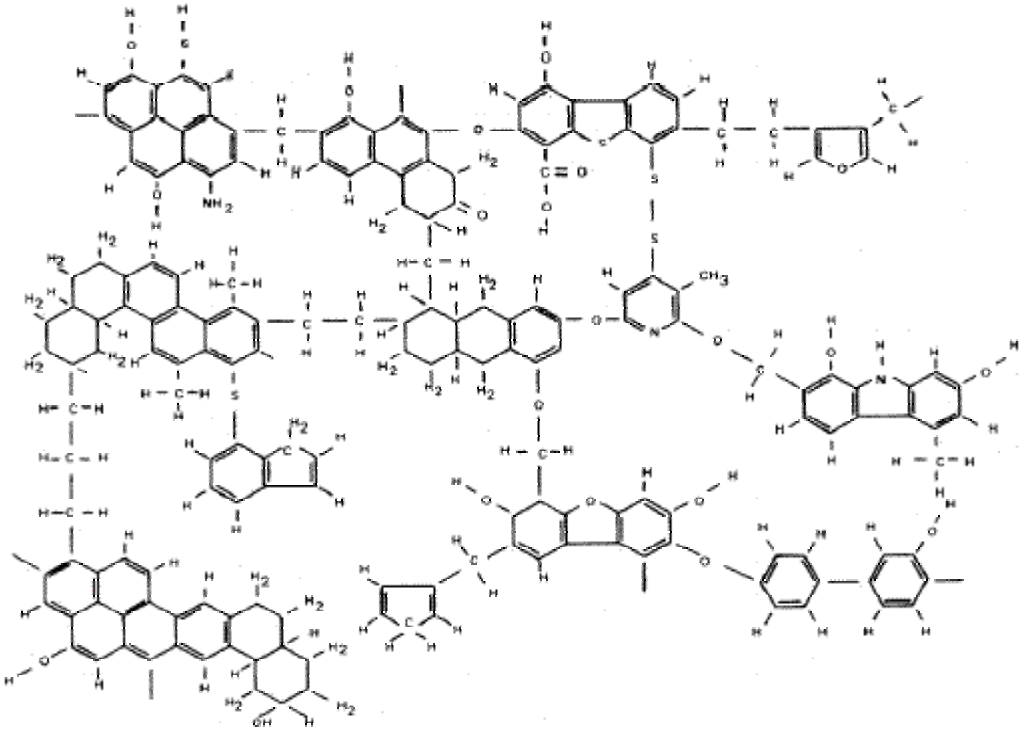

Figure 2-3 – Macromolecular network model of bituminous coals[13]

Some research suggests that coal contains relatively small molecules occluded, or trapped, within a macromolecular network similar to the one in Figure 2-3[14]. This is known as the guest-host model. The guest host model is applicable to some coals, but does not describe some high volatile bituminous coals[15]. Nishioka and Gorbaty judged the guest-host model inadequate for describing Illinois No. 6 high volatile bituminous coal[15]. Nishioka and Gorbaty found no evidence to support to the guest-host model, but did create their own model known as the monophase concept.

The monophase concept postulates that

1) large amounts of neutral small molecules are not tightly occluded inside the coal network and
2) the "mobile phase" consists largely of partial constituent of macromolecules[15].

The reason to favor the monophase model is recent research showing that soluble molecules in coal are solubilized without breaking covalent bonds[16]. This agrees with the hypothesis of coal structure proposed by Stiller in a 1981 patent concerning the solvent extraction of bituminous coals[17].

Section 2.1.3 – Functional Groups of Coal

In addition to carbon, the organic portion of coal contains hydrogen, oxygen, and nitrogen. These are the elements necessary to form the functional groups defined by organic chemistry. Organic chemistry may assist in predicting the behavior of coal in lesser known systems. To determine what functional groups are appended to coal molecules, researchers

use FTIR (Fourier Transform Infrared Analysis), NMR (Nuclear Magnetic Resonance), and XRD (X-ray Diffraction). The relevance of specific functional groups to coal chemistry is summarized below.

R-OH (Hydroxyl)

Hydroxyl groups in coal are interaction sites that solvents use to form hydrogen bonds. Solvent-coal hydrogen bonds are of interest because many solvents are thought to dissolve coal through a process requiring hydrogen bonding. FTIR studies of various coal ranks suggest that as coal rank increases from lignite to bituminous, there is a decrease in oxygen and hydroxyl content[18]. This implies that higher rank coals contain fewer interaction sites with which to form hydrogen bonds with solvents[4].

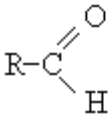

(Aldehyde)

Aldehydes are polar functional groups. The electronegative oxygen pulls the bonding pair of electrons towards itself, creating an electron deficiency at the carbon atom[19]. Treatment of aldehydes with oxidizing agents, such as nitric acide, transforms the aldehydes to carboxylic acids. Coal researchers transform aldehydes to carboxylic acids using oxidizing chemicals such as hydrogen peroxide. Pretreatment of coal with oxidizing agents often results in increased extraction yields.

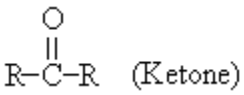

(Ketone)

Ketones are hydrogen bond acceptors, but not hydrogen bond donators. Therefore, ketones can not form hydrogen bonds with themselves. This makes ketones more volatile than alcohols or carboxylic acids of similar molecular weight[19]. A ketone can combine with an electrophile to form resonance stabilized cation.

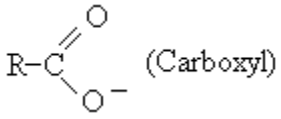

(Carboxyl)

"Carboxyl groups are characteristic constituents of more complex functional groups such as carboxylic acids and amides.[19]"

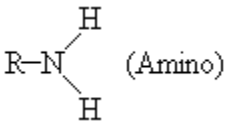

(Amino)

The amino functional group is of interest because the nitrogen can donate its electron pair to the proton of an acid[19]. When the nitrogen donates its electron pair, it becomes positively charged.

R-SH (Sulfhdryl)

In organic chemistry the sulfhdryl group is a functional group composed of a sulfur and a hydrogen. When the sulfhdryl group is connected to a carbon atom, it is known as a thiol, formerly called by the name mercaptan.

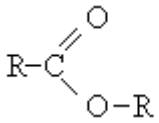

(Ester)

"Esters can participate in hydrogen bonds as hydrogen bond acceptors, but cannot act as hydrogen bond donors, unlike their parent alcohols" and acids.

Examples of the functional groups mentioned can be found in Figure 2-3, the Wiser Model of bituminous coals.

Section 2.2 – Solvent Extraction

Solvent extraction is a mild coal refining technology. Although solvent extraction uses chemicals to dissolve the coal, it's analogous to physical cleaning, as the chemical composition of the coal is preserved.

Section 2.2.1 – Coal Solvents

"In 1951, Oele et al. proposed a system for the classification of coal solvents[20]. Oele et al. grouped solvents used in coal extraction into four general types, which are discussed below.

Group 1) Non-specific solvents – Extract a small amount of coal (up to 10%) at temperatures up to 135°C. These solvents extract the resins and wax residues found in coal. The material extracted with Group 1 solvents is typically aliphatic in nature. Examples of Group 1 solvents include acetone, alcohols, benzene, chloroform, and ethers.

Group 2) Specific solvents – Specific solvents dissolve a larger portion of coal (20 to 40%) than non-specific solvents, and are used at temperatures below 230°C. Specific solvents extract coal by a process of physical dissolution. Dryden showed that effective specific solvents are those that contain a nitrogen atom and an oxygen atom with unshared electrons as a

lone pair[21]. This lone pair of electrons tends to affect the solvent polarity and the coal swelling characteristics of the coal. The nature of the extracted coal is virtually indistinguishable from the original coal.

Group 3) Degrading solvents – Degrading solvents extract the majority of coal (up to 90%) at temperatures up to 425°C. The solvent can be recovered from the solution substantially unaltered. This action is presumed to depend on the mild thermal degradation of coal which produces smaller, more soluble, coal fragments. Anthracene oil and phenanthrene and examples of degrading solvents.

Group 4) Reactive solvents – Reactive solvents extract coal by chemical interaction. The chemical interaction of the solvent promotes degradation during coal extraction. The structure of both the coal and coal solvent change during this process. Examples of reactive solvents include; low temperature alkali hydrolysis of coal by alkaline-alcoholate resulting in partial depolymerization of the coal matrix.[22]"

There is another class of solvents, not considered by Oele, known as super solvents. Super solvents are unique in that they can dissolve of many substances, both polar and non-polar. In 1981 Stiller showed that super solvents are capable of dissolving large amounts of organic material.

Super solvents are a class of dipolar aprotic solvents that are capable of dissolving a large amount of the organic material in coal[17].

"Super Solvents have the general formula.

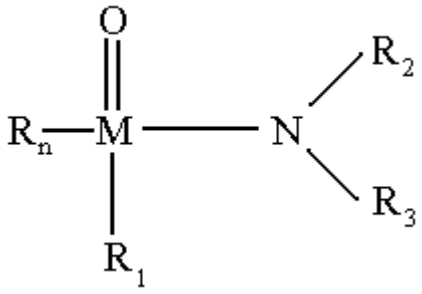

Functional representation of a super solvent

Where:

M is a carbon, sulfur, or phosphorus atom
R2 and R3 are either a hydrogen or lower alkyl group
R1 and Rn are either each a lower alkyl group, another

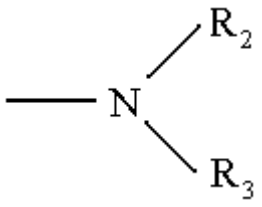

group, a monocyclic group or R1 can be another

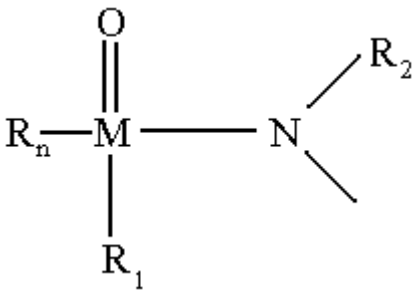

group, or R1 and R3 can represent the atoms necessary to close a heterocyclic ring, and n = 1 where M = Phosphorus and is otherwise 0. Where Rn and R1 are either or both lower akyl groups in this formula akyl can apparently have a carbon content in the range of C1-C4, or possibly C5, of which C1 and C2 are preferable. Preferred substituents for R2 and R3 are methyl and ethyl groups, although it is produced that homologs up to about C4 or possibly higher would produce more or less useful solvent compounds, and the replacement of such groups with one or more hydrogen atoms also appears to be an acceptable alternative. Monocyclic aromatic groups such as benzyl radical might also prove useful as the substituent Rn and R1, because the structure of this group is favorable to the resonance stabilizing function of the solvent. Either or both of Rn and R1 can be another amino group.[17]"

Dimethyl-sulfoxide (DMSO), N-N-dimethyl-acetamide (DMAA), N-methyl-2-pyrrolidone (NMP), hexamethyl phsphoramide (HMPA), and tetra-methyl-urea (TMU) are some commonly used super solvents.

Section 2.2.2 – NMP Extraction

NMP extraction has been the subject of study by the carbon products research group at West Virginia University for over a decade. Like all coal refining technologies, solvent extraction aimed to separate some portion of coal deemed desirable from some portion of coal deemed undesirable. Solvent extraction refers to a process where coal has been refined by dissolution in a solvent, usually at elevated temperatures, followed by filtration or centrifugation. The filtration or centrifugation step separated the soluble carbonaceous portions of coal from the insoluble organic portions of coal. It was hypothesized that coal undergoes no chemical change during solvent extraction; therefore, solvent extraction has been viewed more as a cleaning process than a chemical upgrading process.

Solvent extraction has been used when the inorganic portion of coal would be unacceptably detrimental to a process, or when the increased cost of solvent extraction has reduced the operating cost of the process enough to justify its use. Typically, solvent extraction has been employed when coal cannot be utilized in certain processes due to its inorganic material, or ash. Often this has meant that the inorganic material would adversely affect some piece of equipment, or make some part of a process inoperable. Carbon fuel cells for example, have been poisoned by the inorganic material in coal, and required a fuel that is very low in inorganic content. If coal will be used as an additive to liquid fuels, the inorganic content will need to be minimized. For conventional uses of coal, such as coal combustion for electricity generation, inorganic material has been detrimental. However, solvent extraction has been deemed more expensive than coping with a less pure feedstock.

Solvent extraction, like any coal cleaning technology, operates by exploiting differences between the desirable and undesirable portions of coal. The soluble portions of coal are typically carbonaceous aromatic macromolecules trapped within the 3-dimensional cross linked lattice of coal as illustrated in the Wiser Model of bituminous coals[13]. The insoluble inorganic portion of the coal consists mainly of pyrite, quartz, and clays. These inorganic materials become ash after the coal is combusted, and are the major source of particulate emissions from the combustion of coal. The temperature and pressures at which solvent extraction operates occupies a large range. Some studies have used extraction temperatures as low as room temperature, while others have employed temperatures up to 300°C.

NMP is used as an extraction solvent because it is effective, relatively safe, and widely used in research. NMP is a super solvent. Table 2-4 summarizes the physical and chemical properties of NMP[23].

Table 2-4 – Physical and chemical properties of NMP[23]

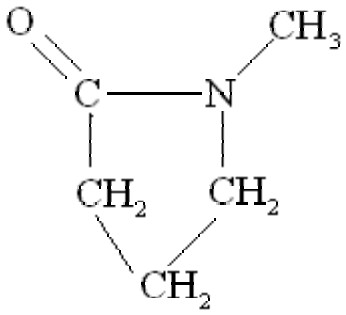

Empirical Formula:	C_5H_9NO
Molecular Weight:	99.13
Physical form:	Liquid with mild amine-like odor.
Color (APHA):	50
Melting Point:	-24ºC (-11.9ºF)
Boiling Point:	202ºC (395ºF) @ 760 mmHg 150ºC (302ºF) @ 162 mmHg 100ºC (212ºF) @ 24 mmHg Tsat = {ln (Psat) + 0.2349} / 0.0156 (Tsat [ºC], Psat [mmHg])
Viscosity (25ºC)	1.65 cp
Specific Gravity:	1.027 @ 25ºC 0.987 @ 75ºC 0.969 @ 100ºC
Specific Heat (Cp):	0.40Kcal/kg at 20ºC CpNMP = 8.04*10^-4 *(T) + .38 (Cp [cal/gm*ºC], T [ºC])
Thermal Conductivity (kNMP):	kNMP = -1*10^-4(T) + 0.1954 (T [ºC], kNMP [W/M/ºC])
Heat of Vaporization	127.3 K cal/kg at 20ºC
Interfacial Surface Tension	(25ºC): 40.7 dynes/cm
Flash Point (open cup):	95ºC (204ºF)
Dipole Moment	4.09+0.04 Debye
Dielectric Constant (25ºC):	32.2
Solubility parameter (δ):	11.0
Miscibility with Other Solvents:	completely miscible with water and most organic solvents including alcohols, esters, ketones, aromatic and chlorinated hydrocarbons and vegetable oil.

Section 2.2.3 – Models of Coal Dissolution via NMP

As discussed previously, models have treated coal as a large 3-dimensional macromolecular network, with extractable carbonaceous substances occluded in the pores in between the macromolecular network[14]. Research by Takanohasi differed in that it concluded coal was a large aggregate, and Takaanohashi proposed different mechanisms for describing coal dissolution[14]. Takanohashi's research suggested that coal is solubilized without breaking covalent bonds[16].

The most common model of solvent extraction treated extraction in terms of the electron donor and acceptor interactions in the solvent coal system[24]. This model assumed that donor-acceptor bonds in coal were responsible for binding together the macromolecular network and the extractable carbonaceous materials that filled the pores of the network[24]. According to this model, "Extraction is in principle, a substitution reaction: pore substances are replaced by a solvent molecule in their $Donor_{network} \rightarrow Acceptor_{pore\ substance}$ or $Donor_{pore\ substance} \rightarrow Acceptor_{network}$ bonds that bind together structural elements of an original coal.[24]"

Section 2.3 – Solvent Swelling of Coal

Solvent swelling of coal occurs when the physical dimensions of coal increase due to the presence of a solvent. Researchers have studied coal swelling to elucidate coal structure. Additionally, researchers have correlated or related coal swelling with other coal properties; such as coal extraction yield or coal surface area. The hypothesis of why coal swells in a solvent is adapted from polymer research. For this reason, coal swelling studies have tended

to be more interdisciplinary than other coal studies. This has led to a wealth of coal swelling studies, the main points of which appear in summary below.

The amount of coal swelling was measured by the swelling ratio, represented by the symbol Q. The swelling ratio was defined as the volume of the swollen coal divided by the volume of the original coal. Coal began to swell as it imbibed a solvent for which it has an affinity. As the coal absorbed solvent, it grew in size, while maintaining its original shape. When the solvent was removed the coal shrank to near its original size and shape. Some destruction of coal samples occurred after swelling and shrinking, but this destruction seemed due to mechanical stresses rather than chemical changes[25]. It is important that coal retained its original shape after swelling and shrinking, because coal swelling models assumed that swelling was a reversible process[26]. Solvents for which coal has a high affinity are referred to as "good swelling solvents." Swelling in good swelling solvents was found to be independent of the solvent to coal weight ratio and grinding direction[11,27]. In good swelling solvents such as NMP and pyridine, coal was capable of swelling to over twice of its original volume, while still retaining its original shape[14].

Good extraction solvents were usually good swelling solvents. A solvent is referred to as a "good extraction solvent" if it was effective at dissolving coal. Good extraction solvents included n-methyl pyrollidone (NMP) and carbondisulfide (CS_2) and therefore were expected to be good swelling solvents[28]. The ability of a solvent to swell coal was a strong function of the electron donating ability of the solvents[14]. Painter and Shenoy proposed that the swelling

of coal took place by a process of chain disinterspersion[29]. It was postulated that the covalent bonds in the coal matrix acted as chains that were stretched by solvents. In this model, the solvent dissociated the non-covalent cross-links of the coal matrix, which resulted in a swollen coal sample.

Because of the anisotropic nature of coal, coal swelled preferentially in a direction perpendicular to the bedding plane of the coal seam[27]. This directional swelling was observed because coal appears to have been more highly cross-linked in the bedding plane than perpendicular to it[27]. This directional swelling of coal was not noted in most studies because traditionally only bulk swelling has been measured, not the swelling of individually oriented coal pieces. Measuring the swelling ratio of individual coal pieces yielded clues to the structure of coal not provided by the study of the bulk swelling behavior of coal. "The perpendicular/parallel swelling ratios are highest in pyridine and lowest in chlorobenzene, indicating a highly anisotropic arrangement of covalent bonds.[27]" Also, the time to reach maximum swell parallel to the bedding plane is shorter than the time to reach maximum swell perpendicular to the bedding plane[27]. Cody et al also discovered that swelling measured as a function of time passed through a maximum due to the formation of a metastable state[27].

Other clues about the structure of coal were obtained by studying the swelling of different ranks of coal in various solvents. Observing the swelling ratios of different ranks in different solvents has provided information about the structural changes across varying ranks. Rincon et al found that swelling ratios were higher for lower ranked coals[30]. Rincon also

found that swelling could be used to improve THF (tetrahydrofuran) soluble materials after liquefaction with H-donor solvents[30]. The trend of increased THF soluble materials correlated with coals of increased swelling ratios[30]. Rincon et al postulated that that liquefaction of coal by H-donor solvents is a surface area dependent reaction, and that preswelling the coal was a good method for producing greater penetration and diffusion of reactants, increasing the liquefaction yield[30].

How quickly coal swells is controlled by how quickly the solvent diffuses into the coal. This is controlled by solvent properties, the size of the coal particles, and the average molecular weight between the crosslinks of the coal matrix[12]. The diffusion of solvent into coal is modeled by either Fickian diffusion or anomalous transport[12]. Coal is a glassy solid at room temperature, but transitions to a flexible state as it absorbs solvent. The flexible nature of the swollen coal suggested lower effective crosslink density, and suggested that the elasticity of the solvent swollen coal may be predominantly rubber-like[26]. The transition from the glassy to rubbery state is generally very sharp[12].

When discussing how swelling affects dissolution, if at all, it was helpful to break coal constituents into soluble and non-soluble materials. Current models for coal dissolution postulate that the soluble portions of coal occupy the pore space of coal and extraction more or less leaves the existing macro molecular network intact[14]. An aggregated structure of coal would imply a model where the coal structure is irrefragably lost upon dissolution.

Chapter 3 – Experimental Plan

By examining process parameters and coal properties, and their effect on the extraction and swelling of bituminous coal, it was possible to develop a correlation describing the solvent extraction and solvent swelling of high-volatile bituminous coal in the super solvent n-methyl-pyrrolidone. It was hypothesized that the developed correlation is general enough to apply to various bituminous coals in super solvent systems.

Section 3.1 – Experimental Matrix

The experimental matrix was a summary of experiments that were performed during the research. The experimental matrix dictated the values of the independent variables during a particular experiment. These variables were manipulated to determine their effect on solvent extraction and solvent swell. The independent variables studied in the experimental matrix were:

1) System temperature
2) Time at temperature
3) Coal size

The system temperature was varied because it may have determined how quickly solvent extraction proceeded. There temperatures of interest ranged from 50°C to 200°C. The time at temperature was varied because it may have determined how far solvent extraction proceeded and to what extent the coal swelled. The times of interest ranged from 2 minutes to 270 minutes. The coal size was varied because it may have determined the rate of solvent extraction and coal swell, and or the extent of solvent extraction and coal swell. There were

three coal sizes of interest, which ranged from a large size of 40 Tyler Mesh (355 μm) to a small size of sub 150 Tyler Mesh (less than 106 μm). These variables and their ranges are illustrated graphically in the experimental matrix, which appears below as Figure 3-1.

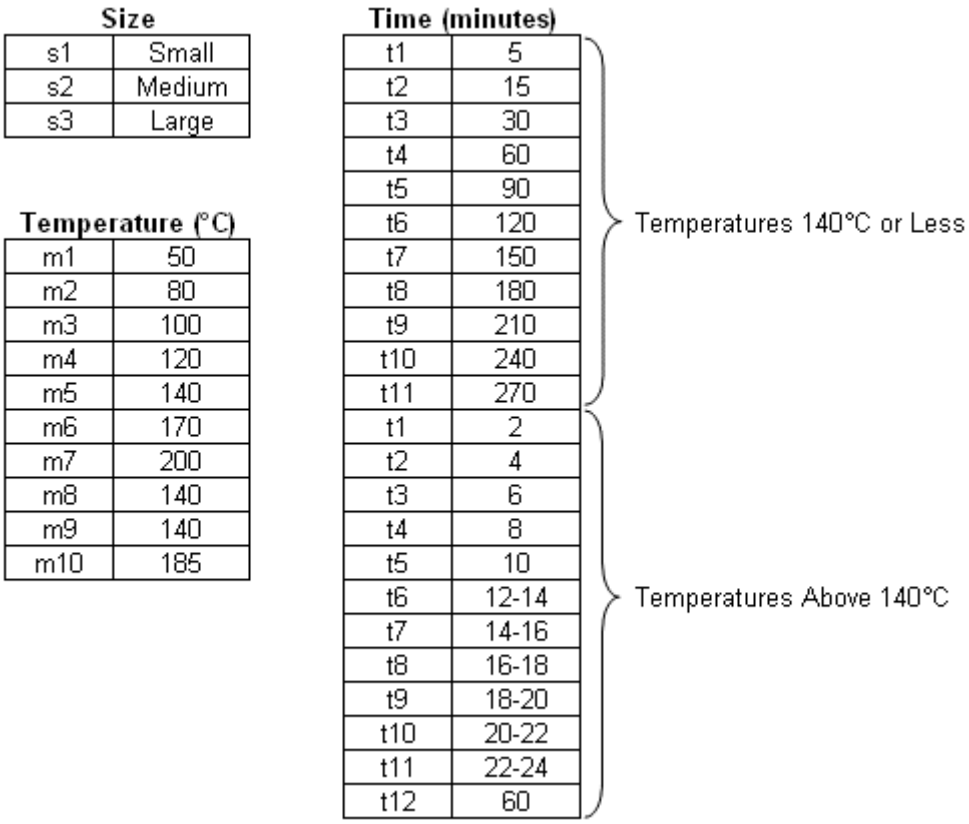

Size	
s1	Small
s2	Medium
s3	Large

Temperature (°C)	
m1	50
m2	80
m3	100
m4	120
m5	140
m6	170
m7	200
m8	140
m9	140
m10	185

Time (minutes)		
t1	5	Temperatures 140°C or Less
t2	15	
t3	30	
t4	60	
t5	90	
t6	120	
t7	150	
t8	180	
t9	210	
t10	240	
t11	270	
t1	2	Temperatures Above 140°C
t2	4	
t3	6	
t4	8	
t5	10	
t6	12-14	
t7	14-16	
t8	16-18	
t9	18-20	
t10	20-22	
t11	22-24	
t12	60	

Figure 3-1 – Experimental matrix

Section 3.2 – Analytical Procedure for Quantifying Coal Swell

Coal swelled when imbibing a solvent. The amount a coal swelled, known as the swelling ratio, was the volume of the swollen coal divided by the volume of the original coal, minus one. The swelling ratio, Q, appears below as Equation 3-1.

$$Q = \frac{h_f}{h_i} - 1 \qquad \textbf{(3-1)}$$

Section 3.3 – Analytical Procedure for Quantifying Coal Solubility

Following solvent extraction, it was necessary to determine how much coal was dissolved in solution. The amount of coal dissolved in the coal-NMP solution was directly proportional to the absorbance of the coal-NMP solution. The absorbance of the coal-NMP solution was measured using a UV-Vis spectrophotometer. Beer's Law was used to calculate the amount of coal in solution. Beer's Law appears below.

$$A = \varepsilon bc \qquad \textbf{(3-2)}$$

In Equation 3-2, A represents the absorbance of the solution, ε is the molar absorbtivity, b is the path length, and c is the concentration. A solution exposed to UV-VIS spectroscopy should have been absorbent enough to absorb some light, but not so absorbent that too little light was transmitted. Without the proper absorbance, useful data would not have been obtained. The absorbance equals the logarithm of the ratio of the power of the light source before and after passing through the solution. The equation used to calculate absorbance appears below.

$$A = \log \frac{P_0}{P} \qquad \textbf{(3-3)}$$

P_0 and P are, respectively, the power of a beam of monochromatic radiation before and after passing through the solution. Another variable in Beer's Law is the path length, represented as term b. The path length is the length of solution that the UV-Vis monochromatic beam must pass through. Figure 3-2 is a graphical illustration of these properties.

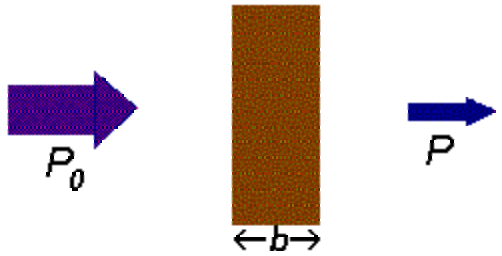

Figure 3-2 – Radiation passing through solution of path length b

Beer's Law (Equation $A = \varepsilon bc$ **(3-2)**) was a non-linear relationship at higher concentrations. For this reason, it was necessary to keep the absorbance of the coal-NMP solutions at or below three. There are two controllable parameters that determined solution absorbency. The first parameter was the path length of the cell that holds the coal-NMP solution. If cell A is ten times the width of cell B, the solution in cell A appeared to have one tenth of the transmittance ($T = P / P_0$) of the solution in cell B. The second adjustable parameter was the dilution of the solution. A relatively dilute solution absorbed less (had a higher transmittance) than a relatively concentrated solution.

It was necessary to know the molar absorbtivity of the coal NMP-solution before the concentration of the coal-NMP solution could be calculated. The molar absorbtivity, a

measure of the amount of light absorbed per unit concentration, was calculated as follows. A Soxhlet Extraction was performed on all coal samples, small, medium, and large. Soxhlet extraction was performed for 24 hours at reflux under vacuum, to ensure complete extraction. The product was then filtered and vacuum dried at ambient temperature. The product and residue weights were added and mass closure was achieved. A known amount of extract was dissolved in a known amount of NMP. The extract dissolved fully in the NMP, and was then diluted 100:1. The absorbance was measured and plotted as a function of concentration. A linear regression was performed and the slope is the product of the molar absorbtivity and the path length.

Section 3.4 – Analytical Procedure for Quantifying Coal Porosity

Porisimetry included the measurement of pore size, pore volume, pore size distribution, density, and other porosity related characteristics. The adsorption, permeability, strength, and density of a material are often influenced by its pore structure. The porosity of the Lower Powellton coal used in this research was characterized via mercury porisimetry. "Mercury porisimetry is based on the capillary law governing liquid penetration into small pores. This law, in the case of a non-wetting liquid like mercury, is expressed by the Washburn equation:

$$D = \left(\frac{1}{P}\right) 4\gamma \cos\phi \qquad \textbf{(3-4)}$$

Where D is the pore diameter, P is the applied pressure, γ the surface tension of the mercury, and ϕ the contact angle between the mercury and the sample, all in consistent units. The volume of mercury V penetrating the pores was measured directly as a function of applied pressure. This P-V information served as a unique characterization of pore structure.[31]" Mercury porisimetry was capable of observing pore sizes over five orders of magnitude, from 0.003μm to 360 μm.

Chapter 4 – Experimental Procedure

The experimental procedure consisted of the methods necessary to perform extraction of coal with NMP, measure coal swell, quantify coal solubility, and analyze coal porosity. Each of these four tasks is described separately in the following sections.

Section 4.1 – Experimental Procedure for Performing Solvent Extraction

Solvent extraction experiments were run in batches. Each batch was performed at a temperature of interest. For example, the first batch was run at 50°C, and contained samples of small coal in NMP. In this particular batch, there were eleven samples, one sample for each of the eleven times of interest as illustrated in the experimental matrix, Figure 3-1. Experimental batches at temperatures above 140°C had twelve time levels, as illustrated in Figure 3-1. All extraction runs were performed individually in a set of 10ml graduated test tubes.

To begin an experimental batch, each empty test tube was numbered and weighed to one milligram accuracy. The test tube was then filled with 1ml of Lower Powellton coal of the appropriate size, and again weighed to the nearest milligram. The graduated test tube was then filled to the 6 ml graduated mark with NMP, and again weighed to the nearest milligram. After the above procedure was complete for all samples in an experimental batch, the set of test tubes were placed in a test tube rack, and lowered into a fluidized sand bath preheated to the batch temperature.

Once a time of interest was reached, a test tube was removed from the sand bath and allowed to air cool. Test tubes were continually removed at the experimental times until no more test tubes remained. Once the test tubes were removed and cooled the solvent extraction was complete. With solvent extraction completed, the next tasks were to quantify the amount that coal swelled during extraction, and to quantify the amount of coal dissolved in NMP.

Section 4.2 – Experimental Procedure for Measuring Coal Swell

After the test tubes described in the previous section were air-cooled, the extraction runs were complete. At this time the test tubes were centrifuged. The graduation mark to which the coal had swollen was noted. The swelling ratio was calculated as the ratio of the post-extraction volume of the coal divided by the pre-extraction volume of the coal, minus one, in accordance with Equation 3-1. For example, if the coal had expanded to the 2.5 ml mark (from the original 1.0 ml mark), that would have indicated a swelling ratio of 150%. After all the swelling ratios in a particular experimental batch were measured, the next step was to quantify coal solubility.

Section 4.3 – Experimental Procedure for Measuring Coal Solubility

After the swelling ratio was recorded, one or two milliliters (depending on solution darkness) of the coal-NMP solution were withdrawn from the test tube via a graduated pipette. The one or two milliliters of the coal-NMP solution were placed in a 100 ml Enerylmeyer Flask. NMP was added to the flask until the 100 milliliter mark was reached. This resulted in

either a 50:1 or 100:1 dilution of the coal-NMP solution. A portion of the diluted solution was placed in a small polyethylene bottle, and stored in a refrigerated room until ready for analysis.

Coal solubility was quantified by analyzing the absorbance of the coal-NMP solution, as described in Section 3.3 – *Analytical Procedure for Quantifying Coal Solubility*. The absorbance of the coal-NMP solution was measured in a UV-Vis spectrophotometer.

Adjustment of both of the coal-NMP solution darkness and cell path length were necessary to obtain solutions with the proper absorbance. A cell width (path length) of 0.1 mm was required, which is small compared to most cells. Dilution of the coal-NMP solution was necessary as well. Some coal-NMP samples were diluted by a factor of 50, while most were diluted by a factor of 100. The dilution factor was chosen depending on the darkness of the coal-NMP solution. Light solutions had a dilution factor of 50:1, while average and dark solutions had a dilution factor of 100:1. These dilution factors placed absorbance readings in an acceptable range.

Section 4.4 – Experimental Procedure for Measuring Coal Porosity

Porosity measurements were made to determine if they could be related to coal extraction and coal swelling. Porosity measurements were made via an AutoPore 9220 Mercury Porisimeter. The mercury porisimeter analyzed samples in a sample holder known as a penetrometer. The penetrometer is cleaned and weighed to the nearest milligram. A small amount of coal, approximately 2 grams, was placed in the penetrometer. The

penetrometer was weighed again to the nearest milligram, and the difference was the sample weight. The penetrometer was placed in the mercury porisimeter for analysis. The mercury porisimeter contained its own dedicated vacuum pump, and the sample penetrometer was evacuated to a pressure of 10 μm Hg, well below the vapor pressure of water at room temperature. Once the evacuation pressure was reached, the porisimeter evacuated the sample for an additional hour to ensure a dry sample. Then the poriosimeter filled the penetrometer with mercury under a pressure 0.5 psia and the analysis began. The mercury pressure slowly increased and the intrusion of mercury was measured at various pressures. When the mercury pressure reached 30 psi, the low pressure analysis was complete. The penetrometer, filled with mercury, was removed from the low pressure ports and again weighed to the nearest milligram. From this information the density of the coal sample was calculated. Then the penetrometer was placed in the high-pressure test station of the mercury porisimeter, which varied the mercury pressure from 30 psia to 60,000 psia. After the pressure increased to 60,000 psia, the sample was slowly depressurized from 60,000 psia to atmospheric pressure. Whereas the increasing pressure was used to measure mercury intrustion, the decreasing pressure was used to measure mercury extrusion. The amount of mercury extruded relative to the amount intruded quantified the amount of "ink bottle" type porosity.

Chapter 5 – Experimental Results

Section 5.1 – Porosity

As detailed in Section 3.4 – *Analytical Procedure for Quantifying Coal Porosity*, mercury porisimetry was used to determine the porosity characteristics of coal. To ensure accurate data, there was one sample and three replicates ran for each coal size, a total of four analyses. The data for the four small coal samples follows as Figure 5-1.

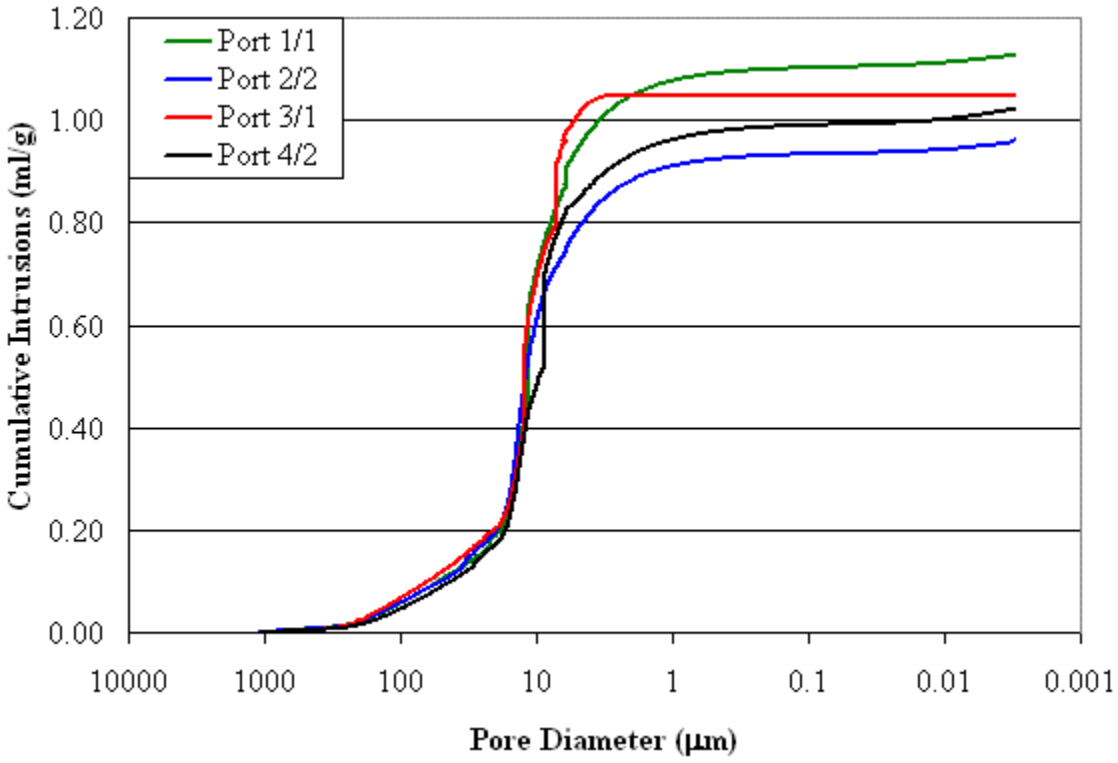

Figure 5-1 – Porosity of small (sub 106 µm) coal

The cumulative intrusion as measured by the mercury porisimeter, in units of ml of mercury per gram of coal sample, is represented by the y-axis. The pore diameter of the coal sample, which was proportional to the mercury over-pressure exerted on the sample by the

porisimeter, is represented by the x-axis. The mercury porisimeter contained four low-pressure analysis ports and two high-pressure analysis ports. The low-pressure and high-pressure ports which the samples were analyzed in are represented by the key in the upper left hand of Figure 5-1. Mercury porisimetry results suggested that most of the porosity in small coal occurred between approximately 80 µm and 20 µm.

Medium sized coal and large sized coal was also analyzed via mercury porisimetry, and the results are represented as Figure 5-2, and Figure 5-3, respectively.

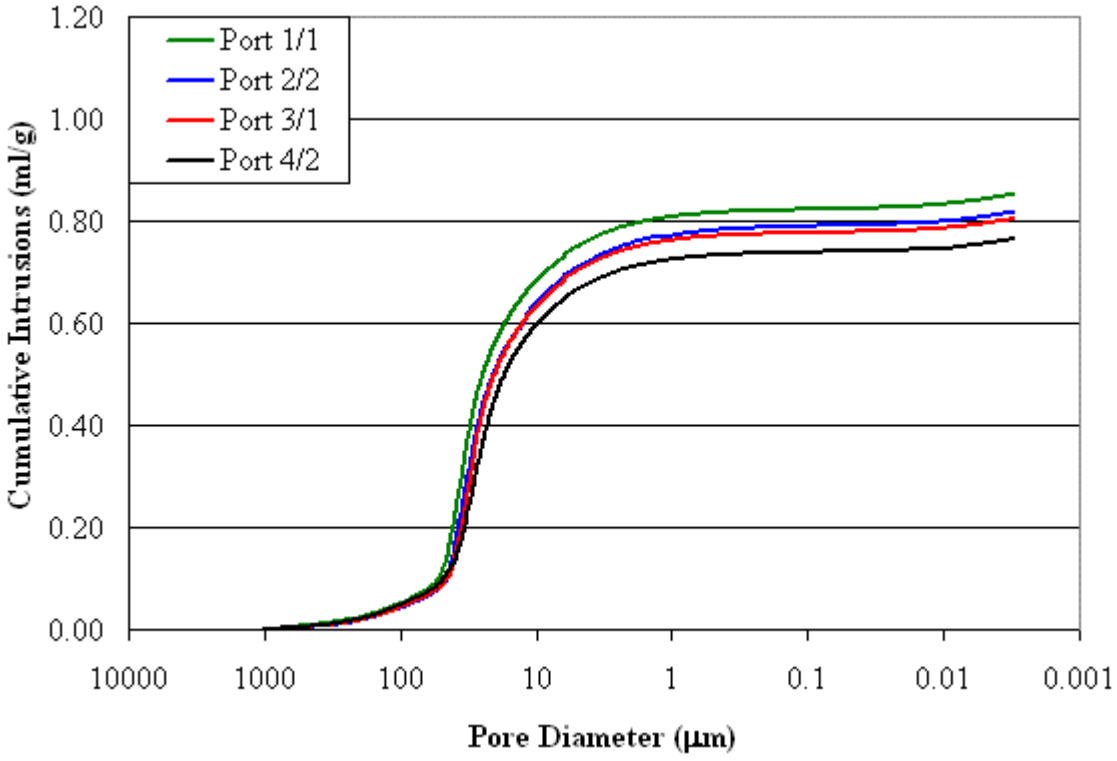

Figure 5-2 – Porosity of medium (106 to 212 µm) coal

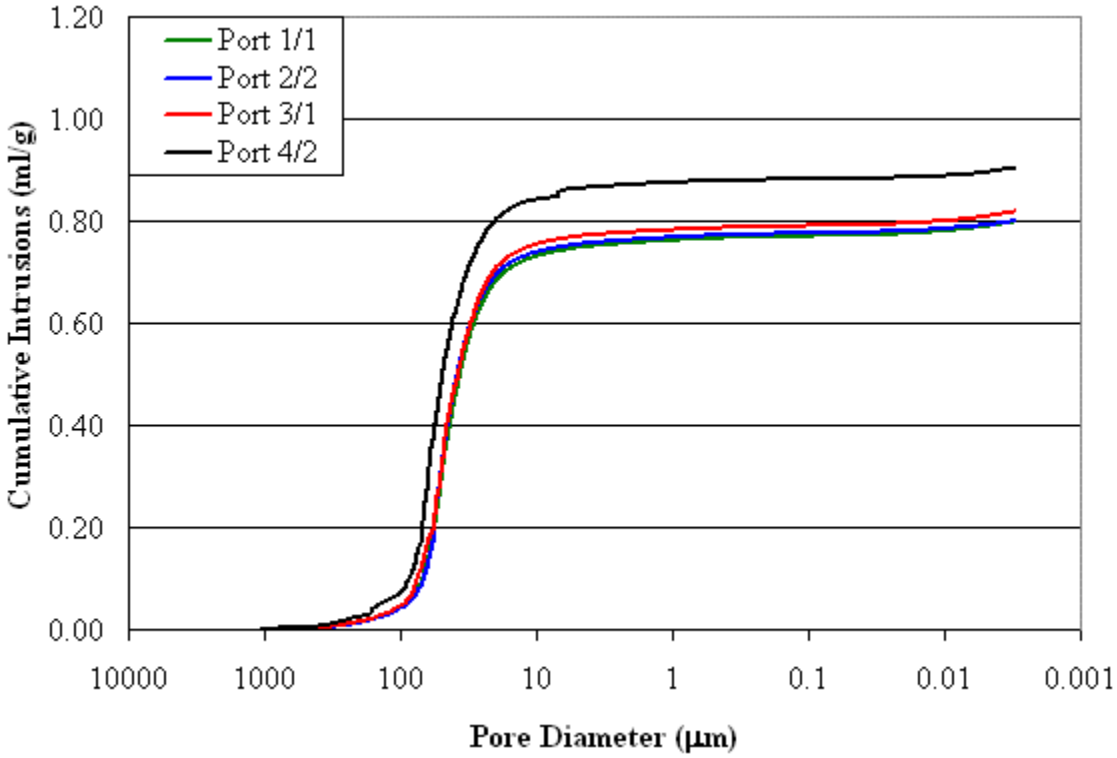

Figure 5-3 – Porosity of large (212 to 355 µm) coal

As with the small coal, porisimetry results suggested that most porosity in medium and large coal occurred between 80 µm and 20 µm. However, medium and large coals exhibited less total porosity than small coals. The discrepancy in coal porosity across the different coal sizes could be explained in two ways. The medium and large coal may have contained closed pores which were not opened until the coal was more finely ground. Additionally, the small coal may have had a different composition than the large and medium coals. Due to differences in the friability of coal macerals, grinding may have caused more porous macerals to be concentrated in the smaller coal sizes. This research suggested no difference in composition between the coal sizes – extraction yields were the same across all three sizes of coal. Furthermore, as will be discussed later, UV-Vis spectroscopy suggested no

difference in composition across extracts from various coal sizes. A graph illustrating the porosity differences between the three different coal sizes is presented below as Figure 5-4.

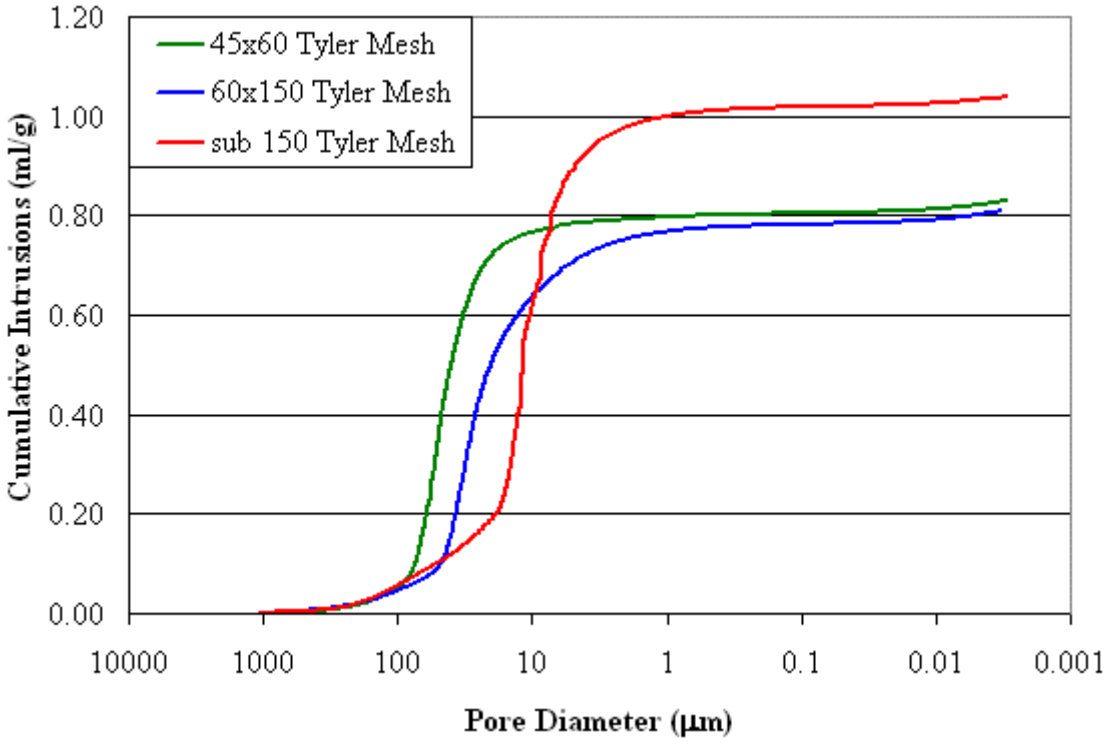

Figure 5-4 – Pore distribution of the three coal sizes

Section 5.2 – Swelling

The amount of coal swell was measured for every solvent extraction run. The swelling ratio appeared to be a function of the extraction temperature, extraction time, and coal size. Coal swelled much more quickly for the higher temperature extractions (140°C to 200°C) than for the lower temperature extractions (50°C to 120°C). For this reason, there are two graphs for each coal size, one for lower extraction temperatures (longer time scales) and one for higher extraction temperatures (shorter time scales). The swelling ratio of small coals at lower extraction temperatures is presented below as Figure 5-5.

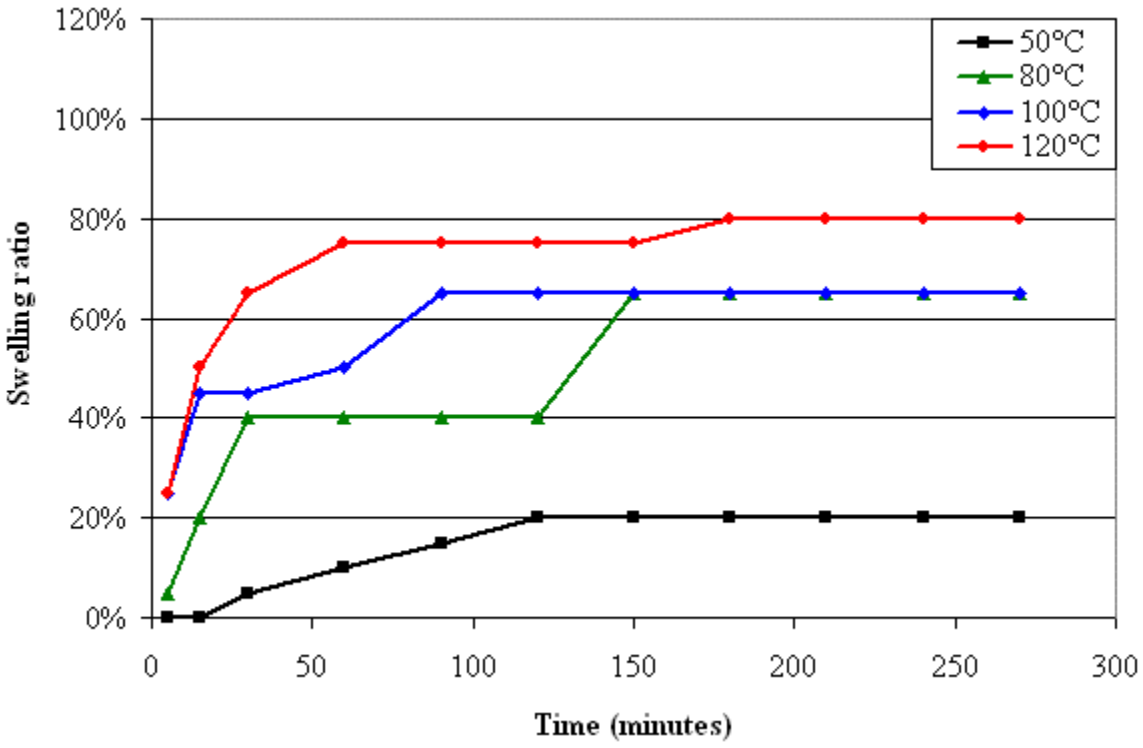

Figure 5-5 – Swell of small coal (sub 106 μm) at low temperatures

Figure 5-5 suggested that appreciable coal swelling occurred at temperatures of 80°C and higher. It was observed that coal swelling increased with increasing extraction time. It was also observed that for lower temperatures, coal swell increased with increasing temperature. This contrasted with the swell of small coal during high temperature extraction runs, which is presented below as Figure 5-6.

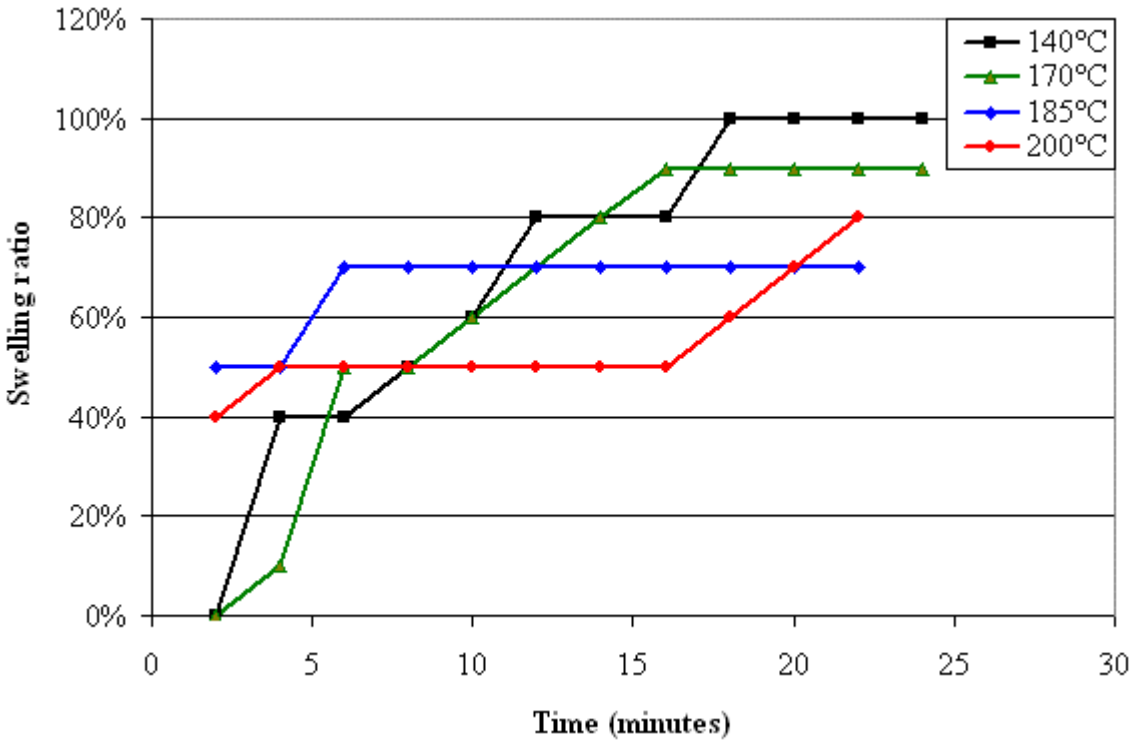

Figure 5-6 – Swell of small coal (sub 106 μm) at high temperatures

Coal swelling passed through a maximum somewhere between 120°C and 140°C. Above 140°C, the coal swelling ratio began to decline with increased temperature. This may be due to dissolution, at higher temperatures more extractable material is removed from the coal matrix. The dissolution of extractable material from the coal matrix may have

counteracted swelling. The next graph, Figure 5-7, illustrated the swelling of medium sized coal as a function of time, at different temperatures.

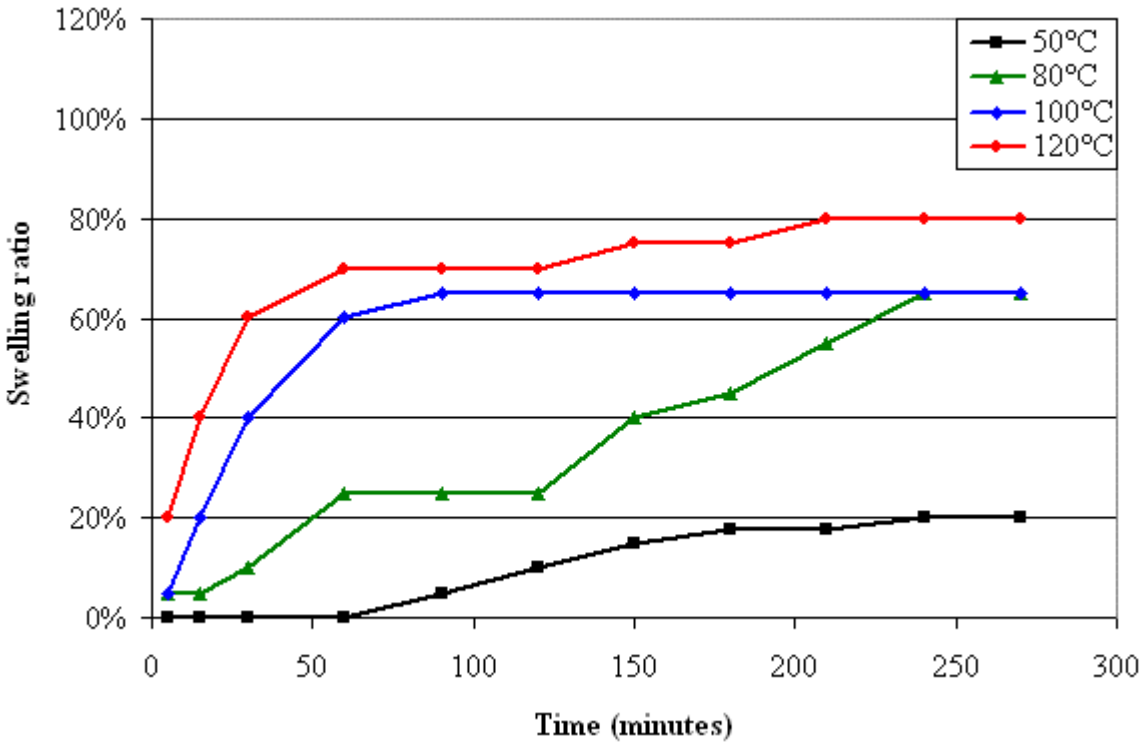

Figure 5-7 – Swell of medium coal (106 - 212 μm) at low temperatures

As with the smaller coal samples discussed earlier, the swelling ratio increased with increasing temperature. Swelling also occurred more quickly for higher temperatures. The swelling ratio of the medium sized coal during high temperature extraction runs is represented by the next graph, Figure 5-8.

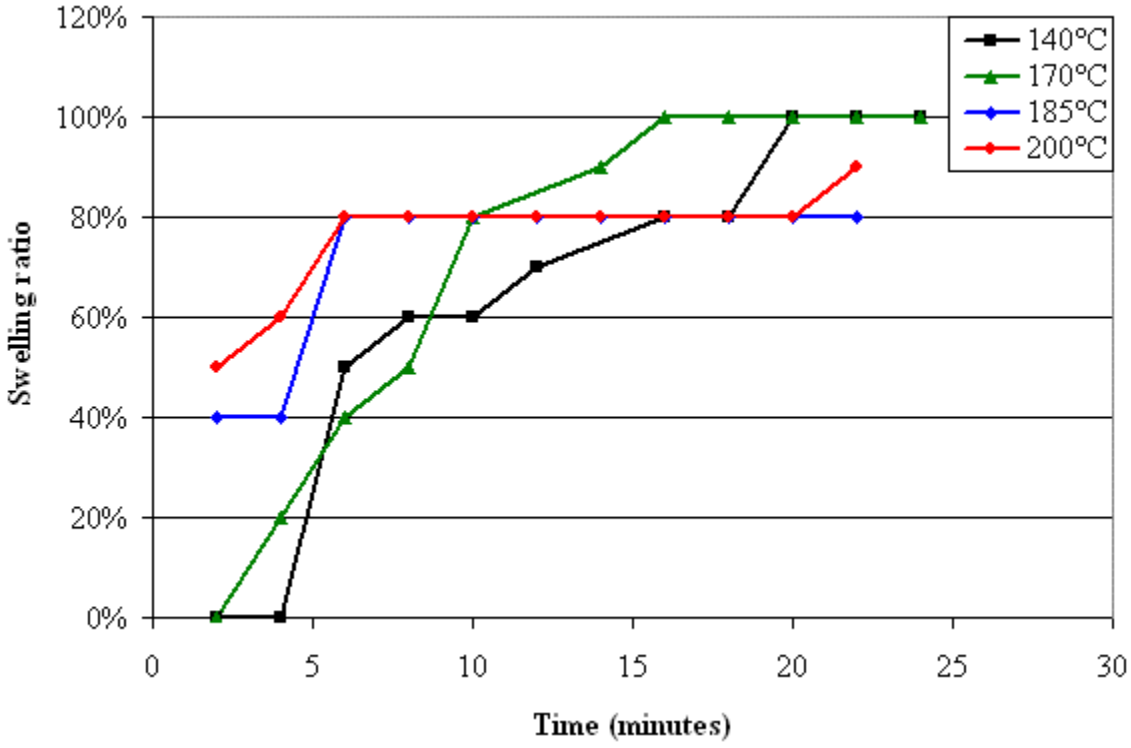

Figure 5-8 – Swell of medium coal (106 - 212 µm) at high temperatures

Similar to the swelling of small coal discussed earlier, the swelling ratio reached a maximum somewhere between 120°C and 140°C. Again, the swelling ratio decreased with increasing temperature. As before, swelling occurred more quickly at higher temperatures, but ultimately lower temperatures swelled more. The amount of swell observed during the low temperature extraction of large coal is presented below as Figure 5-9.

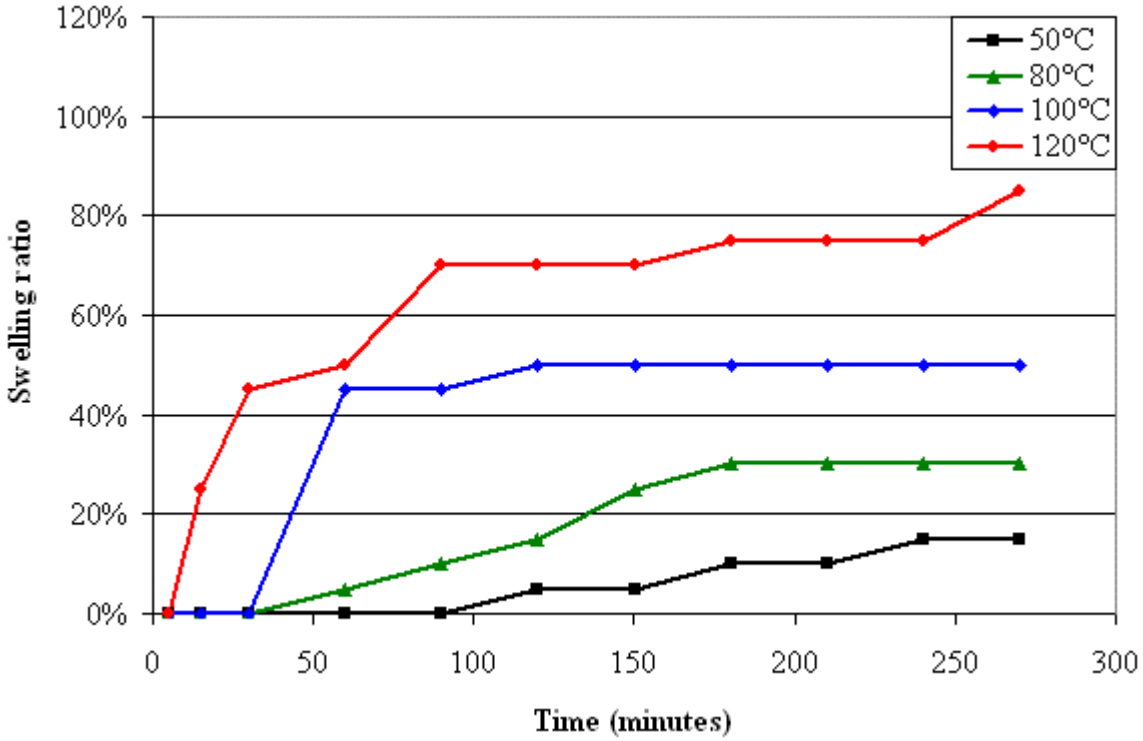

Figure 5-9 – Swell of large coal (212 - 355 μm) at low temperatures

The swell of large coal at lower temperatures resembled the swell of small and medium coals at lower temperatures. The unique aspect of the swelling of large coal is the observed lag time between when extraction starts and when the coal began to swell. This suggested that swelling is a diffusion controlled process. As with medium and small coals, the swelling ratio increased with increased temperature. The swelling of large coals during high temperature extraction runs is presented below as Figure 5-10.

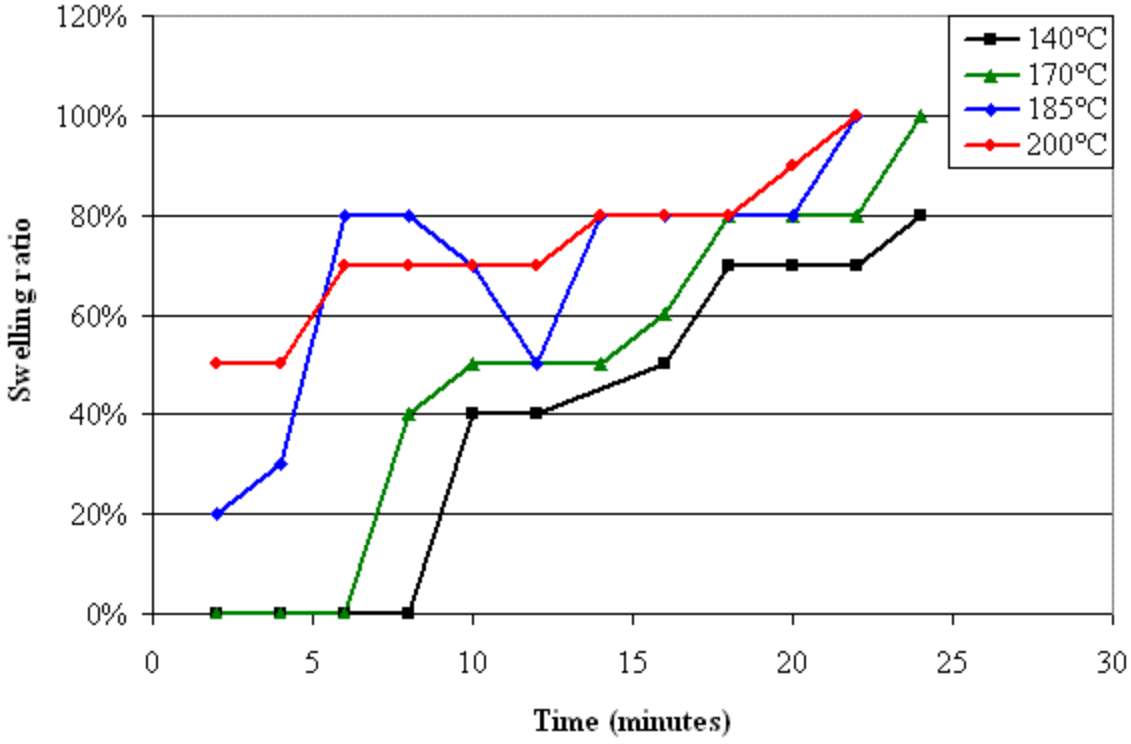

Figure 5-10 – Swell of large coal (212 - 355 μm) at high temperatures

The swelling ratios for large coal at high temperatures differed from the swelling ratios for small and medium coals at high temperatures. Unlike small and medium coals, the large coal swelling ratio continued to increase with increasing temperature. This result was somewhat anomalous, as the maximum swelling (about 100% swell) and extraction yield at higher temperatures were similar across all three coal sizes. The result may have been due to a time scale that was too short to collect sufficient swelling data.

Section 5.3 – Coal Solubility

Before coal solubility measurements began, it was questioned whether the extracted material was the same across all samples. There were three coal sizes and eight temperatures of interest, so it was possible that different material could be extracted from different coal samples. If different materials were extracted from different samples, it would have implied a different molar absorbtivity for each sample or set of samples, which would have made absorbance comparisons across samples difficult. This issue was resolved by noting the wavelength at which maximum absorbance occurred during UV-Vis analysis. Because the wavelength at which maximum absorbance occurred was the same for all samples, it was determined that the same material was being extracted from all coals and concentration comparisons were valid.

Coal solubility was measured using a UV-Vis spectrophotometer, as described in Section 3.3 – *Analytical Procedure for Quantifying Coal Solubility*. The concentration (grams of coal dissolved per liter of NMP) of coal in NMP for the low temperature (50°C to 120°C) extraction of small coal is presented below as Figure 5-11. Notice that the time scale ran from five minutes to four and a half hours. This data suggested that the extraction reached a maximum quickly, and that the temperature determined how much coal was dissolved. Relatively small extraction differences occurred across the temperature range.

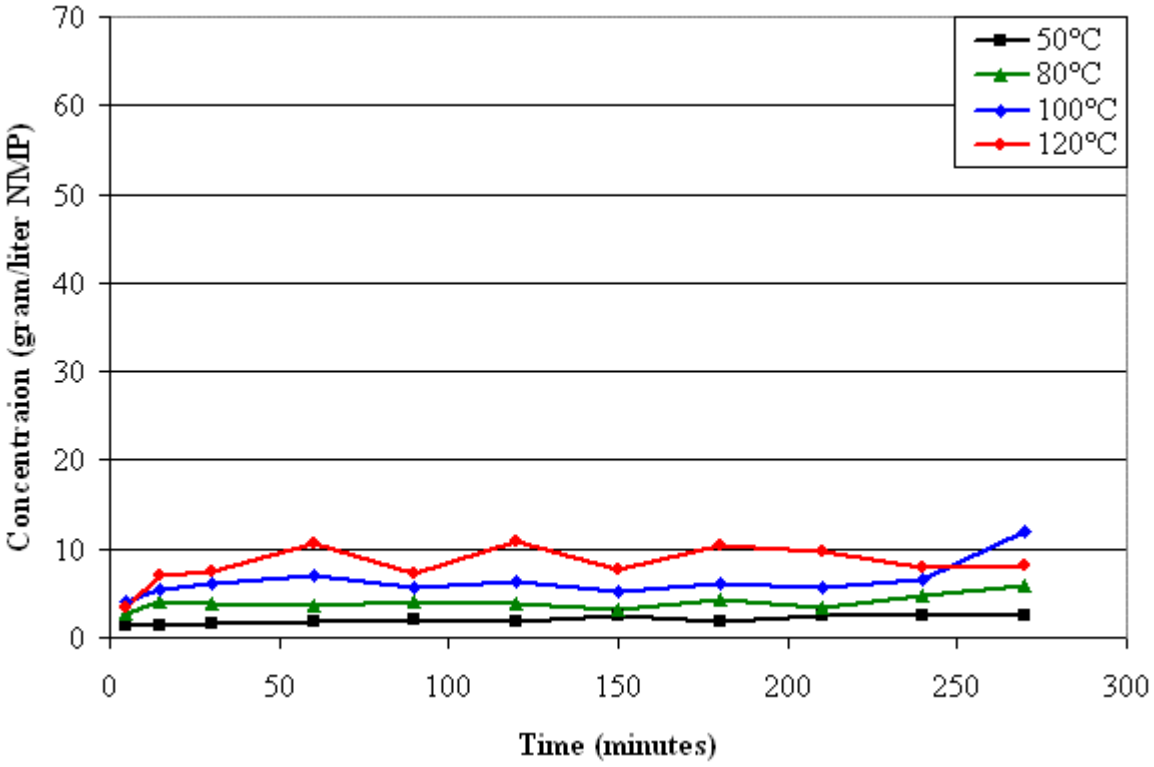

Figure 5-11 – Small coal (sub 106 μm) in NMP at low temperatures

The next set of experimental conditions focused on higher temperature extraction runs, from 140°C to 200°C. During the higher temperature runs, extraction was negligible, until the temperature reached approximately 185°C. At 185°C, a spike in concentration appeared. Extraction yield data for the higher temperature runs appears below as Figure 5-12.

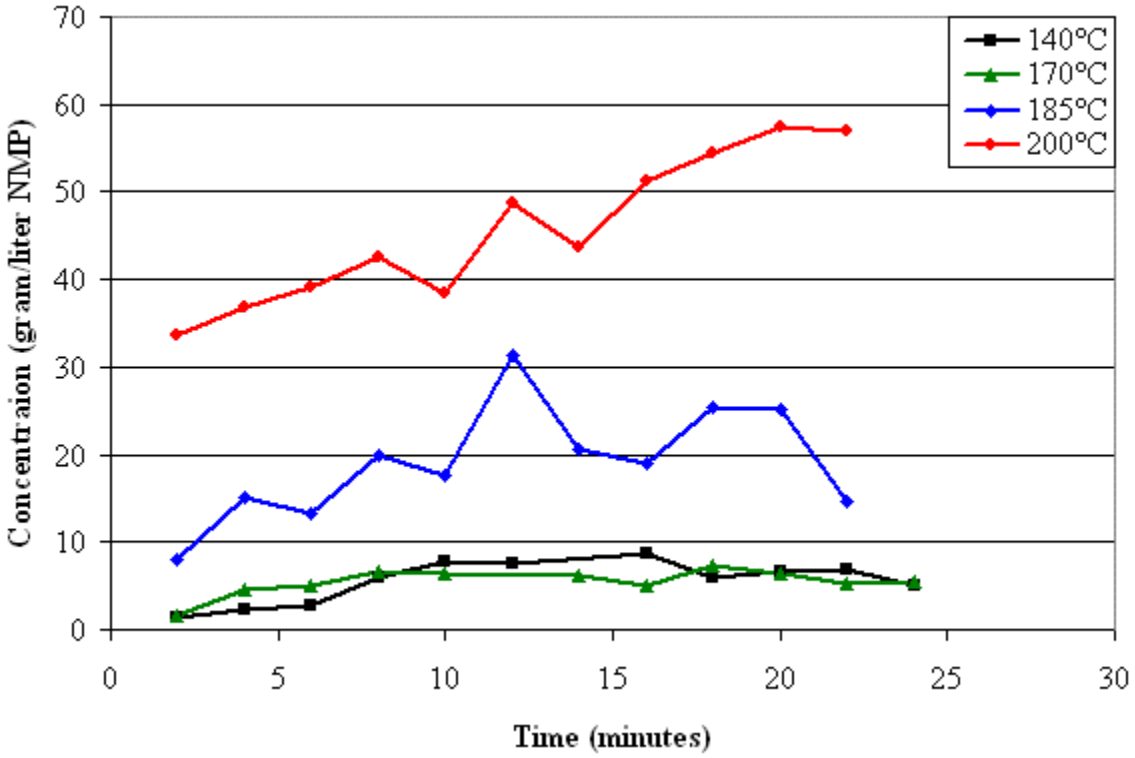

Figure 5-12 – Small coal (sub 106 μm) in NMP at high temperatures

Little extraction occurred before 170°C, significant extraction occurred at 185°C, and maximum extraction occurred at 200°C. This contrasted with swelling – appreciable swelling occurred at all temperatures. This data suggested that swelling and extraction may be independent processes. Extraction yield data for the lower temperature extractions of medium sized coal is presented below as Figure 5-13.

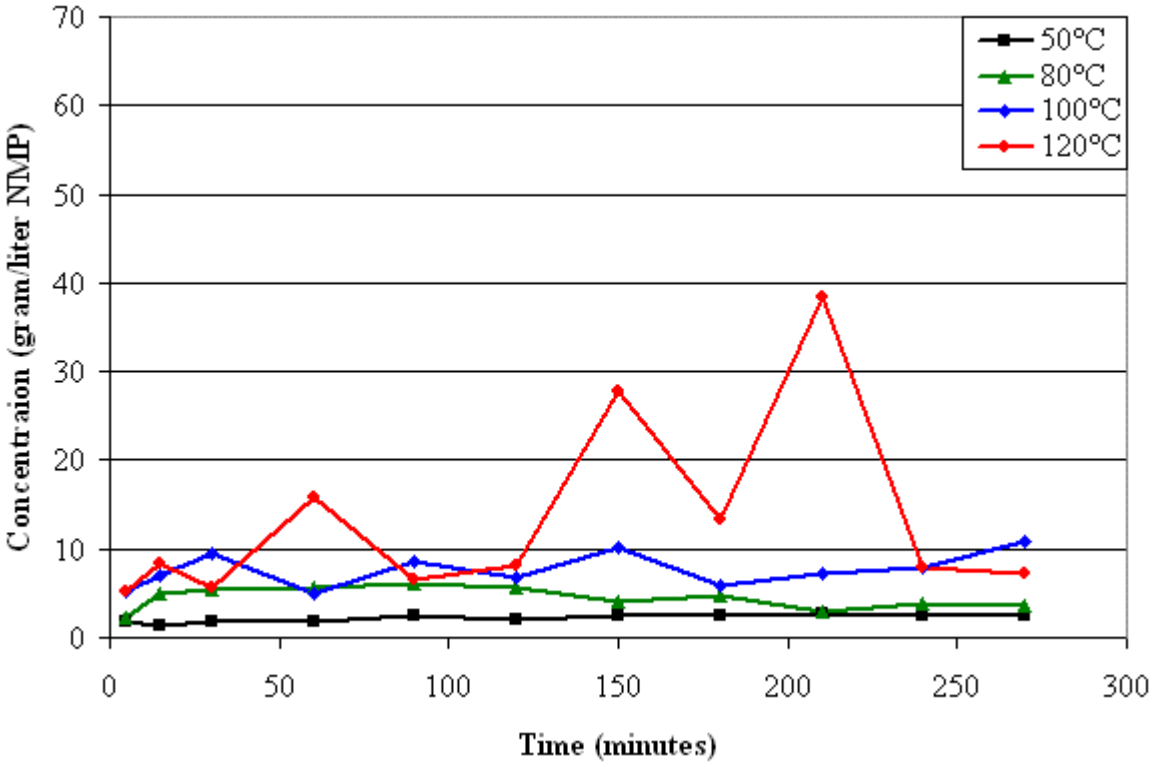

Figure 5-13 – Medium coal (106 - 212 μm) in NMP at low temperatures

Similar to the lower temperature runs on small coal samples, little extraction was observed at the lower temperatures. Except for a few spikes in concentration, observed solubility was flat for most low temperature runs. The extraction yield for high temperature extraction of medium coal is presented below as Figure 5-14.

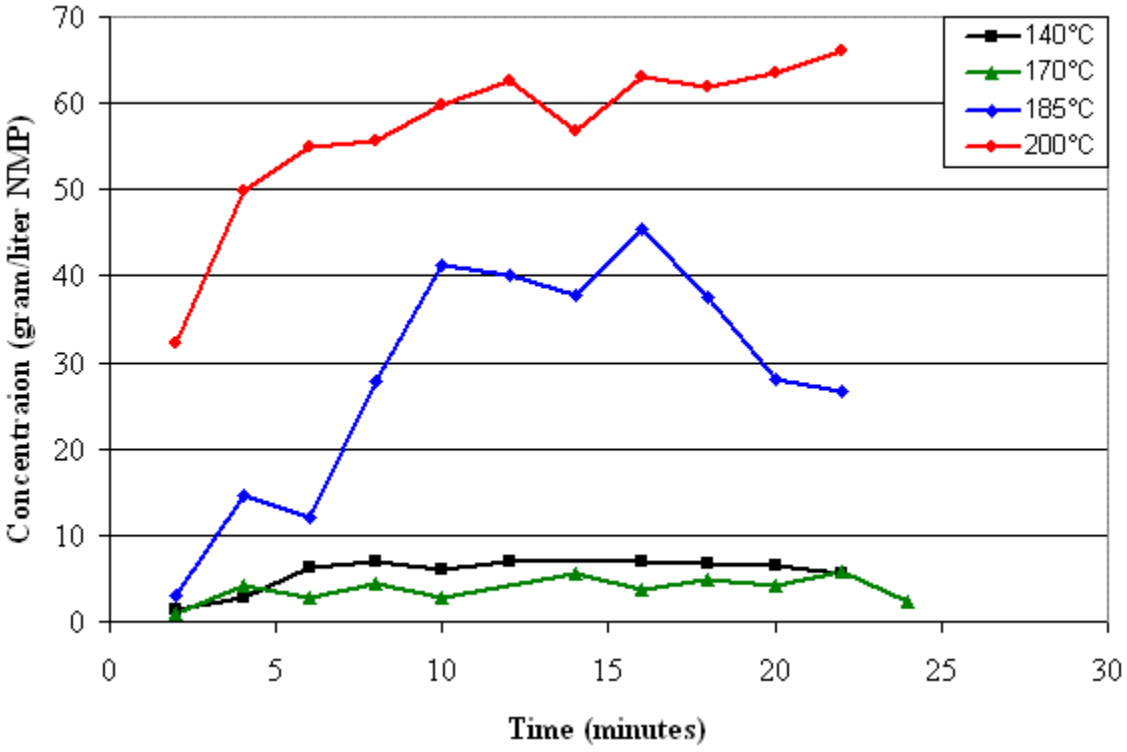

Figure 5-14 – Medium coal (106 - 212 μm) in NMP at high temperatures

The concentration of medium coal at higher temperatures resembled the concentration of small coal at higher temperatures. Little extraction occurred at lower temperatures, 140°C and 170°C. Significant extraction did not occur until 185°C. These parallels between the extraction of small and medium coals extended to the large coal sizes. The extraction of large coals at low and high temperatures is illustrated in the following two graphs, Figure 5-15 and Figure 5-16.

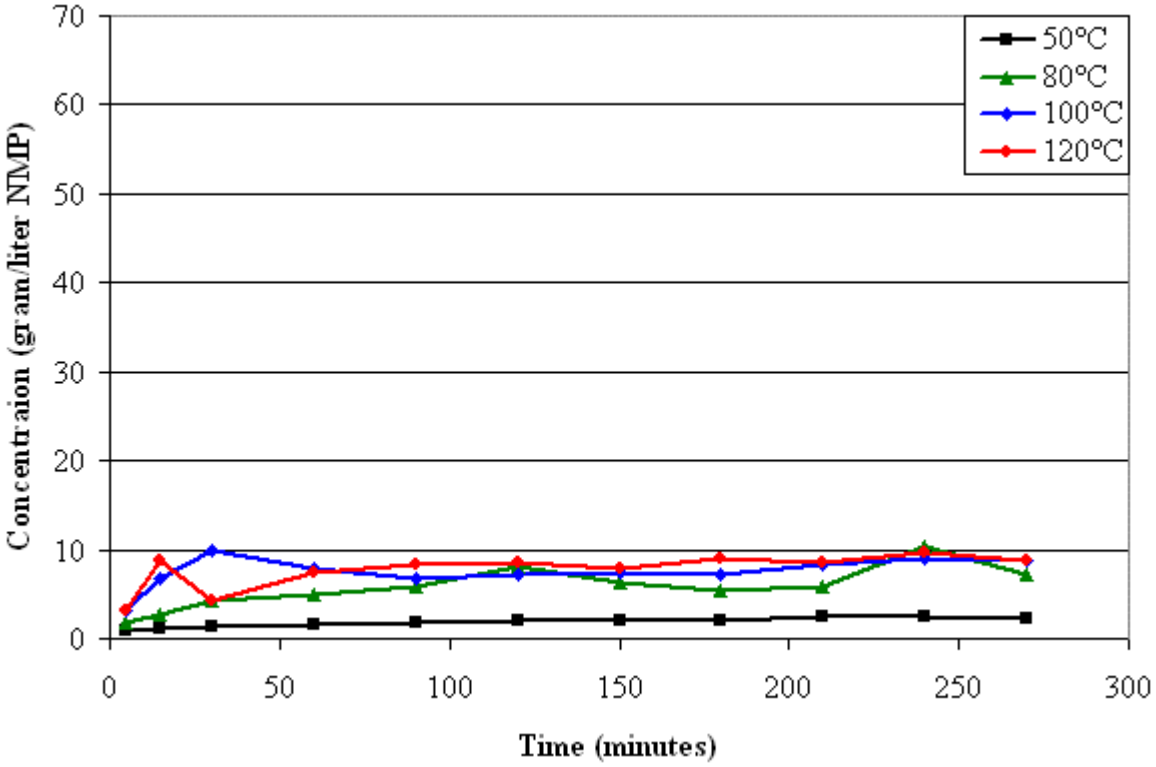

Figure 5-15 – Large coal (212 - 355 μm) in NMP at low temperatures

The data represented in Figure 5-15 illustrated that the same trends observed in the extraction of small and medium coals extended to large coals. Very little extraction occurred at the lower temperatures of 50°C to 120°C. Data for the extraction of larger coal sizes at higher temperatures follows as Figure 5-16.

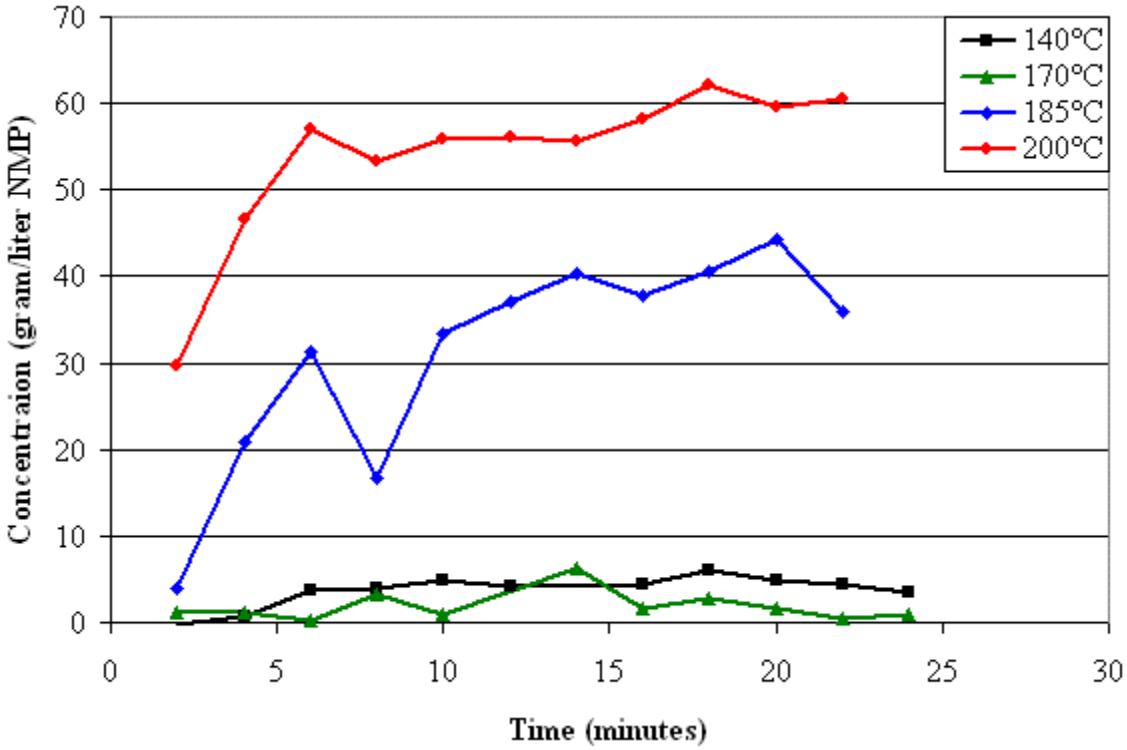

Figure 5-16 – Large coal (212 - 355 µm) in NMP at high temperatures

The dissolution of large coal at higher temperatures resembled the dissolution of smaller and medium coals at lower temperatures. Little extraction occurred at the temperatures of 140°C and 170°C. Significant extraction occurred when the temperature reached 185°C and higher. All swelling and extraction data recorded during research is included in this document as Appendix A.

Examination of the data revealed unusual variability in the amount of coal extraction at 185°C. Preliminary extraction runs, which did not use a sand bath, showed excellent repeatability in concentration measurements. This suggested that the fluidized sand bath may not have had a uniform temperature distribution. This would have been especially obvious around a temperature of 185°C, because the coal-NMP system underwent such drastic

changes around this temperature. The temperature profile of the sand bath was measured using a test tube rack and thermocouple. The holes of the test tube rack served as discrete cells through which the thermocouple was placed and allowed to equilibrate. The resultant temperature profile is presented below as Figure 5-17.

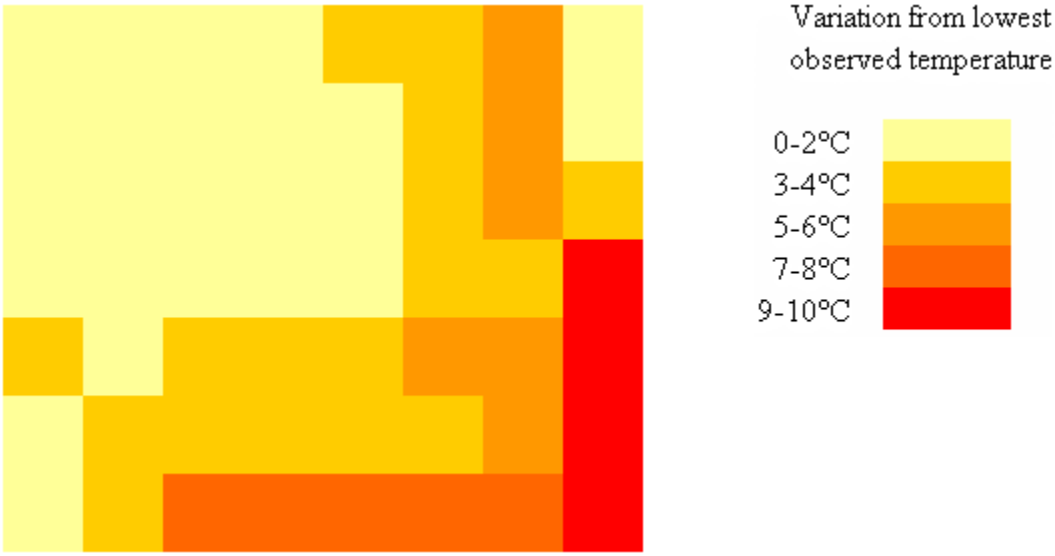

Figure 5-17 – Temperature profile of sand bath used in extraction experiments

Figure 5-17 confirmed that the non-uniformity of the sand bath temperature profile could be responsible for the erratic extraction data observed at a temperature of 185°C.

Chapter 6 – Correlation of Extraction and Swell

Section 6.1 – Developing a correlation for swell and extraction data

It was desired to correlate swell data with process parameters. Several regressions of swelling data were performed. Polynomial, logarithmic, linear, and a reciprocal fits were all applied to swelling data. An example set of swelling data and various fits of the data are presented below as Figure 6-1.

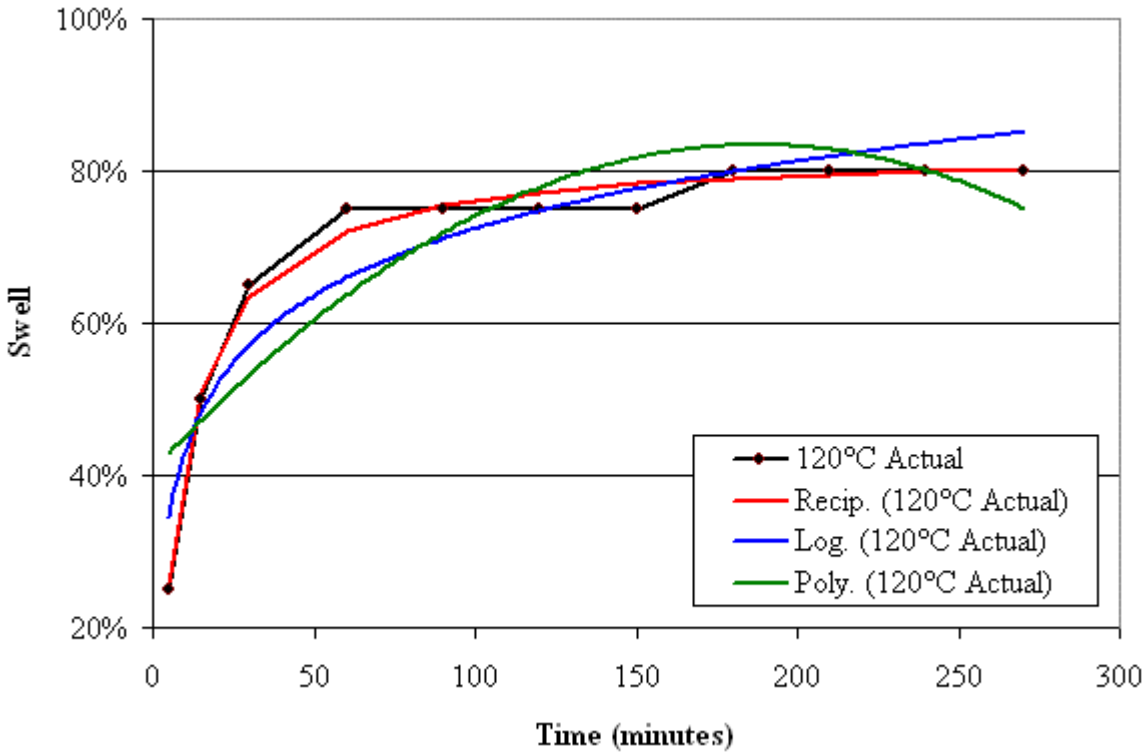

Figure 6-1 – Various fits of swelling data

The reciprocal fit is a custom correlation that was developed during the course of research. The reciprocal fit was developed after it was observed that both swell and extraction

data seemed to approach some maximum asymptotically. For almost all data, the reciprocal fit was superior. By superior, it is meant that the reciprocal fit most often minimized the sum of squares of the residuals between the actual data and predicted fit. . The formula for the reciprocal fit appears below.

$$S_T = S_M \left(1 - \frac{1}{C_S \left(t - \frac{t_l}{l} \right)} \right) \quad \textbf{(6-1)}$$

Where:

S_T = Swell at time t

S_M = Maximum predicted swell

C_S = Swelling curve factor

t = time

t_l = lag time

$$l = \frac{1}{1 - \frac{1}{S_M C_S}}$$

The variable l ensured that the lag time, t_l, offset the curve by the desired time. The effects of the three adjustable parameters of the reciprocal fit, S_M, C_S, and t_l are illustrated below in Figure 6-2, Figure 6-3, and

Figure 6-4.

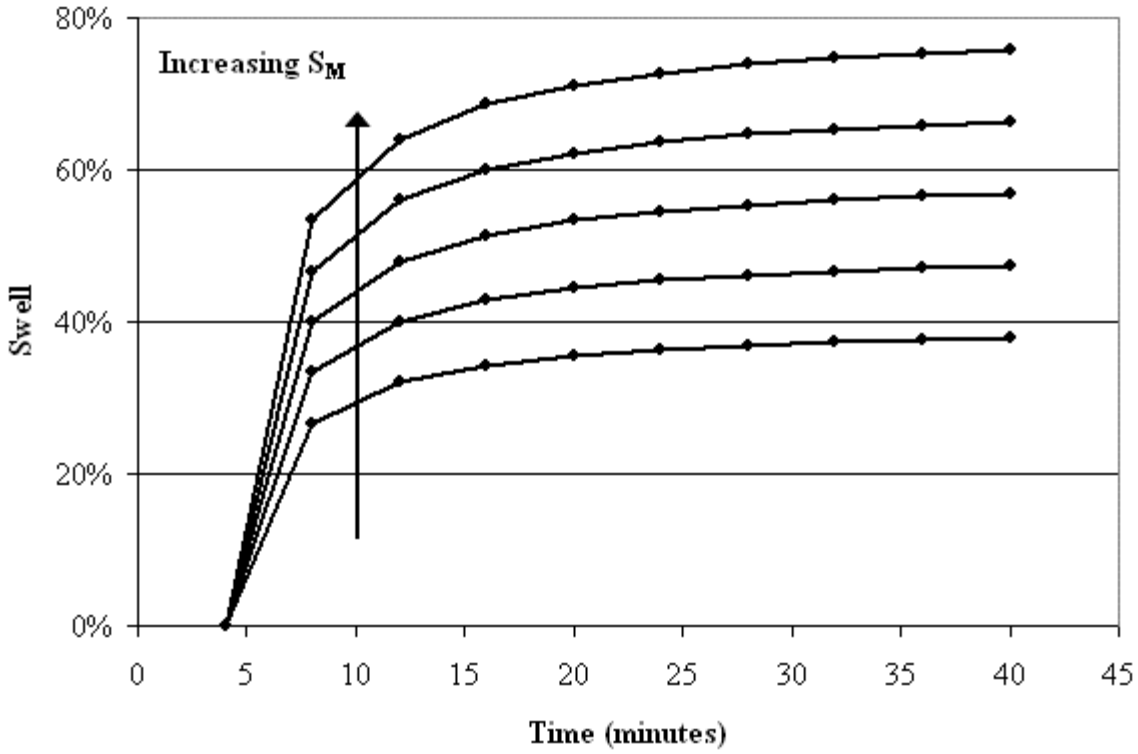

Figure 6-2 – Effect of increasing S_M on reciprocal fit

Figure 6-2 was generated with C_S held constant at 0.5 and t_l held constant at 4. S_M was varied from 0.4 to 0.8. S_M is the maximum swell predicted by the correlation. The predicted swell will reach S_M at infinite time. As can be seen in Figure 6-2, S_M is simply a multiplier of the curve, it does not affect the general shape of the curve. The shape of the curve is affected by C_S, the swelling curve factor. The effect of C_S on the reciprocal fit is presented below as Figure 6-3.

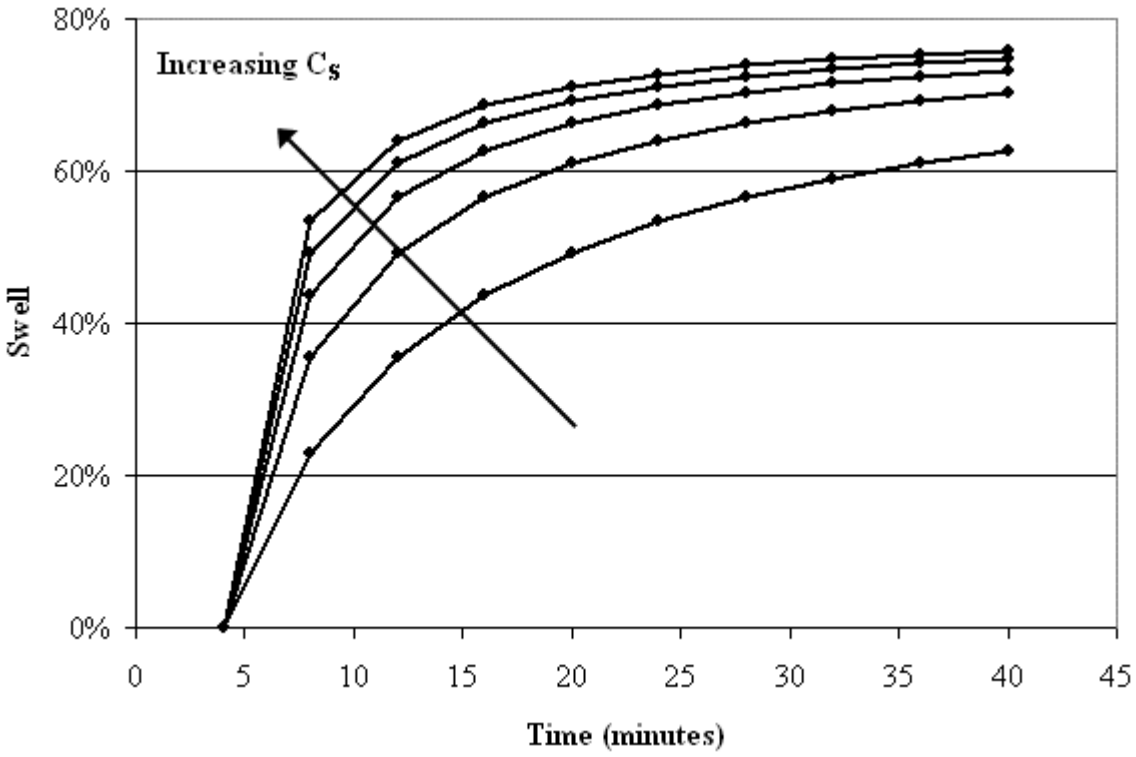

Figure 6-3 – Effect of increasing C_S on reciprocal fit

Figure 6-3 was generated with S_M held constant at 0.8 and t_l held constant at 4. C_S was varied from 0.1 to 0.5. As illustrated in Figure 6-3, C_S represents the curve of the reciprocal fit. It could also be said that C_S determined how quickly the swell approached the maximum predicted swell. Linear data would be best approximated by an extremely small C_S, while step-function data would be best represented by an extremely large C_S. Note that changing both C_S and S_M has no effect on where the reciprocal fit intercepts the x-axis. This is controlled by the lag time parameter, t_l. The effect of various lag times on the reciprocal fit is presented below as Figure 6-4.

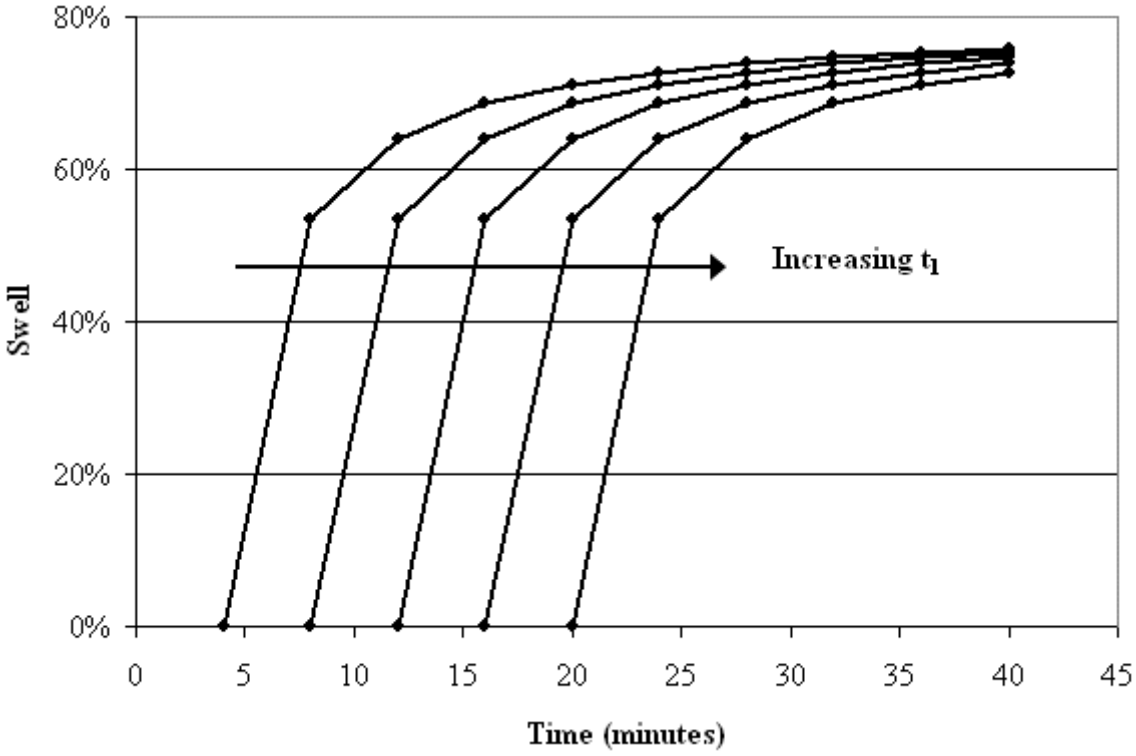

Figure 6-4 – Effect of increasing t_l on reciprocal fit

Figure 6-4 was generated with S_M held constant at 0.8 and C_S held constant at 0.5. t_l was varied from 4 minutes to 20 minutes. As illustrated in Figure 6-4, varying t_l did not affect the shape of the curve or the maximum swell, but simply the x-axis offset of the curve.

The regression to determine the optimum values of S_M, C_S, and t_l operated as follows. A series of nested for loops were created, to run several million combinations of S_M, C_S, and t_l. S_M was divided into 200 increments, from 0.01 to 2.00. C_S was divided into 250 increments, from 0.01 to 2.50. t_l was divided into 100 increments, from 0 to 100. These divisions resulted into a total of five million combinations of S_M, C_S, and t_l. SSR (the sum of squares of residuals) between the

actual data and the reciprocal fit was calculated for all five million points. The one combination of parameters out of five million that minimized SSR was designated as the best fit. The visual basic computer code used to fit the swelling correlation to the data is included in this document as Appendix B.

The extraction data was also best described by a reciprocal fit, fundamentally the same equation as Equation 6-1, but with different terms for the sake of clarity. The equation used to describe extraction data is presented below.

$$E_T = E_M \left(1 - \frac{1}{C_E \left(t - \frac{t_l}{l} \right)} \right) \qquad \textbf{(6-2)}$$

Where:

E_T = Extraction at time t

E_M = Maximum predicted extraction

C_E = Extraction curve factor

t = time

t_l = lag time

$$l = \frac{1}{1 - \frac{1}{E_M C_E}}$$

Because the adjustable parameters E_M and C_E occupied different ranges than their counterparts S_M and C_S, the regression was similar but not exactly the same. E_M was divided into 800 increments, from 0.0 to 80.0. C_E was divided into 250 increments, from 0.00 to 2.50. t_l divided into 10 increments, from 0 to 10. This

resulted in a total of two millions combinations. As before, the best fit was defined as the combination of parameters that minimized SSR.

Section 6.2 – Correlation of swell data

Data for the swell of small coal at low temperatures, along with reciprocal fits laid over the data, are presented below as Figure 6-5. Data for the high temperature swell of small coal follows as Figure 6-6.

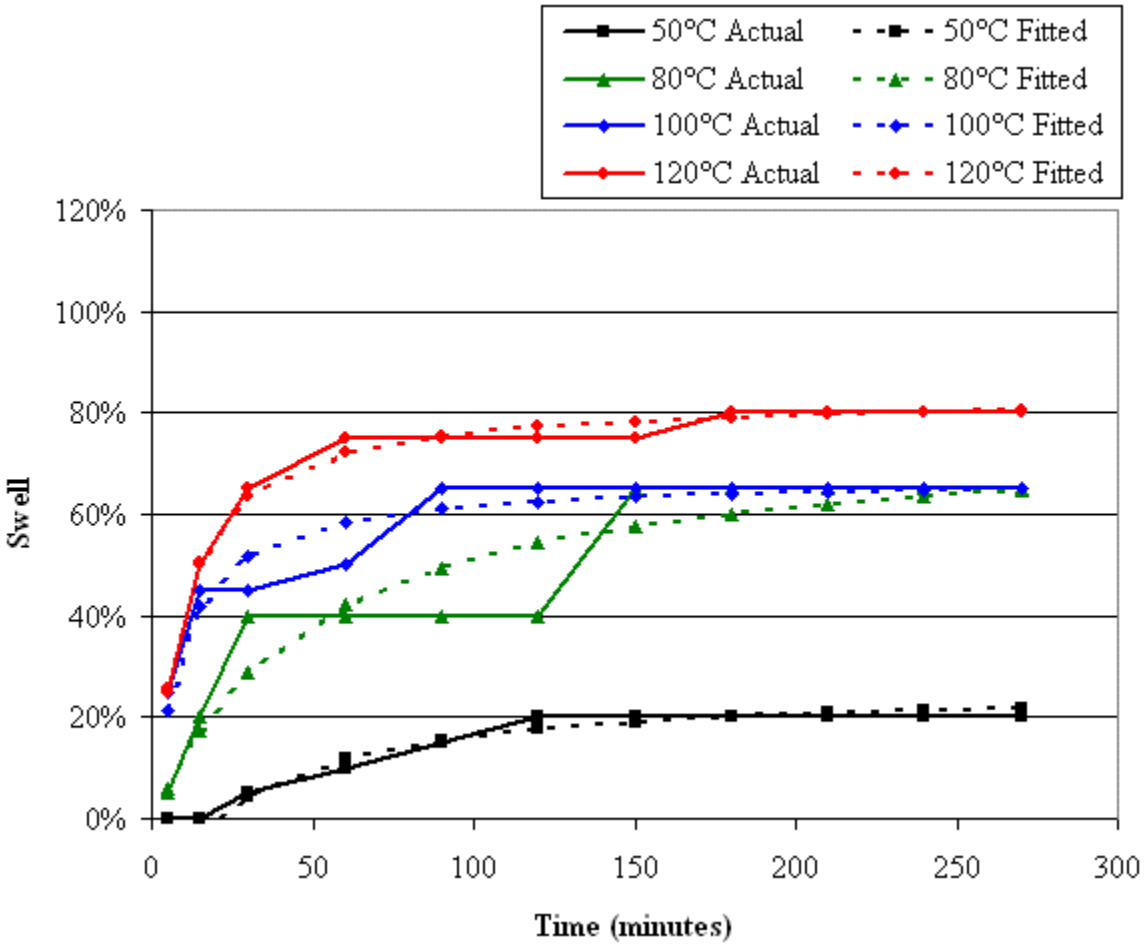

Figure 6-5 – Fitting small coal (sub 106 µm) swell at low temperature

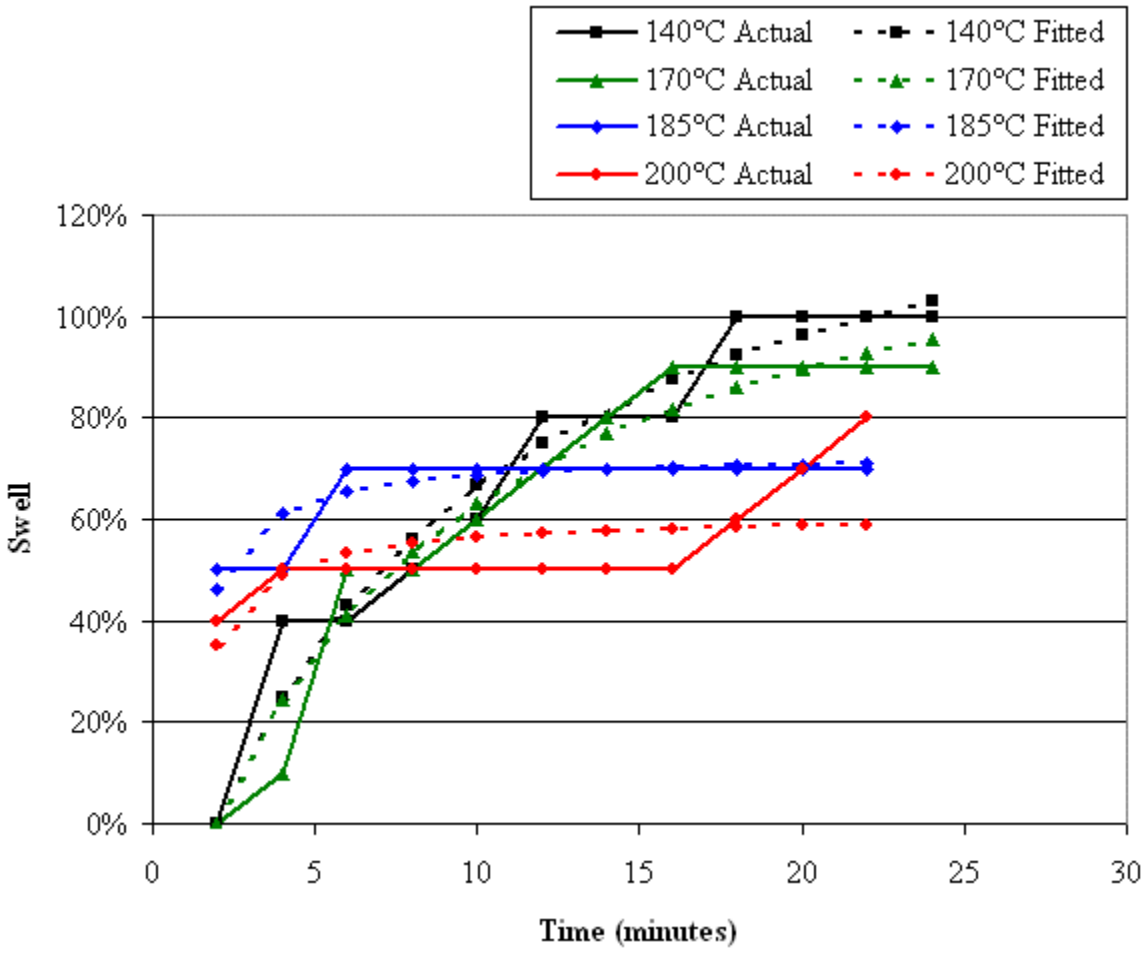

Figure 6-6 – Fitting small coal (sub 106 μm) swell at high temperature

The reciprocal fits correlated well with the data. The reciprocal fit suggested maximum swell occurred at 140°C to 170°C, which is consistent with earlier conclusions. Swelling data and reciprocal fits for the low and high temperature runs of medium sized coal follows as Figure 6-6 and Figure 6-7, respectively.

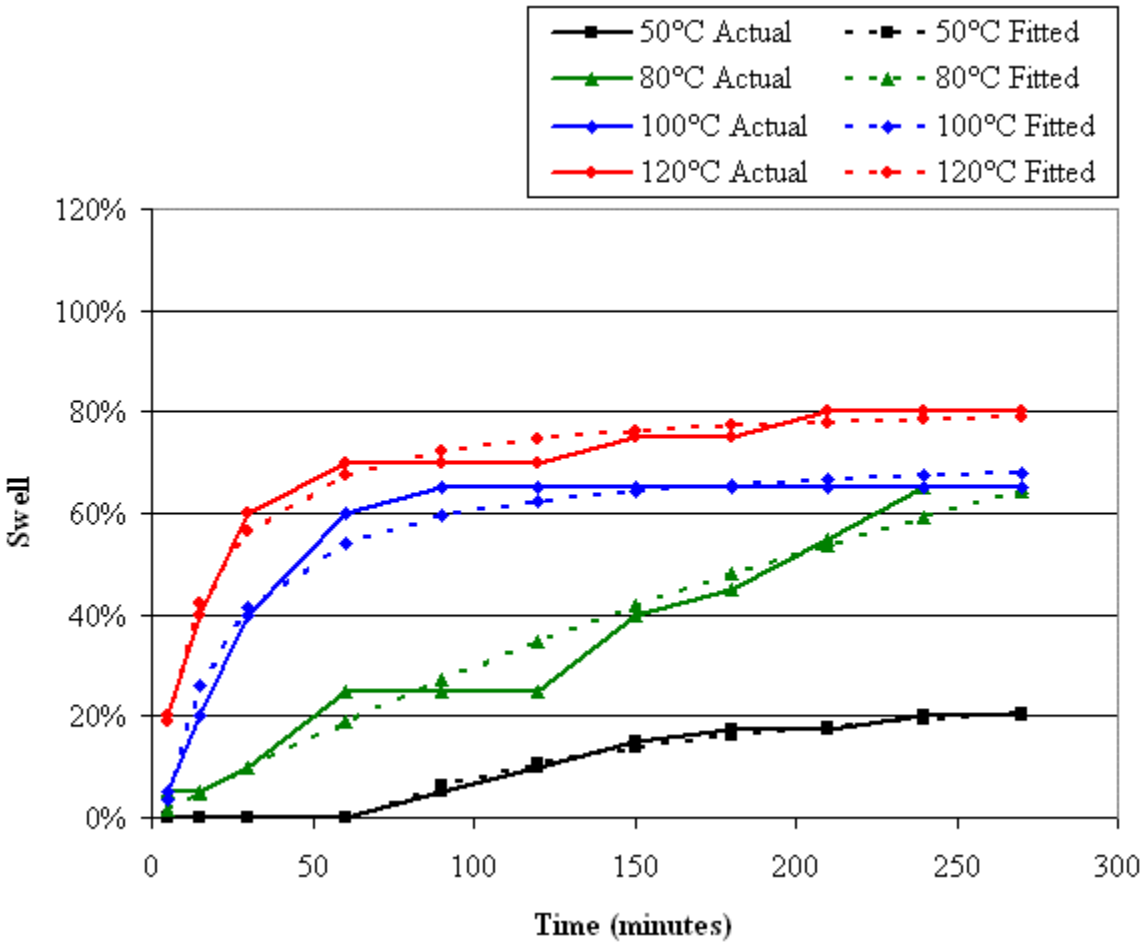

Figure 6-7 – Fitting medium coal (106 - 212 μm) swell at low temperature

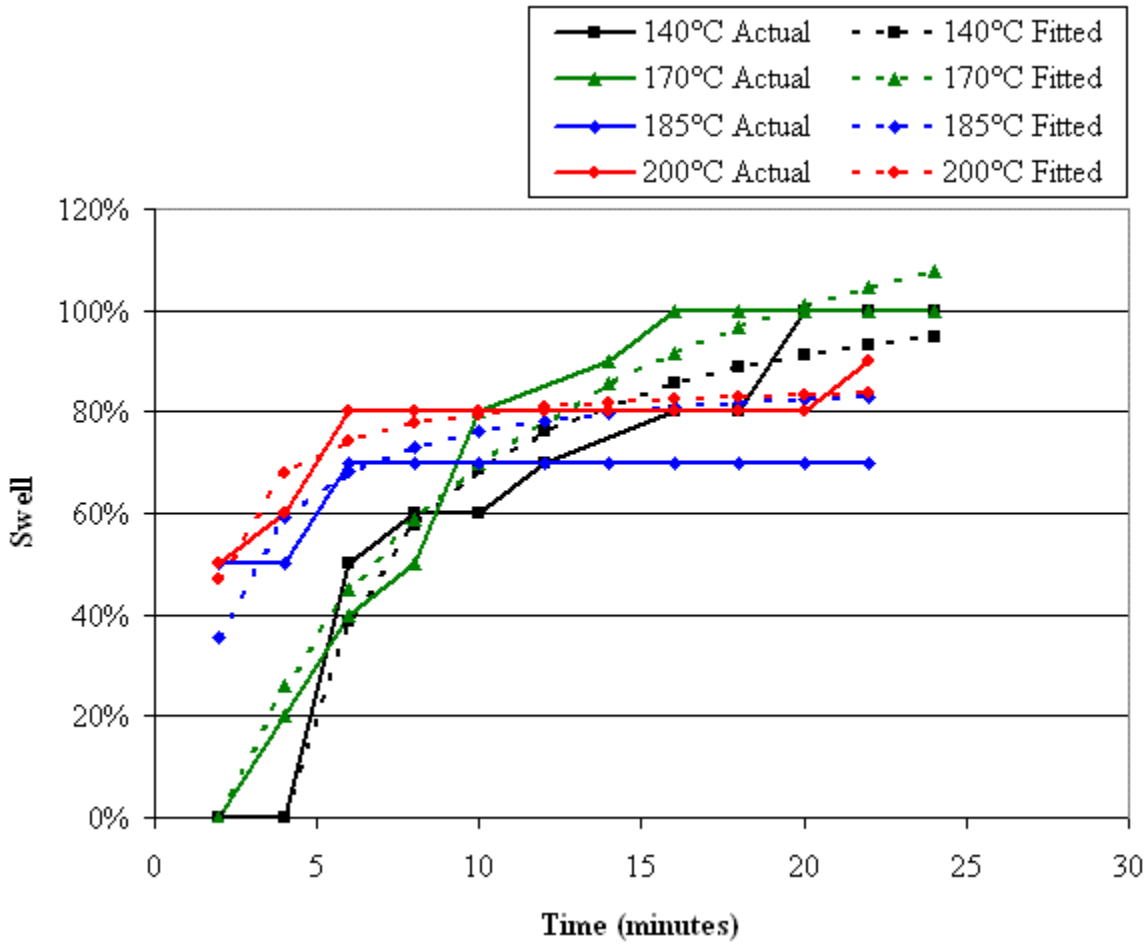

Figure 6-8 – Fitting medium coal (106 - 212 μm) swell at high temperature

As before, swell increased with temperature, until it maximized around 170°C. Swelling data and reciprocal fits for the low and high temperature runs of large sized coal follows as Figure 6-9 and Figure 6-10, respectively.

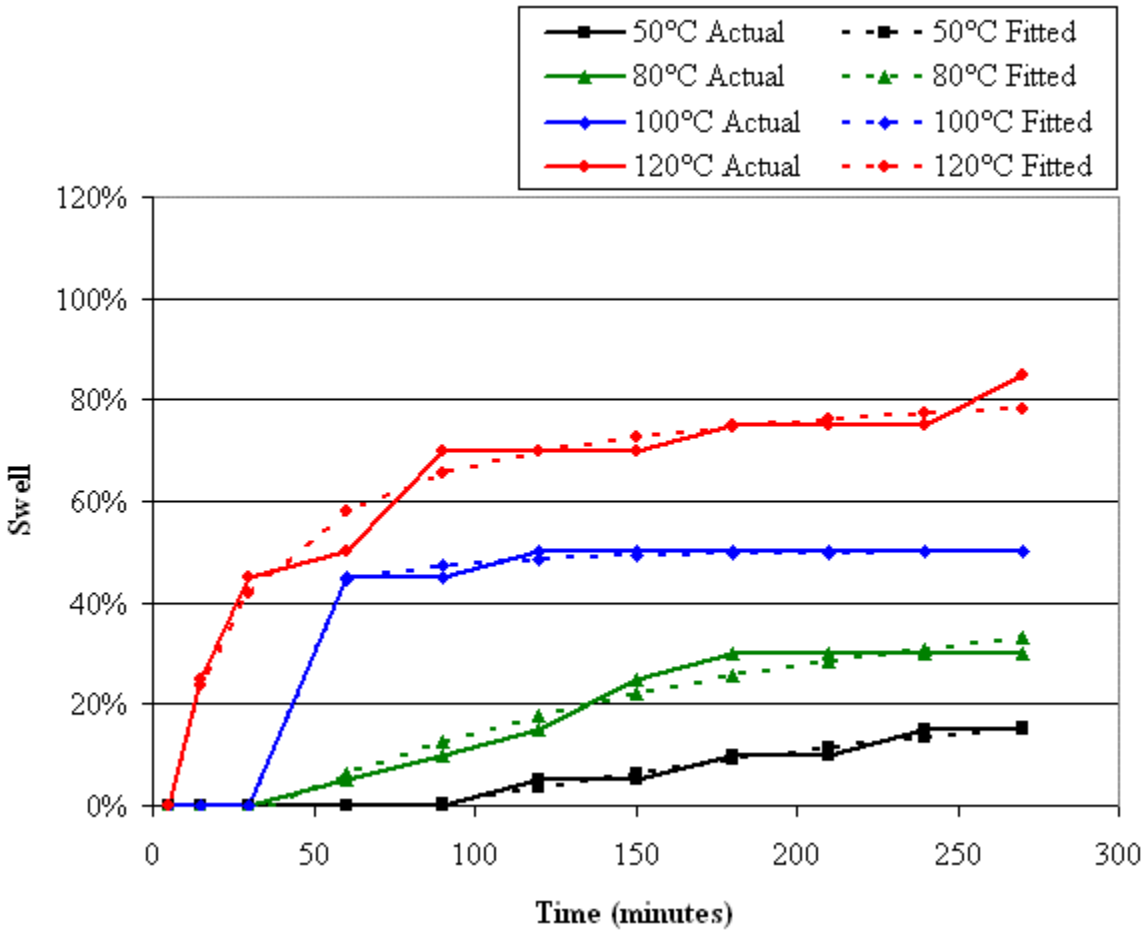

Figure 6-9 – Fitting large coal (212 - 355 µm) swell at low temperature

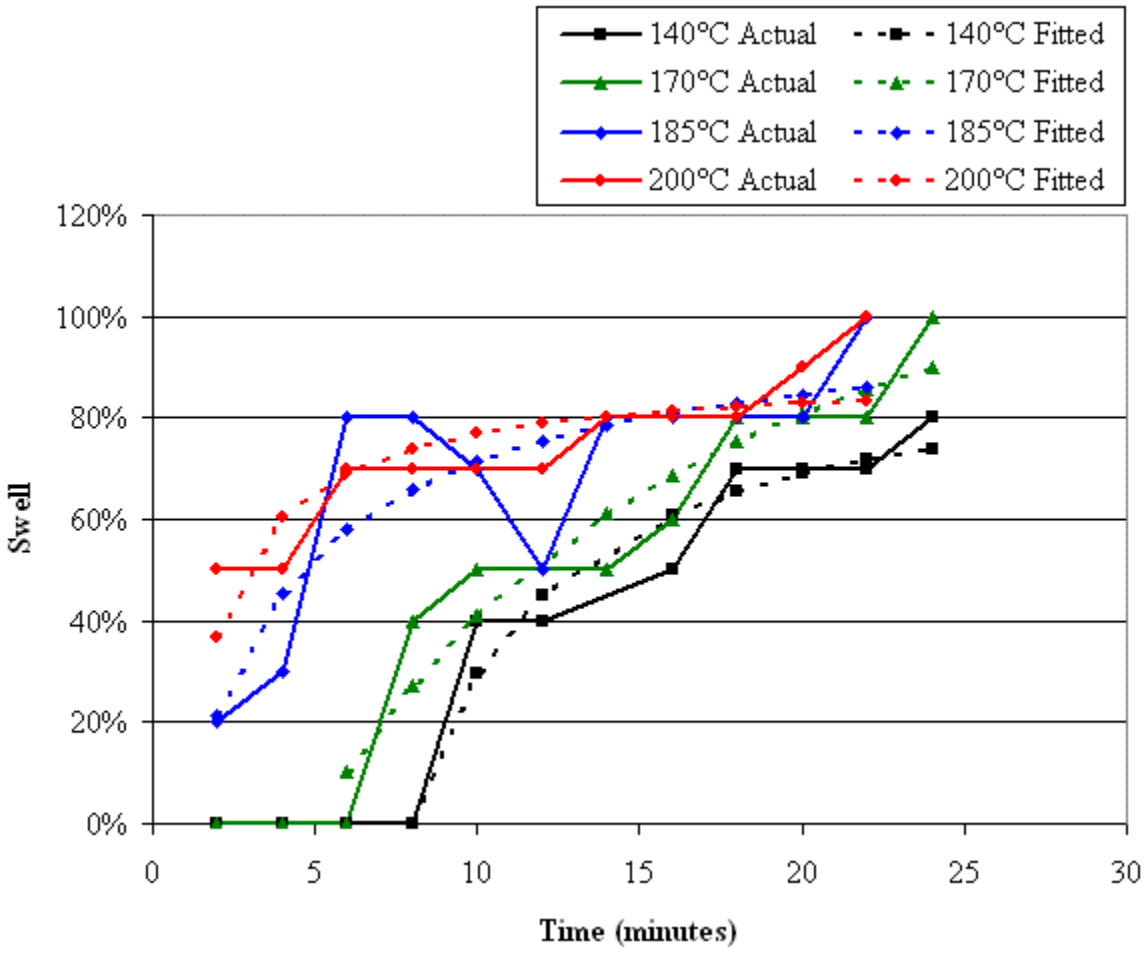

Figure 6-10 – Fitting large coal (212 - 355 µm) swell at high temperature

The large coal followed the same trends as the small and medium coals. The difference was an increased lag time, large coals took longer to begin swelling, especially at lower temperatures. Once swelling began, large coals swelled a similar amount to small and medium coals. Interestingly, the correlation predicted the highest maximum swell at 170°C, which was not observed in the raw data. This supported the idea that maximum swell occurred around 170°C regardless of coal size, but this was not observed in the high temperature swelling of large coals because the time scale was not sufficiently long.

With all six sets of swelling data fit, it was desired to graph the correlation's adjustable parameters, S_M, C_S, and t_l, as a function of temperature. S_M, C_S, and t_l graphed as a function of temperature are presented as Figure 6-11, Figure 6-12, and Figure 6-13, respectively.

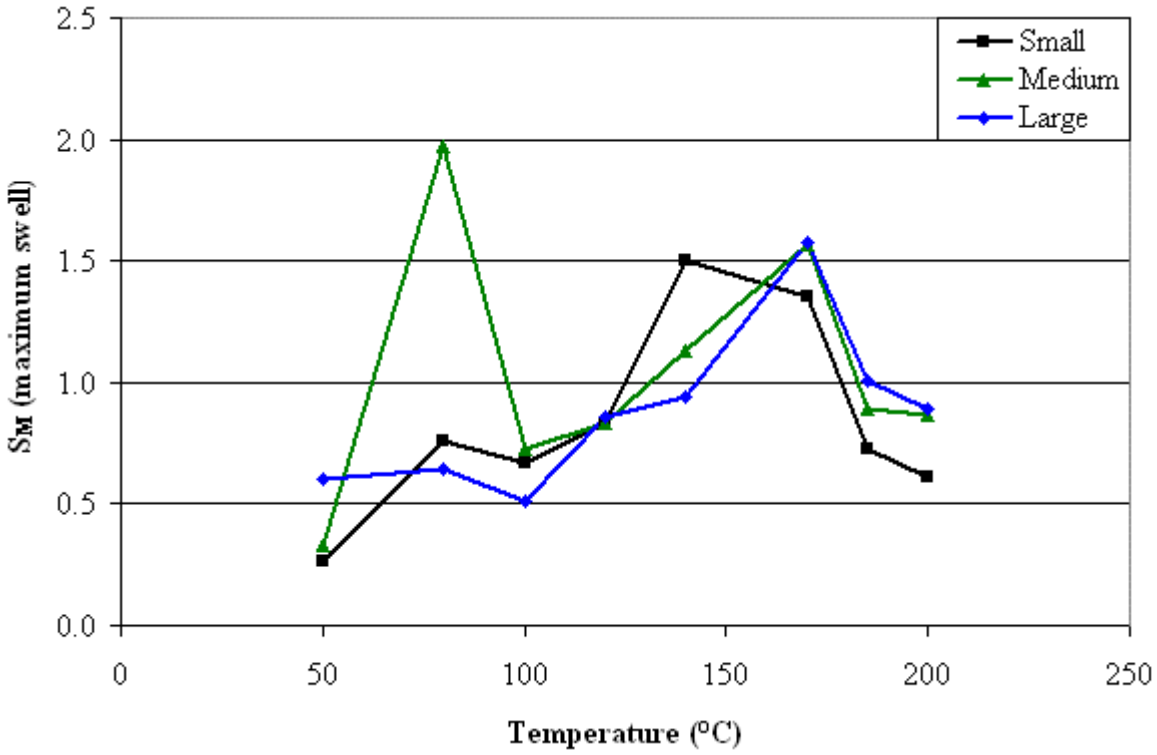

Figure 6-11 – Predicted maximum swell as a function of temperature

As observed, maximum swell increased with temperature until it peaked at 170°C, after which point the maximum swell decreased. The anomalous data point at 80°C is attributed to the somewhat linear looking data of medium coal at that temperature. Linear data is best fit by a reciprocal fit with large S_M and small C_S. The swelling curve factor, C_S, was also graphed as a function of temperature, and follows as Figure 6-12.

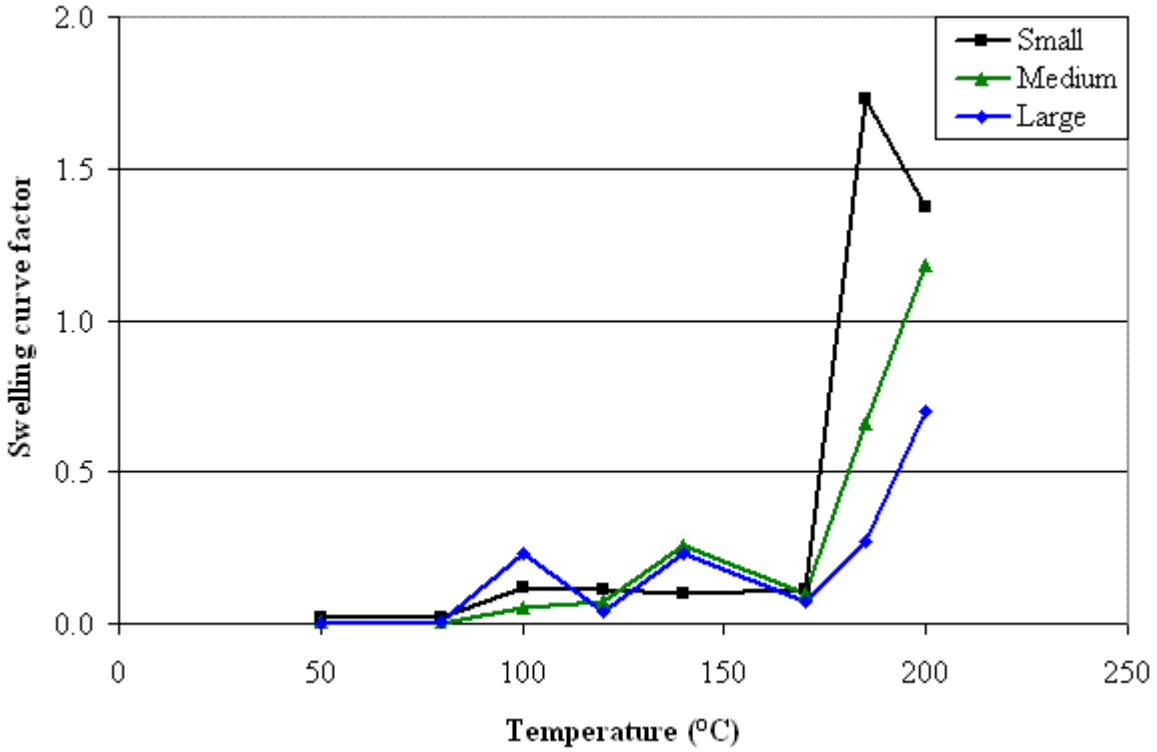

Figure 6-12 – Swelling curve factor as a function of temperature

The swelling curve factor remained relatively flat until it spiked dramatically at a temperature of 185°C. This sudden spike was reminiscent of the sudden spike in extraction yield, which was also observed at 185°C (see Chapter 5 – Experimental Results). The swelling curve factor for small coals was greater than the swelling curve factor for medium coals, which was greater than the swelling curve for large coals. This suggested that small coals approached their maximum swell more quickly, which suggested swelling was at least somewhat diffusion dependent. Next, the swelling lag time was graphed as a function of coal size and temperature, and appears as Figure 6-13.

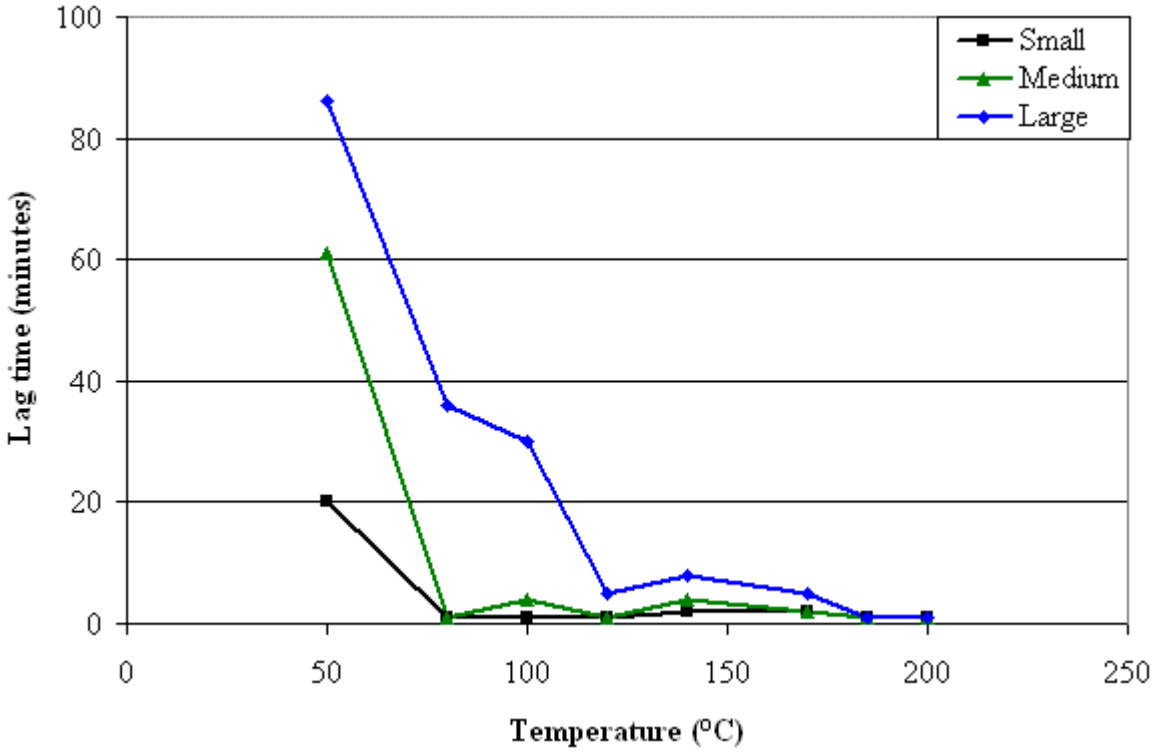

Figure 6-13 – Predicted lag time as a function of temperature

As expected, larger coals had the highest lag times, and swelling lagged until a temperature of 185°C. Medium coal initially had a larger lag time than small coal, but both quickly approached no lag time at 80°C and higher. This data further supported the conclusion that swelling is at least somewhat diffusion controlled. Smaller coals began swelling sooner, and when they began to swell, swelled faster.

Section 6.3 – Correlation of extraction data

The extraction data for low temperature and high temperature runs are presented below as Figure 6-14 and Figure 6-15, respectively.

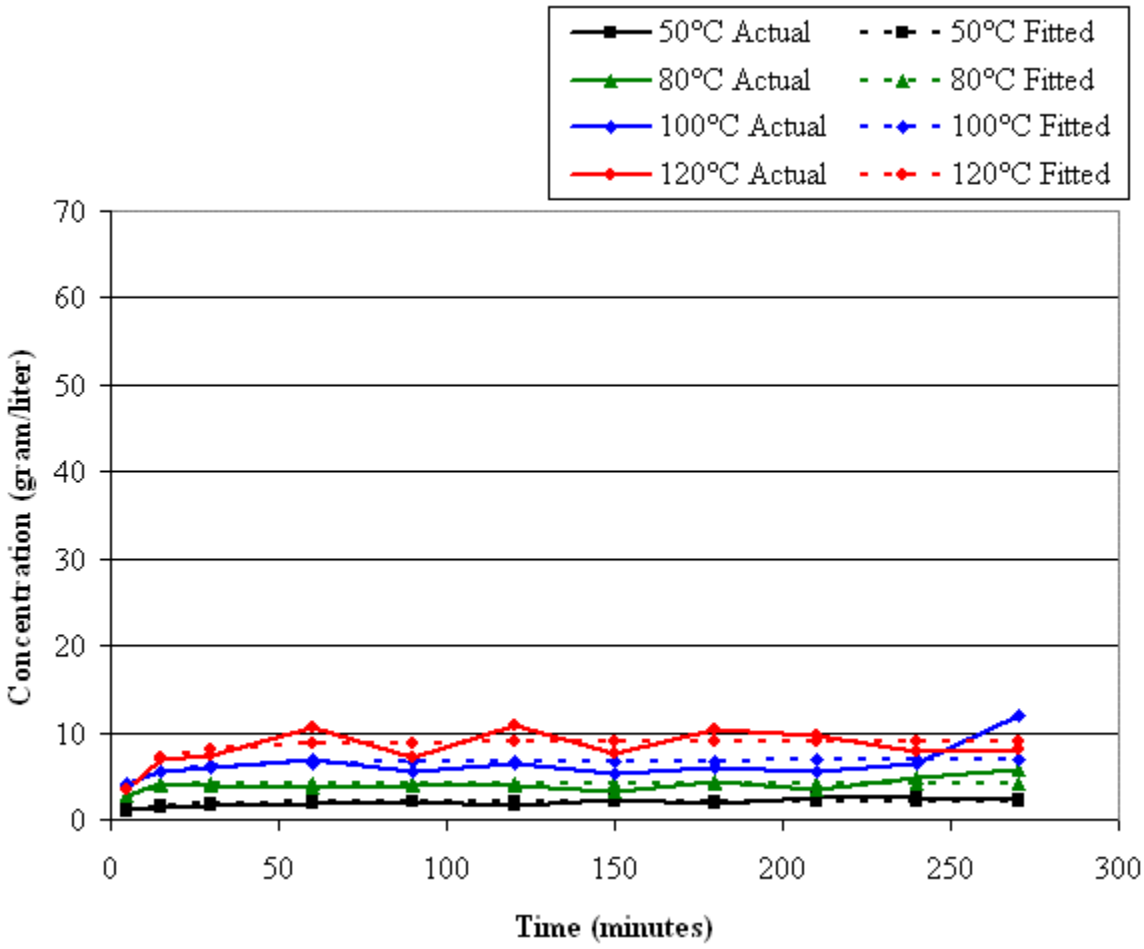

Figure 6-14 – Fitting small coal (sub 106 μm) extraction at low temperature

Note that for the low temperature runs graphed in Figure 6-14, extraction was temperature dependent, but the total observed extraction was relatively small. This contrasted with the extraction of small coal at high temperature, which is presented below as Figure 6-15.

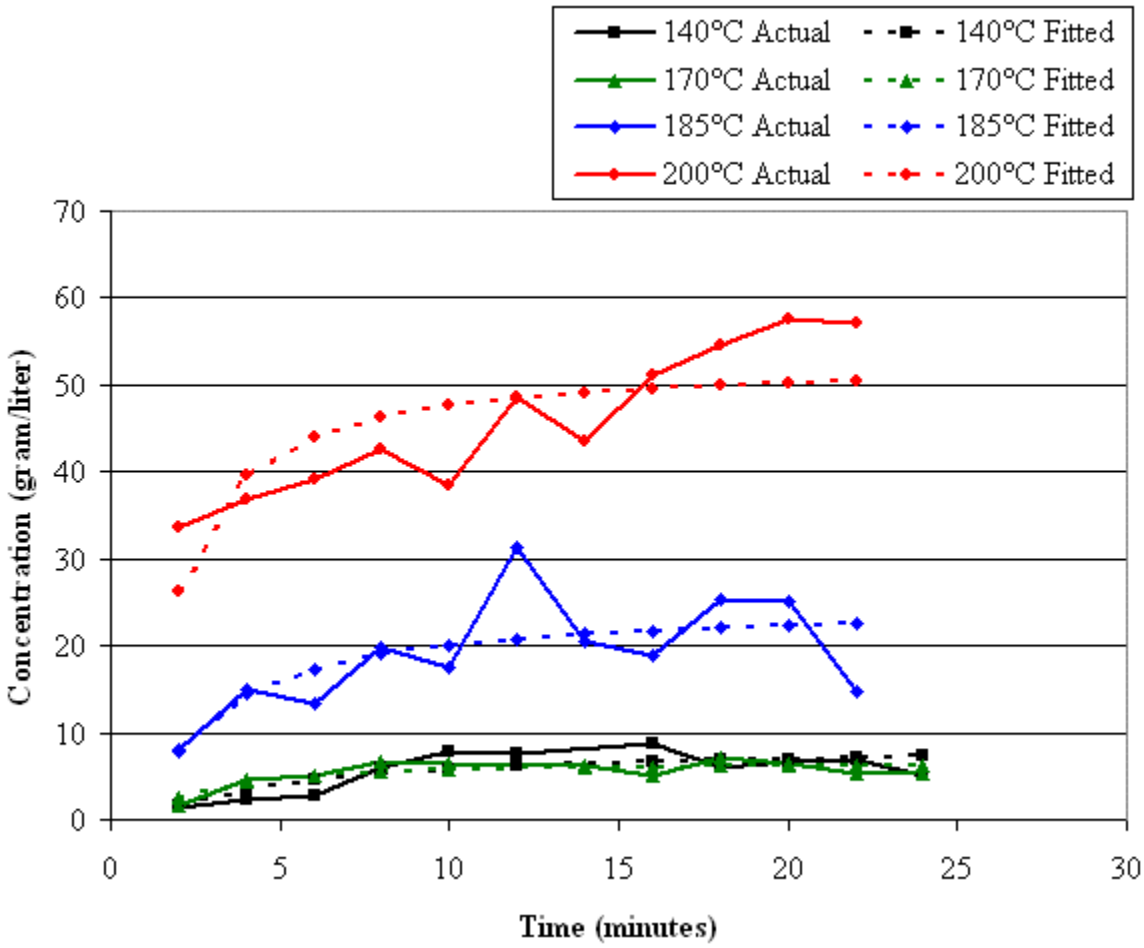

Figure 6-15 – Fitting small coal (sub 106 µm) extraction at high temperature

Little extraction occurred at 140°C and 170°C. When the extraction temperature reached 185°C, significant extraction occurred. The maximum extraction predicted at 200°C was higher than the maximum extraction predicted at 185°C – this was consistent with observed data. This trend was repeated with medium and large sized coal samples. Data for the low temperature and high temperature extraction of medium sized coal are presented below as Figure 6-16 and Figure 6-17.

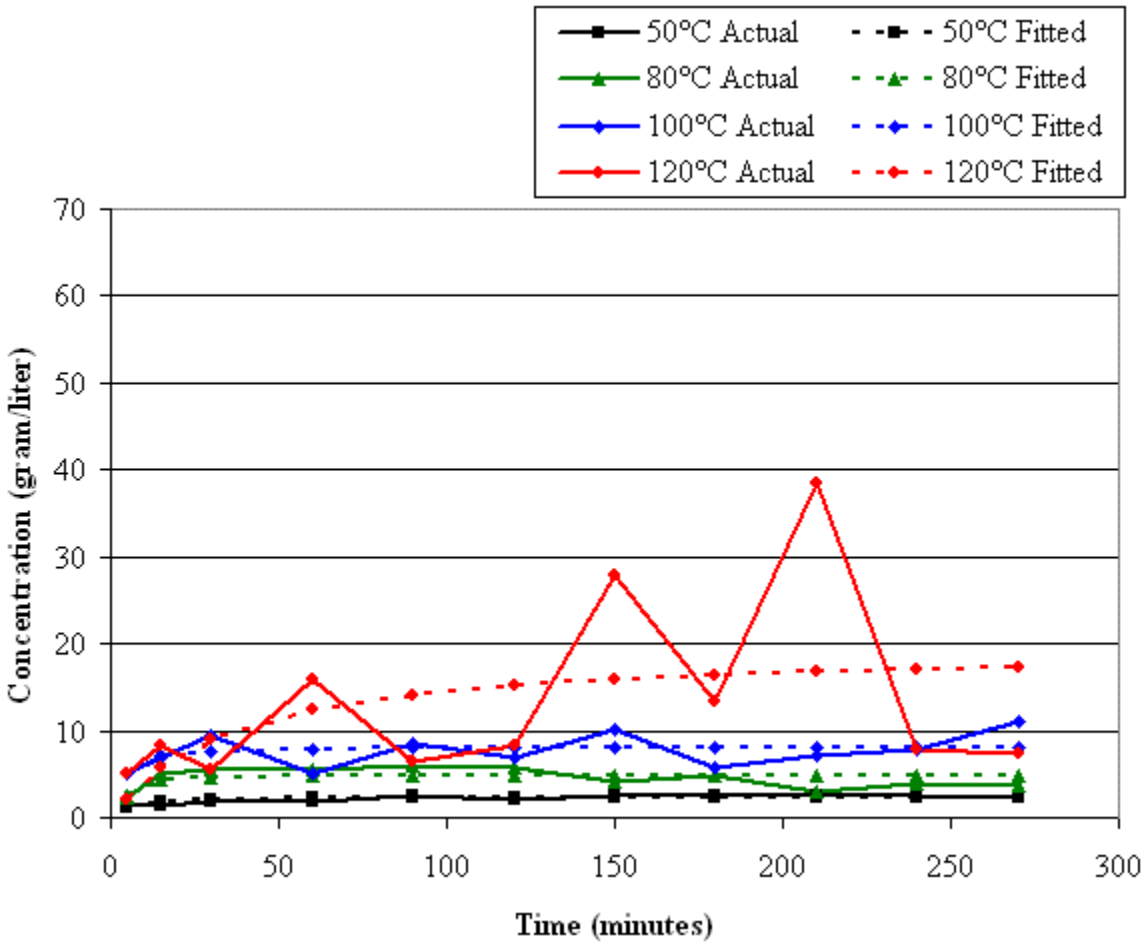

Figure 6-16 – Fitting medium coal (106 - 212 µm) extraction at low temperature

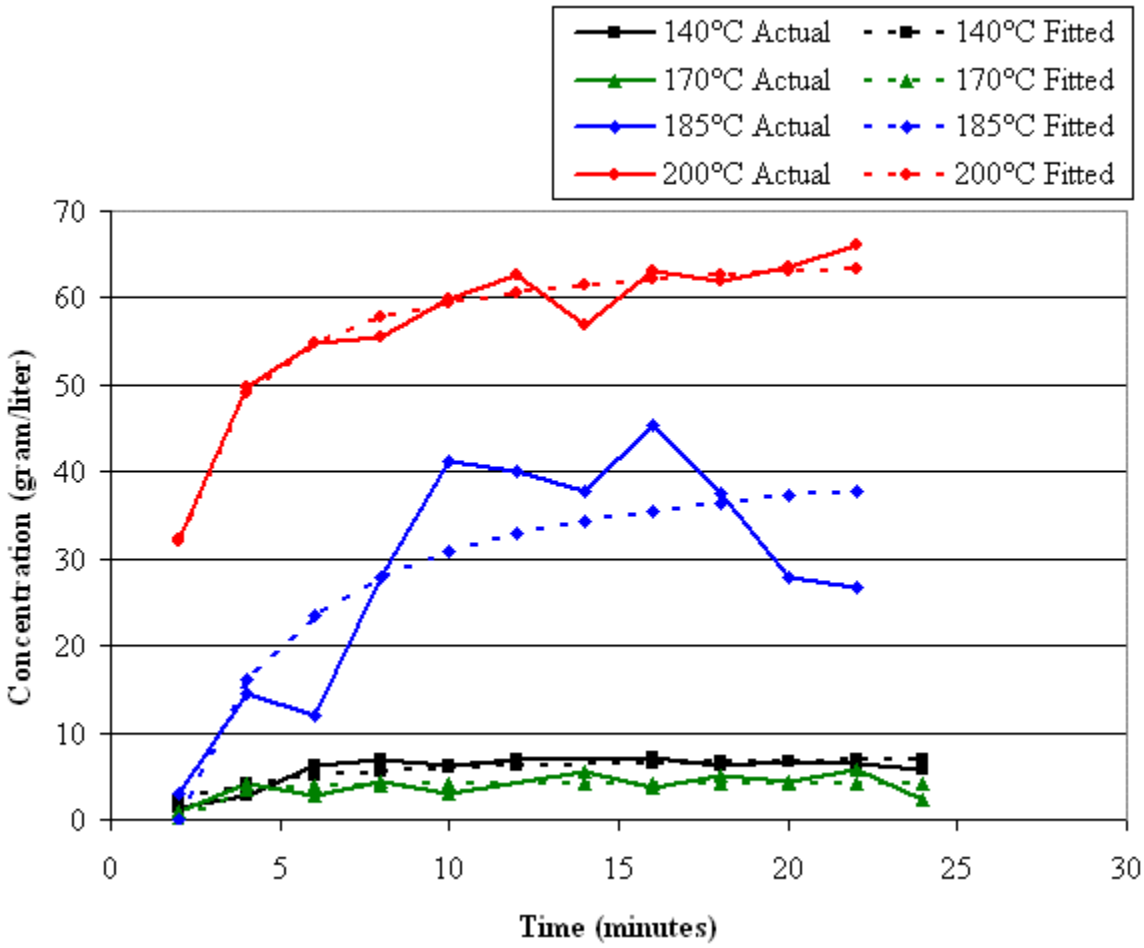

Figure 6-17 – Fitting medium coal (106 - 212 μm) extraction at high temperature

Similar to the small coal samples, little extraction occurred at temperatures up to 170°C. At temperatures of 185°C and higher, the extraction yield immediately spiked. The extraction yield at 200°C was greater than the extraction yield at 185°C. The same trend was observed for the large coal samples. Data for the low temperature and high temperature extraction of large coal are presented below as Figure 6-18 and Figure 6-19.

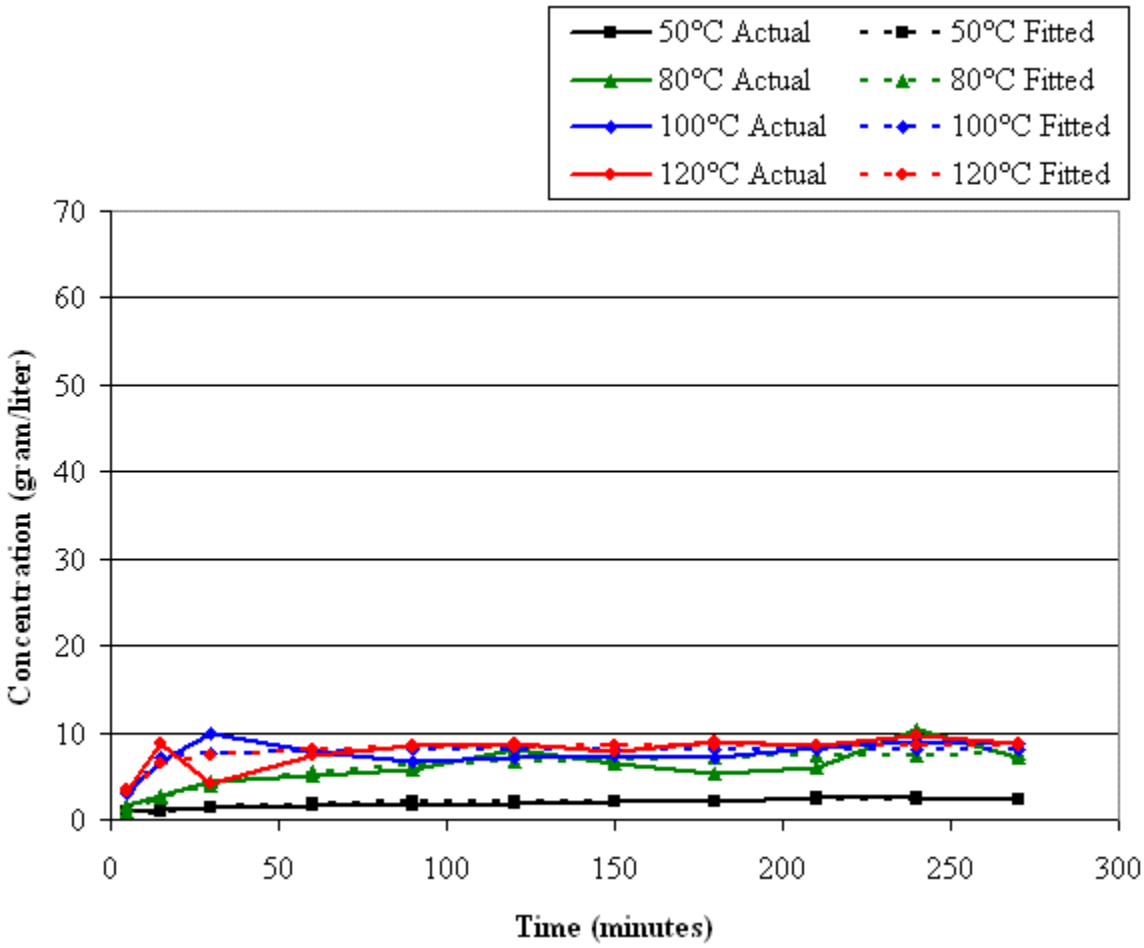

Figure 6-18 – Fitting large coal (212 - 355 μm) extraction at low temperature

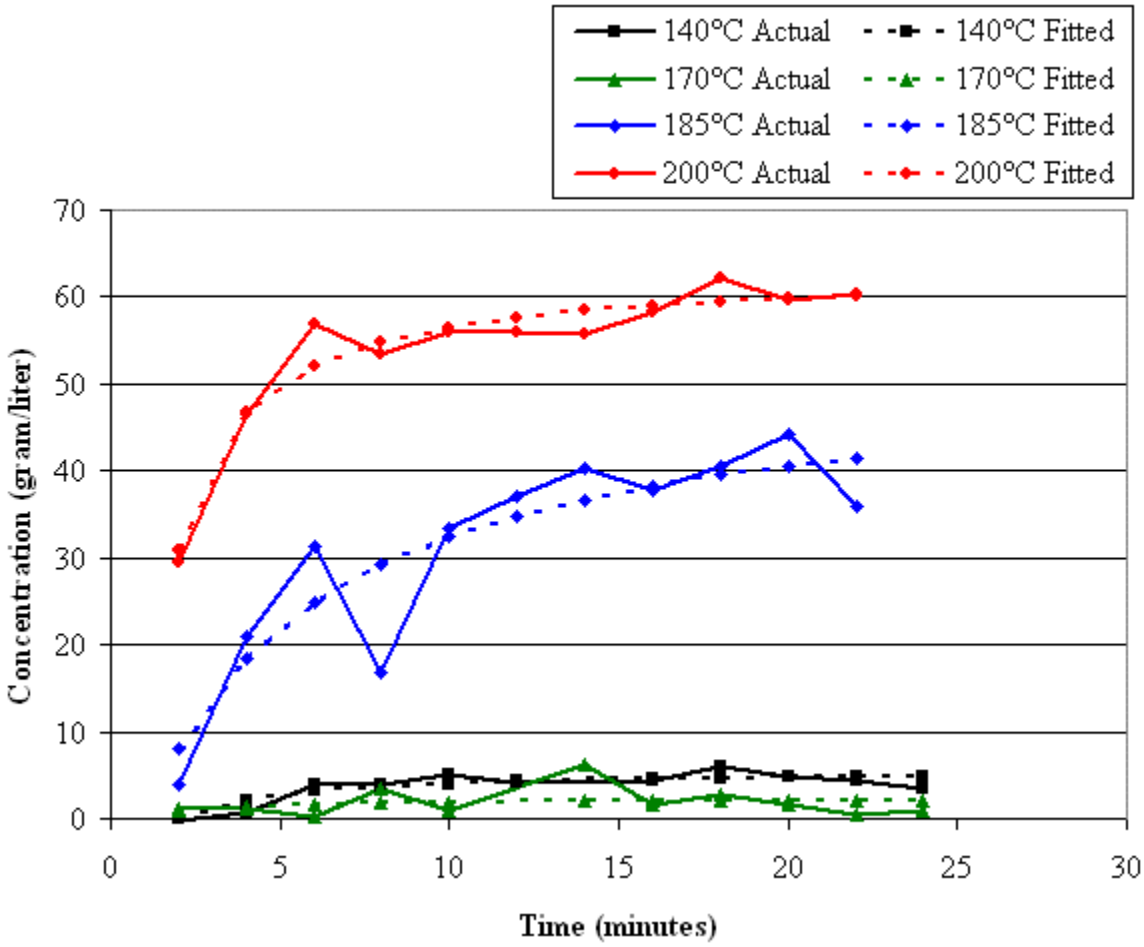

Figure 6-19 – Fitting large coal (212 - 355 μm) extraction at high temperature

After the reciprocal fit was applied to all sets of extraction data, the adjustable parameters E_M and C_E were graphed as a function of temperature. The extraction lag time was not graphed because it was small, less than four minutes, for all extraction runs. The graphs of E_M and C_E are presented below as Figure 6-20 and Figure 6-21.

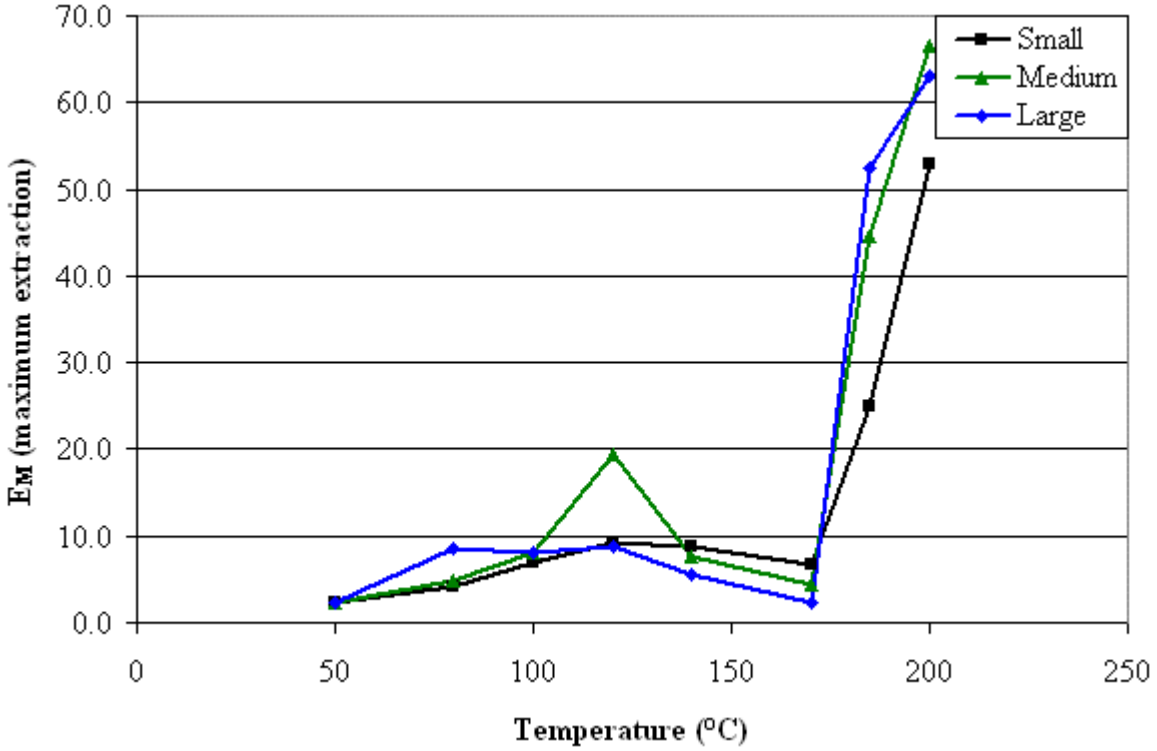

Figure 6-20 – Predicted maximum extraction as a function of temperature

The maximum extraction predicted based on temperature was consistent with observed data. Extraction was relatively flat, until it spiked at a temperature of 185°C. As the data suggested, the maximum extraction was predicted at 200°C, which is near the boiling point of NMP, 202°C. Extraction data contrasted greatly with swelling data. The maximum predicted swell changed relatively smoothly with respect to temperature, where the maximum predicted extraction changed abruptly.

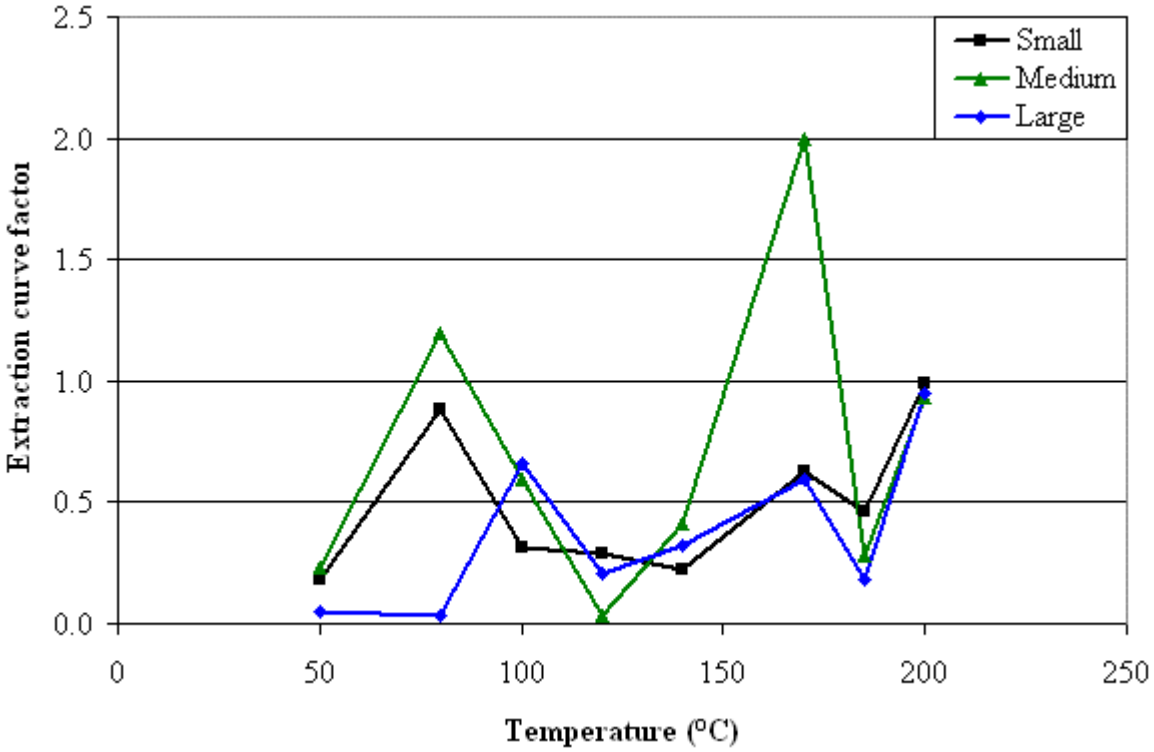

Figure 6-21 – Extraction curve factor as a function of temperature

The extraction curve factor, E_M, appeared erratic across the extraction runs. The extraction lag time, tl, was small for all runs. This suggested that, generally, extraction runs approached their maximum quickly. This contrasted sharply with swelling data, which suggested that lower temperature extractions (less than 185°C) swelled much more slowly than higher temperature extraction runs.

Section 6.4 – Correlation Validation

With the correlation of swell and extraction complete, it was necessary to validate the correlations. The validity of the correlation was qualified by plotting S_M as predicted by the correlation verse S_M as read by eye. This plot is presented below as Figure 6-22.

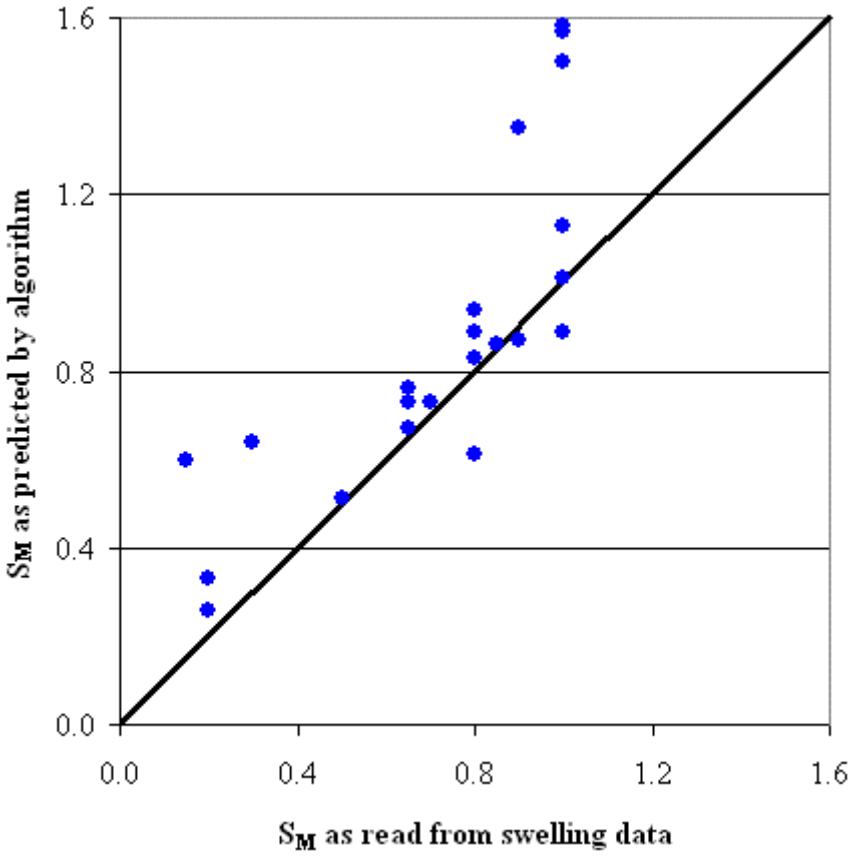

Figure 6-22 – Scatter plot illustrating predicted S_M vs. S_M as read from data

A good correlation would fall along the line $x = y$, verifying that the correlation does not favor certain trends. From Figure 6-22 it is observed that the swelling correlation generally bracketed the $x = y$ line, although there seemed to be a slight preference for the prediction of higher swelling values. The validity of the extraction correlation was qualified in the same

manner. The validity of the correlation was qualified by plotting E_M as predicted by the correlation verse E_M as read by eye. This plot is presented below as Figure 6-23.

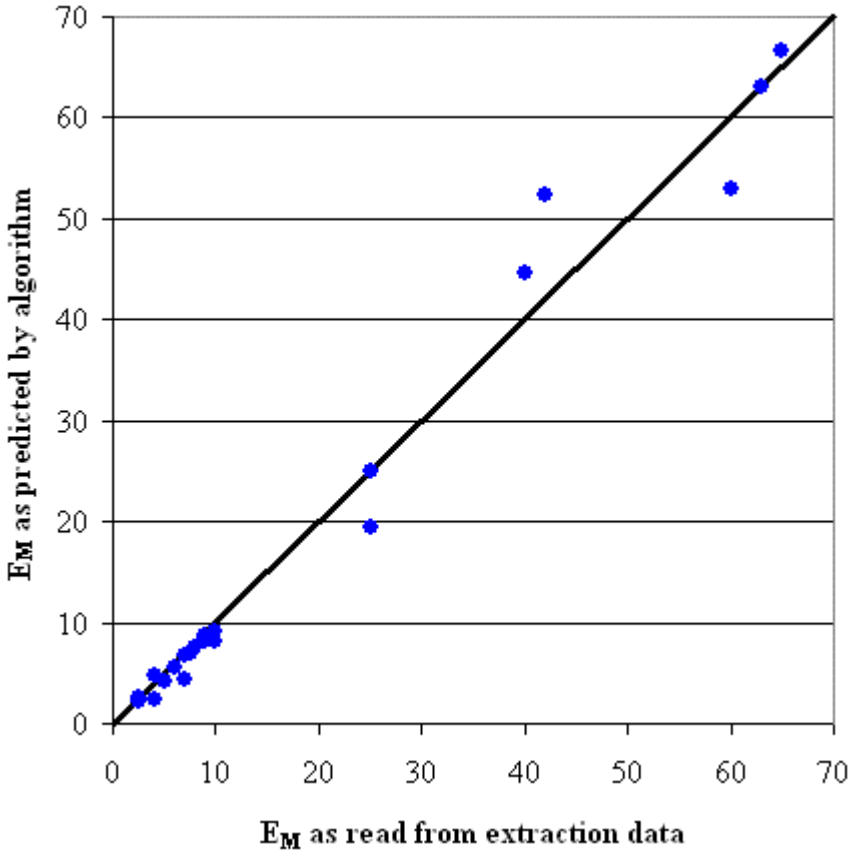

Figure 6-23 – Scatter plot showing predicted E_M vs. E_M read from data

It is observed from Figure 6-23 that the correlation bracketed the $x = y$ line. It is concluded from the above two graphs that the developed correlations were valid in correlating process parameters with swelling and extraction data.

Chapter 7 – Conclusions

The research collected data on the swelling, extraction, and porosity of high volatile bituminous coal (Lower Powellton seam). Swelling and extraction data were collected for over 300 extraction runs. These extraction runs varied temperature, which ranged from 50°C to 200°C, extraction time, which ranged from 2 minutes to 270 minutes, and coal size, which ranged from 355 μm to less than 106 μm. The swell of the bituminous coal post dissolution was measured via optical methods, while the extraction yield was measured via UV-Vis sprectroscopy. The porosity of the coal was measured via mercury porisimetry. Swelling, extraction, and porosity data were examined independently, and a novel correlation was developed between swelling and process parameters, and between extraction and process parameters. Concurrent examination of swelling and extraction correlations suggested a relationship between swelling and extraction.

Data collected during researched showed that the maximum swell observed increased with increasing temperature, until 170°C, after which maximum observed swell decreased. It is hypothesized that swell decreased after 170°C due to the sharp increase in extraction yield that occurred at temperatures higher than 170°C. Increased extraction resulted in significant material being removed from the coal matrix, which may have counteracted swelling. At higher temperatures, temperature weakly affected the maximum observed swell. However, the speed with which the coal swelled increased sharply with increasing temperature. The speed with which the coal swelled maximized at the highest extraction temperature, 200°C.

Data collected during research showed that extraction was relatively negligible with respect to temperature, until a temperature of 185°C, at which point extraction increased dramatically. It was not determined whether this sharp increased in solubility is due to the nature of the extractable material, the nature of the solvent extracting the material, or a combination of the two. All extraction runs showed very little lag time irrespective of coal size, which suggested that the onset of dissolution occurred quickly.

The relationship observed between swelling and extraction is the most significant research result. The research suggested that the maximum observed extraction, E_M, was proportional to the swelling curve factor, C_S. Both of these parameters were fairly flat, until they spiked dramatically at a temperature of 185°C. This suggested that if material was not extracted from the coal matrix, swelling was a relatively slow process. However, when the extractable material was significantly soluble in the solvent, the coal swelled quickly. This result supported the "extraction is a substitution" mechanism proposed by Marzec[24]. It is hypothesized that, as the extractable material in the coal matrix became soluble (at and above 185°C), extractable coal material was replaced with solvent. This sudden introduction of solvent into a coal matrix, which is hypothesized to now be more porous due to the removal of extractable material, may have caused the coal to swell much more quickly.

One novel contribution of this research was the proposed proportionality between the rapidness with which a coal swells and the maximum observed extraction. The other result of this research is a new correlation, a reciprocal fit, used to relate coal swelling and extraction to

processing time and temperature. The optimum parameters for these correlations were found through a "brute force" method, which found the combination of parameters that minimized the sum of squares of the residuals between the correlation and actual data. This research was also significant in that it supported existing literature. It appeared that the dissolution of bituminous coal in a super solvent does take place through a substitution mechanism[24].

Chapter 8 – Recommendations for Future Work

There is an opportunity for further research into super solvent and bituminous coal systems. Research could be performed on other coals, to determine whether the previously developed correlation is general enough to apply to other bituminous coals, other solvents, and even perhaps other ranks of coal. Further research could be performed on the mechanism of the substitution process that is solvent extraction. Does the extractable material dissolve out of the coal matrix, leaving the matrix intact? Or, does the coal matrix cease to exist upon dissolution? The small lag time observed during extraction suggested the latter, but more extraction experiments employing larger coal sizes may be necessary to elucidate the extraction mechanism.

A large area of work remains for anyone willing to investigate why coal swelling and extraction change so dramatically at 185°C, and furthermore, why swelling and extraction are best fit by a reciprocal correlation. Starting from first principles, it should be possible to develop a model describing coal extraction. This model would yield understanding of extraction phenomena observed during this research. Additionally, research could be performed to investigate the relationship between other coal properties and swelling and extraction. In addition to processing time, processing temperature, and coal size, it would be desirous to relate the maceral content of coal to its swelling and extraction behavior.

In summary, many research opportunities still exist concerning the solvent extraction of bituminous coal via super solvents. The research completed herein has raised questions that could serve as the basis of further research.

Chapter 9 – References

[1] Conaway, Shawn, Michael; "CHARACTERIZING TRACE ELEMENT ASSOCIATIONS IN THE PITTSBURGH NO. 8, ILLINOIS NO. 6 AND COALBURG COAL SEAMS"; Thesis, Virginia Polytechnic Institute and State University, July 2001

[2] Hessley, Reasoner, and Riley; page 3 of "Coal Science, an Introduction to Chemistry, Technology, and Utilization"; John Wiley & Sons, New York

[3] Merriam Webster dictionary

[4] Hessley, Reasoner, and Riley; page 4 of "Coal Science, an Introduction to Chemistry, Technology, and Utilization"; John Wiley & Sons, New York

[5] Speight, J.G., *The Chemistry and Technology of Coal,* Marcel Dekker, Inc. New York, NY, 1983

[6] ASTM Designation D 388-84(1984)

[7] Hessley, Reasoner, and Riley; page 74-75 of "Coal Science, an Introduction to Chemistry, Technology, and Utilization"; John Wiley & Sons, New York

[8] Petrakis, L., Grandy, D.W. "Coal Analysis, Characterization, and Petrography," J. Chem. Ed., 57, 691-692 (1980)

[9] "Coal Research Tutorial", Argonne National Laboratories, Chemistry Division, http://chemistry.anl.gov/carbon/coal-tutorial/nomenclature.html

[10] Hessley, Reasoner, and Riley; page 83 of "Coal Science, an Introduction to Chemistry, Technology, and Utilization"; John Wiley & Sons, New York

[11] Ana Maria Mastral, Maria Teresa Izquierdo, Begona Rubio; "Network swelling of coals"; FUEL, 1990, Vol 69, July

[12] Jorge M. Olivares, Nikolaos A Peppas; "THE EFFECT OF TEMPERATURE TREATMENT ON PENETRANT TRANSPORT IN COAL"; Chem. Eng. Comm. 1992, Vol. 115, pp. 183-204

[13] Wiser, W. H. , "Schematic Representation of Structural Groups and Connecting Bridges in Bituminous Coal." 1978

[14] Toshimasa Takanohashi, Masashi Iino; "Investigation of Associated Structure of Upper Freeport Coal by Solvent Swelling"; Energy & Fuels 1995, 9, 788-793

[15] Nishioka, Gorbaty, "Test of the Proposed Two-Phase Model for High-Volatile Bituminous Coals", Energy & Fuels, 1990, 4, pp 70-73

[16] Toshimasa Takanohashi, Hiroyuki Kawashima, Takahiro Yoshida; "The Nature of the Aggregated Structure of Upper Freeport Coal"; (2002 American Chemical Society, 10.1021/ef0101255)

[17] Stiller, Alfred; "US patent # 4,272,356"; June 9, 1981

[18] Chong Chen, Jinsheng Gao, Yongjie Yan; "Role of Noncovalent Bonding in Swelling of Coal"; (1998 American Chemical Society, 10.1021/ef970065w)

[19] Fessenden, Fessenden, "Organic Chemistry"; Fifth Edition, Brooks/Cole Publishing Company, 1994

[20] Oele, A. P., Fuel, Vol. 30, pg.169, 1951.

[21] Dryden, I. G. C., *Fuel*, Vol. 30, pg39, 1951.

[22] Bland, Brian, "Design, Construction, and Evaluation of Coal Extraction Pilot Plant to Manufacture Coal Based Carbon Pitch"; Masters Thesis, West Virginia University, 2000

[23] GAF Corporation, Chemical Division, *M-Pyrol—N-Methyl-2-Pyrrolidone*, New York, NY 1972.

[24] A. Marzec, M. Juzwa, K. Betlej, M. Sobkowiak; "BITUMINOUS COAL EXTRACTION IN TERMS OF ELECTRON-DONOR AND –ACCEPTOR INTERACTIONS IN THE SOLVENT/COAL SYSTEM"; Fuel Processing Technology, 2(1979) 35-44

[25] Douglas Brenner; "In situ microscopic studies of the solvent-swelling of polished surfaces of coal"; FUEL, 1983, Vol 62, November

[26] Douglas Brenner; "Microscopic in-situ studies of the solvent induced swelling of thin sections of coal"; FUEL, 1984, Vol 63, September

[27] George D. Cody, Jr., John W. Larsen, Michael Siskin; "Anisotropic Solvent Swelling of Coals"; Energy & Fuels, Vol. 2, No. 3, 1988

[28] Xiaolin Yang, Bernard G. Silbernagel, John W. Larsen; "Phase Behavior and Macromolecular Structure of Swollen Coals: A Low-Temperature ^{1}H and ^{2}H NMR Study"; Energy & Fuels 1994, 8, 266-275

[29] Paul Painter, Suresh Shenoy; "A New Model for the Swelling of Coal"; Energy & Fuels 1995, 9, 364-371

[30] Jose M. Rincon, Sergio Cruz; "Influence of preswelling on liquefaction of coal"; (FUEL, 1988, Vol 67, August)

[31] Micromeretics sales brochure for Autopore 9220 mercury porisimeter

Appendix A – Solvent Extraction Data and UV-Vis Data

Sample	Absorbance	Size	Time (minutes)	Temperature (Celsius)	Swell Percentage	Cell Width (mm)	Dilution Factor	Concentration (gram/liters)
s1t1m1	0.215655	Small	5	50	0%	1.0	50	1.25
s1t1m2	0.462085	Small	5	80	5%	1.0	50	2.68
s1t1m3	0.706077	Small	5	100	25%	1.0	50	4.09
s1t1m4	0.59738	Small	5	120	25%	1.0	50	3.46
s1t1m5	0.011656	Small	2	140	0%	0.1	100	1.35
s1t1m6	0.014086	Small	2	170	0%	0.1	100	1.63
s1t1m7	0.290784	Small	2	200	40%	0.1	100	33.72
s1t2m1	0.246269	Small	15	50	0%	1.0	50	1.43
s1t2m2	0.701211	Small	15	80	20%	1.0	50	4.07
s1t2m3	0.941461	Small	15	100	45%	1.0	50	5.46
s1t2m4	1.198031	Small	15	120	50%	1.0	50	6.95
s1t2m5	0.019577	Small	4	140	40%	0.1	100	2.27
s1t2m6	0.039843	Small	4	170	10%	0.1	100	4.62
s1t2m7	0.316997	Small	4	200	50%	0.1	100	36.76
s1t3m1	0.27472	Small	30	50	5%	1.0	50	1.59
s1t3m2	0.680152	Small	30	80	40%	1.0	50	3.94
s1t3m3	1.045143	Small	30	100	45%	1.0	50	6.06
s1t3m4	1.288682	Small	30	120	65%	1.0	50	7.47
s1t3m5	0.024022	Small	6	140	40%	0.1	100	2.79
s1t3m6	0.043081	Small	6	170	50%	0.1	100	5.00
s1t3m7	0.337046	Small	6	200	50%	0.1	100	39.08
s1t4m1	0.300744	Small	60	50	10%	1.0	50	1.74
s1t4m2	0.631173	Small	60	80	40%	1.0	50	3.66
s1t4m3	1.193777	Small	60	100	50%	1.0	50	6.92
s1t4m4	1.82791	Small	60	120	75%	1.0	50	10.60
s1t4m5	0.051258	Small	8	140	50%	0.1	100	5.94
s1t4m6	0.056732	Small	8	170	50%	0.1	100	6.58
s1t4m7	0.367046	Small	8	200	50%	0.1	100	42.56
s1t5m1	0.33842	Small	90	50	15%	1.0	50	1.96

Sample	Absorbance	Size	Time (minutes)	Temperature (Celsius)	Swell Percentage	Cell Width (mm)	Dilution Factor	Concentration (gram/liters)
s1t5m2	0.69337	Small	90	80	40%	1.0	50	4.02
s1t5m3	0.971235	Small	90	100	65%	1.0	50	5.63
s1t5m4	1.233181	Small	90	120	75%	1.0	50	7.15
s1t5m5	0.066993	Small	10	140	60%	0.1	100	7.77
s1t5m6	0.054647	Small	10	170	60%	0.1	100	6.34
s1t5m7	0.332268	Small	10	200	50%	0.1	100	38.53
s1t6m1	0.295141	Small	120	50	20%	1.0	50	1.71
s1t6m2	0.67963	Small	120	80	40%	1.0	50	3.94
s1t6m3	1.10884	Small	120	100	65%	1.0	50	6.43
s1t6m4	1.88452	Small	120	120	75%	1.0	50	10.93
s1t6m5	0.064551	Small	12	140	80%	0.1	100	7.49
s1t6m6	0.054136	Small	14	170	80%	0.1	100	6.28
s1t6m7	0.419913	Small	12	200	50%	0.1	100	48.69
s1t7m1	0.411803	Small	150	50	20%	1.0	50	2.39
s1t7m2	0.542663	Small	150	80	65%	1.0	50	3.15
s1t7m3	0.912347	Small	150	100	65%	1.0	50	5.29
s1t7m4	1.319627	Small	150	120	75%	1.0	50	7.65
s1t7m5	0.074583	Small	16	140	80%	0.1	100	8.65
s1t7m6	0.043647	Small	16	170	90%	0.1	100	5.06
s1t7m7	0.376216	Small	14	200	50%	0.1	100	43.62
s1t8m1	0.311908	Small	180	50	20%	1.0	50	1.81
s1t8m2	0.753912	Small	180	80	65%	1.0	50	4.37
s1t8m3	1.041502	Small	180	100	65%	1.0	50	6.04
s1t8m4	1.776194	Small	180	120	80%	1.0	50	10.30
s1t8m5	0.051384	Small	18	140	100%	0.1	100	5.96
s1t8m6	0.062282	Small	18	170	90%	0.1	100	7.22
s1t8m7	0.441011	Small	16	200	50%	0.1	100	51.14
s1t9m1	0.442999	Small	210	50	20%	1.0	50	2.57
s1t9m2	0.594815	Small	210	80	65%	1.0	50	3.45
s1t9m3	0.963346	Small	210	100	65%	1.0	50	5.59
s1t9m4	1.66924	Small	210	120	80%	1.0	50	9.68

Sample	Absorbance	Size	Time (minutes)	Temperature (Celsius)	Swell Percentage	Cell Width (mm)	Dilution Factor	Concentration (gram/liters)
s1t9m5	0.057691	Small	20	140	100%	0.1	100	6.69
s1t9m6	0.055228	Small	20	170	90%	0.1	100	6.40
s1t9m7	0.469789	Small	18	200	60%	0.1	100	54.47
s1t10m1	0.440595	Small	240	50	20%	1.0	50	2.55
s1t10m2	0.817559	Small	240	80	65%	1.0	50	4.74
s1t10m3	1.123437	Small	240	100	65%	1.0	50	6.51
s1t10m4	1.361536	Small	240	120	80%	1.0	50	7.89
s1t10m5	0.059521	Small	22	140	100%	0.1	100	6.90
s1t10m6	0.046292	Small	22	170	90%	0.1	100	5.37
s1t10m7	0.495697	Small	20	200	70%	0.1	100	57.48
s1t11m1	0.411263	Small	270	50	20%	1.0	50	2.38
s1t11m2	0.99951	Small	270	80	65%	1.0	50	5.79
s1t11m3	2.046176	Small	270	100	65%	1.0	50	11.86
s1t11m4	1.400272	Small	270	120	80%	1.0	50	8.12
s1t11m5	0.044129	Small	24	140	100%	0.1	100	5.12
s1t11m6	0.04659	Small	24	170	90%	0.1	100	5.40
s1t11m7	0.492031	Small	22	200	80%	0.1	100	57.05
s2t1m1	0.295717	Medium	5	50	0%	1.0	50	1.71
s2t1m2	0.40109	Medium	5	80	5%	1.0	50	2.33
s2t1m3	0.88353	Medium	5	100	5%	1.0	50	5.12
s2t1m4	0.876652	Medium	5	120	20%	1.0	50	5.08
s2t1m5	0.012557	Medium	2	140	0%	0.1	100	1.46
s2t1m6	0.007573	Medium	2	170	0%	0.1	100	0.88
s2t1m7	0.277821	Medium	2	200	50%	0.1	100	32.21
s2t2m1	0.233244	Medium	15	50	0%	1.0	50	1.35
s2t2m2	0.867766	Medium	15	80	5%	1.0	50	5.03
s2t2m3	1.203003	Medium	15	100	20%	1.0	50	6.97
s2t2m4	1.426751	Medium	15	120	40%	1.0	50	8.27
s2t2m5	0.024619	Medium	4	140	0%	0.1	100	2.85
s2t2m6	0.03633	Medium	4	170	20%	0.1	100	4.21
s2t2m7	0.429409	Medium	4	200	60%	0.1	100	49.79

Sample	Absorbance	Size	Time (minutes)	Temperature (Celsius)	Swell Percentage	Cell Width (mm)	Dilution Factor	Concentration (gram/liters)
s2t3m1	0.303353	Medium	30	50	0%	1.0	50	1.76
s2t3m2	0.933809	Medium	30	80	10%	1.0	50	5.41
s2t3m3	1.641679	Medium	30	100	40%	1.0	50	9.52
s2t3m4	0.968863	Medium	30	120	60%	1.0	50	5.62
s2t3m5	0.054158	Medium	6	140	50%	0.1	100	6.28
s2t3m6	0.023545	Medium	6	170	40%	0.1	100	2.73
s2t3m7	0.473403	Medium	6	200	80%	0.1	100	54.89
s2t4m1	0.308144	Medium	60	50	0%	1.0	50	1.79
s2t4m2	0.961098	Medium	60	80	25%	1.0	50	5.57
s2t4m3	0.859009	Medium	60	100	60%	1.0	50	4.98
s2t4m4	2.725953	Medium	60	120	70%	1.0	50	15.80
s2t4m5	0.059108	Medium	8	140	60%	0.1	100	6.85
s2t4m6	0.037278	Medium	8	170	50%	0.1	100	4.32
s2t4m7	0.478981	Medium	8	200	80%	0.1	100	55.54
s2t5m1	0.417745	Medium	90	50	5%	1.0	50	2.42
s2t5m2	1.043606	Medium	90	80	25%	1.0	50	6.05
s2t5m3	1.468052	Medium	90	100	65%	1.0	50	8.51
s2t5m4	1.117643	Medium	90	120	70%	1.0	50	6.48
s2t5m5	0.05279	Medium	10	140	60%	0.1	100	6.12
s2t5m6	0.024855	Medium	10	170	80%	0.1	100	2.88
s2t5m7	0.516444	Medium	10	200	80%	0.1	100	59.88
s2t6m1	0.369273	Medium	120	50	10%	1.0	50	2.14
s2t6m2	0.985115	Medium	120	80	25%	1.0	50	5.71
s2t6m3	1.181288	Medium	120	100	65%	1.0	50	6.85
s2t6m4	1.419483	Medium	120	120	70%	1.0	50	8.23
s2t6m5	0.060114	Medium	12	140	70%	0.1	100	6.97
s2t6m6	0.047937	Medium	14	170	90%	0.1	100	5.56
s2t6m7	0.539434	Medium	12	200	80%	0.1	100	62.55
s2t7m1	0.41904	Medium	150	50	15%	1.0	50	2.43
s2t7m2	0.708638	Medium	150	80	40%	1.0	50	4.11
s2t7m3	1.740047	Medium	150	100	65%	1.0	50	10.09

Sample	Absorbance	Size	Time (minutes)	Temperature (Celsius)	Swell Percentage	Cell Width (mm)	Dilution Factor	Concentration (gram/liters)
s2t7m4	4.8015	Medium	150	120	75%	1.0	50	27.84
s2t7m5	0.060727	Medium	16	140	80%	0.1	100	7.04
s2t7m6	0.032474	Medium	16	170	100%	0.1	100	3.77
s2t7m7	0.490266	Medium	14	200	80%	0.1	100	56.85
s2t8m1	0.419988	Medium	180	50	18%	1.0	50	2.43
s2t8m2	0.824009	Medium	180	80	45%	1.0	50	4.78
s2t8m3	1.008589	Medium	180	100	65%	1.0	50	5.85
s2t8m4	2.297709	Medium	180	120	75%	1.0	50	13.32
s2t8m5	0.053759	Medium	18	140	80%	0.1	100	6.23
s2t8m6	0.042836	Medium	18	170	100%	0.1	100	4.97
s2t8m7	0.543577	Medium	16	200	80%	0.1	100	63.03
s2t9m1	0.453485	Medium	210	50	18%	1.0	50	2.63
s2t9m2	0.514296	Medium	210	80	55%	1.0	50	2.98
s2t9m3	1.240968	Medium	210	100	65%	1.0	50	7.19
s2t9m4	6.622657	Medium	210	120	80%	1.0	50	38.40
s2t9m5	0.057996	Medium	20	140	100%	0.1	100	6.72
s2t9m6	0.036837	Medium	20	170	100%	0.1	100	4.27
s2t9m7	0.533786	Medium	18	200	80%	0.1	100	61.90
s2t10m1	0.436786	Medium	240	50	20%	1.0	50	2.53
s2t10m2	0.680413	Medium	240	80	65%	1.0	50	3.94
s2t10m3	1.34635	Medium	240	100	65%	1.0	50	7.81
s2t10m4	1.355118	Medium	240	120	80%	1.0	50	7.86
s2t10m5	0.055499	Medium	22	140	100%	0.1	100	6.44
s2t10m6	0.049639	Medium	22	170	100%	0.1	100	5.76
s2t10m7	0.547994	Medium	20	200	80%	0.1	100	63.54
s2t11m1	0.41548	Medium	270	50	20%	1.0	50	2.41
s2t11m2	0.626592	Medium	270	80	65%	1.0	50	3.63
s2t11m3	1.888403	Medium	270	100	65%	1.0	50	10.95
s2t11m4	1.265699	Medium	270	120	80%	1.0	50	7.34
s2t11m5	0.048678	Medium	24	140	100%	0.1	100	5.64
s2t11m6	0.019441	Medium	24	170	100%	0.1	100	2.25

Sample	Absorbance	Size	Time (minutes)	Temperature (Celsius)	Swell Percentage	Cell Width (mm)	Dilution Factor	Concentration (gram/liters)
s2t11m7	0.570505	Medium	22	200	90%	0.1	100	66.15
s3t1m1	0.15745	Large	5	50	0%	1.0	50	0.91
s3t1m2	0.296178	Large	5	80	0%	1.0	50	1.72
s3t1m3	0.524417	Large	5	100	0%	1.0	50	3.04
s3t1m4	0.539334	Large	5	120	0%	1.0	50	3.13
s3t1m5	-0.001503	Large	2	140	0%	0.1	100	-0.17
s3t1m6	0.009569	Large	2	170	0%	0.1	100	1.11
s3t1m7	0.25511	Large	2	200	50%	0.1	100	29.58
s3t2m1	0.182266	Large	15	50	0%	1.0	50	1.06
s3t2m2	0.46464	Large	15	80	0%	1.0	50	2.69
s3t2m3	1.166741	Large	15	100	0%	1.0	50	6.76
s3t2m4	1.520466	Large	15	120	25%	1.0	50	8.82
s3t2m5	0.005388	Large	4	140	0%	0.1	100	0.62
s3t2m6	0.009006	Large	4	170	0%	0.1	100	1.04
s3t2m7	0.401728	Large	4	200	50%	0.1	100	46.58
s3t3m1	0.224182	Large	30	50	0%	1.0	50	1.30
s3t3m2	0.74333	Large	30	80	0%	1.0	50	4.31
s3t3m3	1.690993	Large	30	100	0%	1.0	50	9.80
s3t3m4	0.719289	Large	30	120	45%	1.0	50	4.17
s3t3m5	0.032782	Large	6	140	0%	0.1	100	3.80
s3t3m6	0.002084	Large	6	170	0%	0.1	100	0.24
s3t3m7	0.491274	Large	6	200	70%	0.1	100	56.97
s3t4m1	0.269082	Large	60	50	0%	1.0	50	1.56
s3t4m2	0.863416	Large	60	80	5%	1.0	50	5.01
s3t4m3	1.355006	Large	60	100	45%	1.0	50	7.86
s3t4m4	1.285229	Large	60	120	50%	1.0	50	7.45
s3t4m5	0.034646	Large	8	140	0%	0.1	100	4.02
s3t4m6	0.028798	Large	8	170	40%	0.1	100	3.34
s3t4m7	0.46068	Large	8	200	70%	0.1	100	53.42
s3t5m1	0.297636	Large	90	50	0%	1.0	50	1.73
s3t5m2	0.997472	Large	90	80	10%	1.0	50	5.78

Sample	Absorbance	Size	Time (minutes)	Temperature (Celsius)	Swell Percentage	Cell Width (mm)	Dilution Factor	Concentration (gram/liters)
s3t5m3	1.150154	Large	90	100	45%	1.0	50	6.67
s3t5m4	1.45456	Large	90	120	70%	1.0	50	8.43
s3t5m5	0.042876	Large	10	140	40%	0.1	100	4.97
s3t5m6	0.008764	Large	10	170	50%	0.1	100	1.02
s3t5m7	0.482493	Large	10	200	70%	0.1	100	55.95
s3t6m1	0.332129	Large	120	50	5%	1.0	50	1.93
s3t6m2	1.398643	Large	120	80	15%	1.0	50	8.11
s3t6m3	1.236225	Large	120	100	50%	1.0	50	7.17
s3t6m4	1.49379	Large	120	120	70%	1.0	50	8.66
s3t6m5	0.035452	Large	12	140	40%	0.1	100	4.11
s3t6m6	0.053685	Large	14	170	50%	0.1	100	6.23
s3t6m7	0.48292	Large	12	200	70%	0.1	100	56.00
s3t7m1	0.349071	Large	150	50	5%	1.0	50	2.02
s3t7m2	1.10354	Large	150	80	25%	1.0	50	6.40
s3t7m3	1.279285	Large	150	100	50%	1.0	50	7.42
s3t7m4	1.344527	Large	150	120	70%	1.0	50	7.80
s3t7m5	0.038689	Large	16	140	50%	0.1	100	4.49
s3t7m6	0.014354	Large	16	170	60%	0.1	100	1.66
s3t7m7	0.480745	Large	14	200	80%	0.1	100	55.75
s3t8m1	0.361865	Large	180	50	10%	1.0	50	2.10
s3t8m2	0.932874	Large	180	80	30%	1.0	50	5.41
s3t8m3	1.248511	Large	180	100	50%	1.0	50	7.24
s3t8m4	1.537391	Large	180	120	75%	1.0	50	8.91
s3t8m5	0.052306	Large	18	140	70%	0.1	100	6.07
s3t8m6	0.023118	Large	18	170	80%	0.1	100	2.68
s3t8m7	0.502346	Large	16	200	80%	0.1	100	58.25
s3t9m1	0.419722	Large	210	50	10%	1.0	50	2.43
s3t9m2	1.01292	Large	210	80	30%	1.0	50	5.87
s3t9m3	1.43632	Large	210	100	50%	1.0	50	8.33
s3t9m4	1.47068	Large	210	120	75%	1.0	50	8.53
s3t9m5	0.041469	Large	20	140	70%	0.1	100	4.81

Sample	Absorbance	Size	Time (minutes)	Temperature (Celsius)	Swell Percentage	Cell Width (mm)	Dilution Factor	Concentration (gram/liters)
s3t9m6	0.014631	Large	20	170	80%	0.1	100	1.70
s3t9m7	0.536398	Large	18	200	80%	0.1	100	62.20
s3t10m1	0.432026	Large	240	50	15%	1.0	50	2.50
s3t10m2	1.791915	Large	240	80	30%	1.0	50	10.39
s3t10m3	1.545973	Large	240	100	50%	1.0	50	8.96
s3t10m4	1.667961	Large	240	120	75%	1.0	50	9.67
s3t10m5	0.038294	Large	22	140	70%	0.1	100	4.44
s3t10m6	0.003015	Large	22	170	80%	0.1	100	0.35
s3t10m7	0.514215	Large	20	200	90%	0.1	100	59.63
s3t11m1	0.403897	Large	270	50	15%	1.0	50	2.34
s3t11m2	1.228681	Large	270	80	30%	1.0	50	7.12
s3t11m3	1.524784	Large	270	100	50%	1.0	50	8.84
s3t11m4	1.495289	Large	270	120	85%	1.0	50	8.67
s3t11m5	0.030242	Large	24	140	80%	0.1	100	3.51
s3t11m6	0.007993	Large	24	170	100%	0.1	100	0.93
s3t11m7	0.521108	Large	22	200	100%	0.1	100	60.43

Sample	Absorbance	Size	Time (minutes)	Temperature (Celsius)	Swell Percentage	Cell Width (mm)	Dilution Factor	Concentration (gram/liters)
s2t1e	0.412598	Medium	5	200	30%	0.1	100	12502.97
s2t1f	0.394171	Medium	5	200	30%	0.1	100	11944.58
s2t1g	0.456292	Medium	5	200	30%	0.1	100	13827.03
s2t2e	0.456359	Medium	10	200	60%	0.1	100	13829.06
s2t2f	0.476154	Medium	10	200	60%	0.1	100	14428.91
s2t2g	0.416354	Medium	10	200	60%	0.1	100	12616.79
s2t3e	0.468711	Medium	15	200	70%	0.1	100	14203.36
s2t3f	0.450855	Medium	15	200	70%	0.1	100	13662.27
s2t3g	0.485044	Medium	15	200	70%	0.1	100	14698.30
s2t4e	0.49862	Medium	20	200	90%	0.1	100	15109.70
s2t4f	0.476364	Medium	20	200	90%	0.1	100	14435.27

Sample	Absorbance	Size	Time (minutes)	Temperature (Celsius)	Swell Percentage	Cell Width (mm)	Dilution Factor	Concentration (gram/liters)
s2t4g	0.490532	Medium	20	200	90%	0.1	100	14864.61
s2t1a	0.440604	Medium	30	200	90%	0.1	100	13351.64
s2t1b	0.494685	Medium	30	200	90%	0.1	100	14990.45
s2t1c	0.505487	Medium	30	200	90%	0.1	100	15317.79
s2t2a	0.919077	Medium	60	200	90%	0.1	100	27850.82
s2t2b	0.510847	Medium	60	200	90%	0.1	100	15480.21
s2t2c	0.517143	Medium	60	200	90%	0.1	100	15671.00
s2t3a	0.495664	Medium	90	200	90%	0.1	100	15020.12
s2t3b	0.441334	Medium	90	200	90%	0.1	100	13373.76
s2t3c	0.517433	Medium	90	200	90%	0.1	100	15679.79
s2t4a	0.480106	Medium	120	200	90%	0.1	100	14548.67
s2t4b	0.462723	Medium	120	200	90%	0.1	100	14021.91
s2t4c	0.514511	Medium	120	200	90%	0.1	100	15591.24

Sample	Absorbance	Size	Time (minutes)	Temperature (Celsius)	Swell Percentage	Cell Width (mm)	Dilution Factor	Concentration (gram/liters)
Shaking								
s1t1m8	0.069884	Small	2	140	0%	0.1	100	2117.70
s1t2m8	0.034141	Small	4	140	10%	0.1	100	1034.58
s1t3m8	0.057279	Small	6	140	60%	0.1	100	1735.73
s1t4m8	0.053619	Small	8	140	60%	0.1	100	1624.82
s1t5m8	0.069755	Small	10	140	70%	0.1	100	2113.79
s1t6m8	0.07191	Small	12	140	50%	0.1	100	2179.09
s1t7m8	0.069529	Small	14	140	80%	0.1	100	2106.94
s1t8m8	0.067916	Small	16	140	80%	0.1	100	2058.06
s1t9m8	0.080673	Small	18	140	80%	0.1	100	2444.64
s1t10m8	0.069723	Small	20	140	80%	0.1	100	2112.82
s1t11m8	0.073424	Small	25	140	80%	0.1	100	2224.97
s2t1m8	0.03656	Medium	2	140	20%	0.1	100	1107.88
s2t2m8	0.039867	Medium	4	140	20%	0.1	100	1208.09
s2t3m8	0.029357	Medium	6	140	40%	0.1	100	889.61

Sample	Absorbance	Size	Time (minutes)	Temperature (Celsius)	Swell Percentage	Cell Width (mm)	Dilution Factor	Concentration (gram/liters)
s2t4m8	0.033828	Medium	8	140	50%	0.1	100	1025.09
s2t5m8	0.038933	Medium	10	140	60%	0.1	100	1179.79
s2t6m8	0.079134	Medium	12	140	60%	0.1	100	2398.00
s2t7m8	0.047248	Medium	14	140	70%	0.1	100	1431.76
s2t8m8	0.038316	Medium	16	140	80%	0.1	100	1161.09
s2t9m8	0.06216	Medium	18	140	80%	0.1	100	1883.64
s2t10m8	0.046221	Medium	20	140	80%	0.1	100	1400.64
s2t11m8	0.048971	Medium	25	140	80%	0.1	100	1483.97
s3t1m8	0.024946	Large	2	140	0%	0.1	100	755.94
s3t2m8	0.024072	Large	4	140	20%	0.1	100	729.45
s3t3m8	0.013833	Large	6	140	20%	0.1	100	419.18
s3t4m8	0.018276	Large	8	140	30%	0.1	100	553.82
s3t5m8	0.013663	Large	10	140	40%	0.1	100	414.03
s3t6m8	0.032254	Large	12	140	40%	0.1	100	977.39
s3t7m8	0.016957	Large	14	140	50%	0.1	100	513.85
s3t8m8	0.01773	Large	16	140	50%	0.1	100	537.27
s3t9m8	0.039943	Large	18	140	50%	0.1	100	1210.39
s3t10m8	0.025296	Large	20	140	60%	0.1	100	766.55
s3t11m8	0.048493	Large	25	140	60%	0.1	100	1469.48

Appendix B – Visual Basic Code used to Fit Correlation to Data

```
Sub regression()
'
' regression Macro
' Macro recorded 3/26/2006 by Joe Stoffa
'
' These variables will determine the resolution of the optimization
Dim nSwellLevels
Dim nConstantLevels
Dim nTimeLevels

' These variables represent the correlation's adjustable parameters
Dim nSwell
Dim nConstant
Dim nTime

' These variables are the optimum values found during optimization
Dim nOptimumSwell
Dim nOptimumConstant
Dim nOptimumTime
Dim lnOptimumSSR

' Initialize the optimum SSR to something high
lnOptimumSSR = 999

' Turn off screen updating before we start
Application.ScreenUpdating = False

' There are three loops here, two nested and parent
' These loops examine all combinations of adjustable parameters
For nLoop1 = 1 To 200
   For nLoop2 = 1 To 250
      For nLoop3 = 1 To 100
         ' First, we set the current swell, constant, and time

         ' Set the maximum swell
         nSwell = 0.1 * nLoop1

         ' Set the constant
         nConstant = 0.01 * nLoop2

         ' Set the lag time
```

```
            nTime = nLoop3

            ' adjust the spreadsheet
            Range("swellMaximum").Value = nSwell
            Range("curveFactor").Value = nConstant
            Range("lagTime").Value = nTime

            ' Check to make sure we don't divide by zero
            ' If we're going to, we'll simply skip that combination
            If Range("SSR").Text <> "#DIV/0!" And Range("SSR").Text <> "#VALUE!" Then
               If Range("SSR").Value < lnOptimumSSR Then
                  lnOptimumSSR = Range("SSR").Value
                  nOptimumSwell = Range("swellMaximum").Value
                  nOptimumConstant = Range("curveFactor").Value
                  nOptimumTime = Range("lagTime").Value
               End If
            End If

         Next ' For nLoop3 = 0 To nTimeLevels
      Next ' For nLoop2 = 0 To nConstantLevels
   Next ' For nLoop = 0 To nSwellLevels

   ' Turn on screen updating before we end
   Application.ScreenUpdating = True

   Range("swellMaximum").Value = nOptimumSwell
   Range("curveFactor").Value = nOptimumConstant
   Range("lagTime").Value = nOptimumTime

   End Sub
```